De Jaime-Soguero, Chabier; Mujal, Eudald; Oms, Oriol; [et al.]. «Palaeoenvironmental reconstruction of a lower to middle Permian terrestrial composite succession from the Catalan Pyrenees : Implications for the evolution of tetrapod ecosystems in equatorial Pangaea». Palaeogeography, Palaeoclimatology, Palaeoecology, Vol. 632 (December 2023), art. 111837. DOI 10.1016/j.palaeo.2023.111837

Supplementary material for:

Palaeoenvironmental reconstruction of a lower to middle Permian terrestrial composite succession from the Catalan Pyrenees: implications for the evolution of tetrapod ecosystems in equatorial Pangaea

De Jaime-Soguero, C.[1], Mujal, E.[2,1], Oms, O.[3], Bolet, A.[4,1,5], Dinarès-Turell, J.[6], Ibáñez-Insa, J.[7], Fortuny, J.[1]

[1]*Institut Català de Paleontologia Miquel Crusafont (ICP-CERCA), Universitat Autònoma de Barcelona, Edifici ICTA-ICP, c/ Columnes s/n, Campus de la UAB, 08193 Cerdanyola del Vallès, Barcelona, Spain.*

[2]*Staatliches Museum für Naturkunde Stuttgart, Rosenstein 1, D-70191 Stuttgart, Germany.*

[3]*Departament de Geologia, Universitat Autònoma de Barcelona, E-08193 Bellaterra, Catalonia, Spain.*

[4]*Departamento de Estratigrafía y Paleontología, Universidad de Granada, Avda. Fuente Nueva s/n, 18071 Granada, Spain*

[5]*School of Earth Sciences, University of Bristol, Wills Memorial Building, Queens Road, Bristol BS8 1RJ, United Kingdom*

[6]*Istituto Nazionale di Geofisica e Vulcanologia, Via di Vigna Murata 605, I-00143 Roma, Italy*

[7]*Geosciences Barcelona (GEO3BCN-CSIC), C/ Lluís Solé i Sabarís s/n, 08028 Barcelona, Spain*

Supplementary Text S1. Indeterminated tetrapod tracks, invertebrate traces and plant remains

Systematic ichnology

Tetrapod ichnology

Indeterminate morphotype

Fig. S7

Material. Lower Upper Red Unit (lower URU): one unrecovered isolated partial right footprint in concave epirelief from CR section (CR-15-4) (Fig. S7).

Description. Semiplantigrade, medium-sized track (28.80 mm long) composed of three robust digit imprints. The imprint shows a moderately ectaxonic shape, with the digits markedly separated without overlapping, and the digit length increases from digit I to III. Digits II and III imprints are the deepest, being completely preserved, showing a slightly inward rotation and ending with pointed claw traces, whereas digits I is only represented by isolated, shallow and rounded tip imprint. Digit II imprint shows two phalangeal pads, being the proximal the deepest. Digit III imprint presents three phalangeal pads being also, the proximal the deepest. The lack of the digit IV and V precludes an accurate measurement of the ichnite, making also impossible to distinguish if the footprint belong to a pes or a manus. The sole/palm impression is short, and it is deeper impressed below digits II and III.

Remarks. The low preservation degree (1) and the lack of additional samples precludes the identification of the ichnotaxon. The overall shape and the relative length of the digits are features observed in the ichnogenus *Dromopus* and *Varanopus*. However, in both, several diagnostic features are absent. The robust digits with clawed digit tips could be characteristic features of the ichnogenus *Varanopus*, a widespread ichnotaxon of the Cisuralian–Guadalupian related to captorhinomorphs and bolosaurian parareptiles (Haubold and Lucas, 2003; Gand and Durand, 2006; Voigt, 2012; Voigt et al., 2013, Voigt and Haubold, 2015; Marchetti et al., 2021a). This ichnogenus has been recovered in the Catalan Pyrenees (Voigt and Haubold, 2015; Mujal et al., 2016a), France (Gand, 1988; Marchetti et al., 2022b), Italy (Nicosia et al., 2000, Marchetti et al., 2022a), Germany (Müller, 1954; Haubold and Stapf, 1998), USA (Haubold and Lucas, 2001, 2003; Lucas and Spielmann, 2009) and Canada (Van Allen et al., 2005). However, the shallow impression of the digit I and the slightly inward curvature of the digits II and III are features inconsistent with this ichnogenus. Moreover, the absence of an elongated digit IV, subequal in length with the digit III, and the digit V, subequal in length as digit I and II, precludes the assignment to *Varanopus*. On the other hand, the increasing digit length, their curvature, and the shallow impression of digit I are typical characteristics of the ichnogenus *Dromopus*. However, this ichnogenus is also defined by a markedly elongated digit IV and a proximal position of the short digit V, showing slender elongated digits with tiny digit tips. Therefore, the lack of digits IV and V, and the robust digital impressions with rounded clawed tips observed in this footprint makes impossible to assign it to this ichnogenus.

Invertebrate ichnology

Acripes (Matthew, 1910)

Acripes multiformis Gand et al., 2008

Material. Upper Upper Red Unit (upper URU): two samples with invertebrate traces recovered from the massive mudstone deposits of the RM section (IPS128903, IPS128906).

Description. Small-size lineal (1.3 to 5 mm as maximum width) traces generally composed by two symmetric and parallel groves (sometimes only one is preserved) separated by one medial ridge, which generally are displayed in straight or sinuous lines. The width of each grove can variate along the trace. The edges of each row display a rounded shape, and sometimes appear in contact with resting traces (*Rusophycus* see below).

Discussion. The rectilinear or sinuous shallow impression of two symmetric furrows associated with invertebrate traces of *Rusophycus* are diagnostic features of the ichnospecies *Acripes multiformis*. They are interpreted as walking traces (*Repichnia*), being in the same levels as resting traces (*Cubichnia)* of clam shrimp arthropods (triopsids) (Gand et al., 2008). It has been recovered in different fluvial and shallow lacustrine Permian deposits of the LRU and URU of the Catalan Pyrenees (Mujal et al., 2016, 2017). In the studied succession, it is mostly related to small water bodies in floodplain deposits and lacustrine ponds.

Rusophycus Hall, 1852

***Rusophycus* isp.**

Fig. S8A–B

Material. Lower Red Unit (LRU): Several surfaces with bioturbation activity (not recovered) recorded in floodplain and overbank deposits of the LRU (at 180 m, 192 m and 232 m from the base of CnH section), one sample related with vegetal impressions at CnH section (IPS128889). Upper Upper Red Unit (upper URU): several samples (Fig. S8A–B) recovered from the outcrops of the massive mudstone deposits at 145 m, 180 m and 208 m from the base of RM section (IPS88736, IPS88737, IPS128897, IPS128900, IPS128903, IPS128906, IPS128907, IPS12908) and at 164 m from the base of CR section (IPS88728, IPS88729, IPS88730, IPS128879).

Description. Small-sized (2-5 mm), oval-shaped smooth traces with bilateral symmetry. They are divided in two elongated loves by an intermedial space, giving them a "coffee grain" shape. The internal edges are parallel to the midline; however, the lateral edges tend be curved, producing a thicker area in the middle of each love and, showing a gradual reduction of the thickness in extremes distal and anterior limit of each love, producing pointed shapes.

Discussion. The small size, oval and bilobated shape with bilateral symmetry are diagnostic features of the ichnogenus *Rusophycus*, a common Permian-Triassic resting trace (*Cubichnia*) related with notostracan arthropods (triopsids) (Gand et al., 2008). They appear related with walking traces (*Repichnia*) of the same trackmakers *(Acripes* see above). This ichnogenus is conspicuously abundant in shallow water deposits with mudstone or very fined sandstones as the ephemeral ponds of the playa lake system or the overbank deposits of the floodplains in the studied succession. In fact, it has been recovered in river and playa-lake systems of the LRU and URU of the Catalan Pyrenees (Mujal et al., 2016, 2017). Sometimes several globular structures possibly corresponding to pellets associated with these notostracan traces (Fig. S7B).

Plant remains

Despite the long wide succession studied in this work, only a few vegetal remains have been recorded. Also, the partial and bad preservation of this palaeontological material, make most of the samples cannot be identified at family, genus nor specific level. Just a few fossils preserve recognizable morphologies to reveal the floristic diversity of the studied Permian red beds.

The oldest biotic remains recovered in the studied area is the specimen IPS88725. This sample contain three small trunk fragments of horsetail plant have been recovered from a medium grain-sized yellowish sandstone (IPS88725, Fig. S8C). They measure between 7.73 mm and 1.02 mm width, and they present a vertical ribbing, however no segmentation nodule and no other structure is observed, considering the three remains as internodular fragments. This sample was recovered in a covered area, relatively close to the lowermost layers of the CnH section. However, this ex-situ sample show a clear different feature in comparison with these Permian deposits, showing similar colour and granulometry to those facies identified as the Transition Unit in the studied area (Gisbert et al., 1985). All these observations precludes that these horsetail remains probably belong to sandstone levels of the Transition Unit, identified in the Pyrenean Basin as late Carboniferous-early Permian sediments (Nagtegaal, 1969; Gisbert, 1981; Mujal et al., 2018), being the oldest sample of the studied sub-basin.

In the Lower Red Unit deposits of CnH section, some vegetal remains appear in the overbank deposits of the LRU (IPS128895, at 232.5 m of the base of CnH section), however, the bad preservation of the remains precludes a detailed identification of them.

Most of the plant remains were recovered in the Upper Red Unit (URU). In the first deposits of the lower URU, some few vegetal impressions appear in a fine-grained sandstone level (IPS128889, IPS128890; Fig. S7D). Despite presenting an elongated and straight shape, like a needle leaf, the poor preservation makes impossible to recognise any structure. On the other hand, the shallow lacustrine deposits of the upper URU of RM section (IPS128898, IPS128900, IPS128905, IPS128892, IPS128893) and CR section (IPS88730) preserve several samples of straight branches of ferns (Fig. S7E). The general morphology consists of a principal branch that splits in two homologous branches, which in turn, split in two branches. The branches usually show stretch marks parallel to the main axis of the branch. Despite they do not preserve any leaf structure, their morphology shares several features with fern fronds (i.e. *Schizopteris*) and fern leaves (i.e. *Sphenopteris*). These plants only appear in shallow lacustrine facies, related with ephemeral water ponds. Sometimes invertebrate traces (*Rusophicus* and *Acripes*) appear in the same slabs as these plant remains. Similar samples have been recovered in lacustrine environments of Cisuralian deposits of the Collio Formation related with hygromorphic vegetation (Southern Alps, Northern Italy) (Marchetti et al., 2022).

Finally, several trunk marks have been identified in a mud-cracked level at 190 m of the base of CR section. They show radial cracks surrounding the diameter of an arborescent plant (Fig. S8F). These trunk marks appear grouped, spaced between them just for 20-50 cm.

References

Gand G., Garric, J., Schneider, J., Walter, H., Lapeyrie, J., Martin, C., Thiery, A., 2008. Notostraca trackways in Permian playa environments of the Lodève basin (France). J. Iber. Geol. 34 (1), 73–108.

Gisbert, J., 1981. Estudio geológicopetrológico del Estefaniense-Pérmico de la sierra del Cadí (Pirineo de Lérida): Diagénesis y Sedimentología. PhD Thesis, Universidad de Zaragoza, Spain.

Gisbert, J., Martí, J., Gascón, F., 1985. Guía de la excursión al Stephaniense, Pérmico y Triásico inferior del Pirineo catalán. II Coloquio de estratigrafía y paleogeografía del Pérmico y Triásico de España, La Seu d’Urgell, 1–78.

Marchetti, L., Forte, G., Kustatscher, E., DiMichele, W.A., Lucas, S.G., Roghi, G., Juncal, M.A., Hartkopf-Fröder, C., Krainer, K., Morelli, C., Ronchi, A., 2022. The Artinskian Warming Event: an Euramerican change in climate and the terrestrial biota during the early Permian. Earth Sci. Rev. 226, 103922. https://doi.org/10.1016/j.earscirev.2022.103922

Mujal, E., Fortuny, J., Marmi, J., Dinarès-Turell, J., Bolet, A., Oms, O., 2018. Aridification across the Carboniferous–Permian transition in central equatorial Pangea: The Catalan Pyrenean succession (NE Iberian Peninsula). Sediment. Geol. 363, 48–68. https://doi.org/10.1016/j.sedgeo.2017.11.005

Mujal, E., Fortuny, J., Oms, O., Bolet, A., Galobart, À., Anadón, P., 2016. Palaeoenvironmental reconstruction and early Permian ichnoassemblage from the NE Iberian Peninsula (Pyrenean Basin). Geol. Mag. 153, 578–600. https://doi.org/10.1017/S0016756815000576

Mujal, E., Fortuny, J., Pérez-Cano, J., Dinarès-Turell, J., Ibáñez-Insa, J., Oms, O., Vila, I., Bolet, A., Anadón, P., 2017. Integrated multi-stratigraphic study of the Coll de Terrers late Permian–Early Triassic continental succession from the Catalan Pyrenees (NE Iberian Peninsula): A geologic reference record for equatorial Pangaea. Glob. Planet. Change 159, 46–60. https://doi.org/10.1016/j.gloplacha.2017.10.004

Nagtegaal, P.J.C., 1969. Sedimentology, paleoclimatology, and diagenesis of post-Hercynian continental deposits in the south-central Pyrenees, Spain. Leidse Geologische Mededelingen 42, 143–238.

Supplementary material for:

Palaeoenvironmental reconstruction of a lower to middle Permian terrestrial composite succession from the Catalan Pyrenees: implications for the evolution of tetrapod ecosystems in equatorial Pangaea

De Jaime-Soguero, C.[1], Mujal, E.[2,1], Oms, O.[3], Bolet, A.[4,1,5], Dinarès-Turell, J.[6], Ibáñez-Insa, J.[7], Fortuny, J.[1]

[1]Institut Català de Paleontologia Miquel Crusafont (ICP-CERCA), Universitat Autònoma de Barcelona, Edifici ICTA-ICP, c/ Columnes s/n, Campus de la UAB, 08193 Cerdanyola del Vallès, Barcelona, Spain.

[2]Staatliches Museum für Naturkunde Stuttgart, Rosenstein 1, D-70191 Stuttgart, Germany.

[3]Departament de Geologia, Universitat Autònoma de Barcelona, E-08193 Bellaterra, Catalonia, Spain.

[4]Departamento de Estratigrafía y Paleontología, Universidad de Granada, Avda. Fuente Nueva s/n, 18071 Granada, Spain

[5]School of Earth Sciences, University of Bristol, Wills Memorial Building, Queens Road, Bristol BS8 1RJ, United Kingdom

[6]Istituto Nazionale di Geofisica e Vulcanologia, Via di Vigna Murata 605, I-00143 Roma, Italy

[7]Geosciences Barcelona (GEO3BCN-CSIC), C/ Lluís Solé i Sabarís s/n, 08028 Barcelona, Spain

Supplementary Text S2. XRD analysis

Powder x-ray diffraction (XRD) measurements were performed in order to characterize the mineralogy of the investigated samples (see Table S4). The XRD results were also employed to shed light on the possible origin of samples that were not identified unambiguously in the flied thin section. In particular, we found that in several cases, both in hand specimens and in thin section, the distinction between volcanic and fluvial materials was not straightforward. This is probably related, in part, to the fact that volcaniclastics were highly represented in the source areas of the sedimentary materials.

Figures S9 to S11 show XRD scans from selected samples. In general, it is found that the qualitative mineralogy of the analysed samples, regardless of their origin (volcanic or sedimentary), is similar. Most of the scans are dominated by strong reflections of quartz. Other major phases that show up in the scans include plagioclase (albite), mica (muscovite 2M1), chlorite (clinochlore), calcite and small amounts of hematite. As is well known, the latter is responsible for the red colour of the Permian-Triassic materials.

The relative amount of the different major minerals in the investigated samples shows significant variations, as revealed by the relative intensities of the XRD peaks of the different phases. Fig. S9A shows the XRD scans of the samples CH-8 and CH-9 recovered from the Lower Red Unit (LRU) of CnH section. According to field sedimentological observations can be attributed, respectively, to volcanic material (CH-8;) and to fluvial sediments (CH-9). Although the mineralogy and the thin section (see Table S4) of these two samples share several features, it is found that the volcaniclastic material contains larger amounts of plagioclase and of quartz. Small amounts of calcite are only detected in the fluvial material. In turn, stronger reflections from chlorite show up in the scan of the fluvial sediments. Nevertheless, chlorite is typically found in volcaniclastic samples and, therefore, it is not expected to be particularly indicative of the provenance of volcano-sedimentary materials because it may be related to multiple processes like, for instance: I) recrystallization after weathering of volcanic materials, which can be later incorporated in the fluvial sediments; II) hydrothermal alteration of the volcano-sedimentary rocks; III) incorporation of metamorphic materials from the source area in the fluvial sediments, IV) Incorporation of chlorite-rich clasts in the volcanic materials through pyroclastic density currents.

With these ideas in mind, we show in Fig. S9B the XRD scan of sample CH-13, which corresponds to the lower Upper Red Unit (lURU) of Castellar de n'Hug, i.e., above the last registered volcanic materials. In this case, the intensity of the plagioclase peaks is relatively low, in agreement with the above considerations. In contrast, a somewhat larger amount of calcite is detected, which can be attributed to pedogenetic processes or to fluid circulation in the more porous, non-volcanic sediments. Interestingly, weak signal from microcline is also detected, which may be attributed to a change of source area for the lURU sediments. Similar observations are found in Fig. S10A for samples CH-14 (lURU in Coll Roig) and RM-m254-pre upper Upper Red Unit (UURU) of Riera de Monell. As discussed for the case of sample CH-9 (Fig. S9), chlorite peaks are also evident for these two samples.

Interestingly, the XRD measurements allowed us to identify the possible origin of samples that, in the field, showed particular colorations or morphologies. This is the case, for instance, of sample RM-m254 from the uURU of Riera del Monell, which did not display the typical red colour of the Permian-Triassic sediments. As can be seen in the XRD results (Fig. S10B), this sample contains small amounts of barite and larger amounts of calcite and chlorite. According to these findings, this sample can be attributed to a highly reduced organic-matter-rich fluvial sediment that contains a metal-rich mineralization deposited through hydrothermal circulation.

Finally, we discuss the case of samples from the LURU of Sant Vicenç de Rus, the identification of which was unclear in thin section. As can be seen in Fig. S11 for the case of sample RUS-1, and bearing in mind the above discussion, this sample might be tentatively attributed to a fluvial sediment due to the relatively low amount of plagioclase that shows up in the scan. The presence of calcite may be attributed to the larger porosity of the sedimentary material relative to the volcanic materials. However, the XRD data alone do not allow us to reach definitive conclusions about the origin of these unclear LURU samples since, for instance, pedogenetic processes or subsequent weathering of volcaniclastic materials might have yielded the observed mineralogy. This example is basically aimed at illustrating the complexity of correctly assigning the origin of these volcano-sedimentary materials. More work is required in order to unambiguously identify the nature of all the materials registered in Castellar de n'Hug and related outcrops.

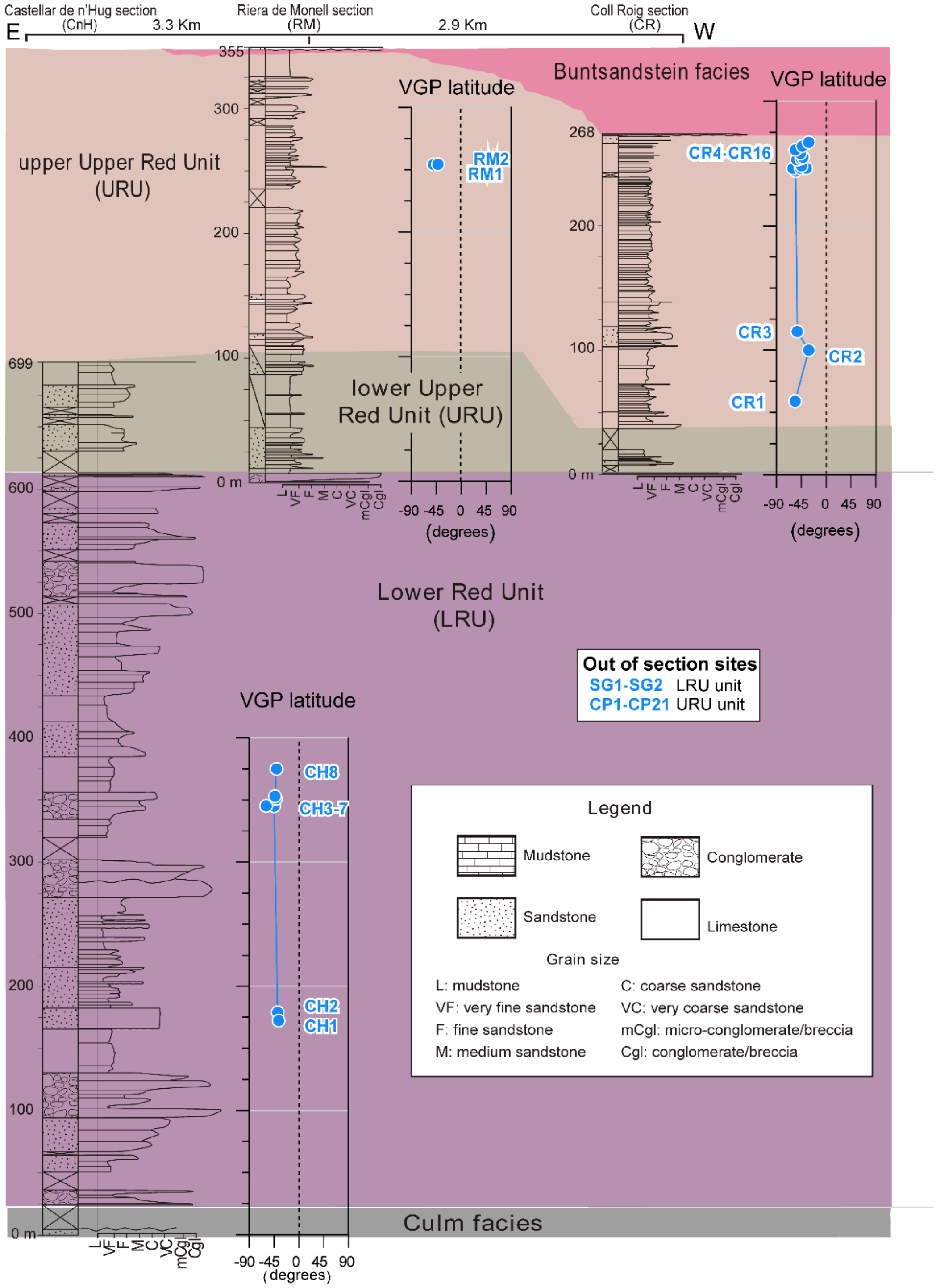

Castellar de n'Hug section (CnH)
Riera de Monell section (RM)
Coll Roig section (CR)
E
3.3 Km
2.9 Km
W
Buntsandstein facies
upper Upper Red Unit (URU)
lower Upper Red Unit (URU)
Lower Red Unit (LRU)
Culm facies
VGP latitude
(degrees)
RM2
RM1
CR4-CR16
CR3
CR2
CR1
CH8
CH3-7
CH2
CH1
Out of section sites
SG1-SG2 LRU unit
CP1-CP21 URU unit
Legend
Mudstone
Conglomerate
Sandstone
Limestone
Grain size
L: mudstone
VF: very fine sandstone
F: fine sandstone
M: medium sandstone
C: coarse sandstone
VC: very coarse sandstone
mCgl: micro-conglomerate/breccia
Cgl: conglomerate/breccia

Figure S1.

284

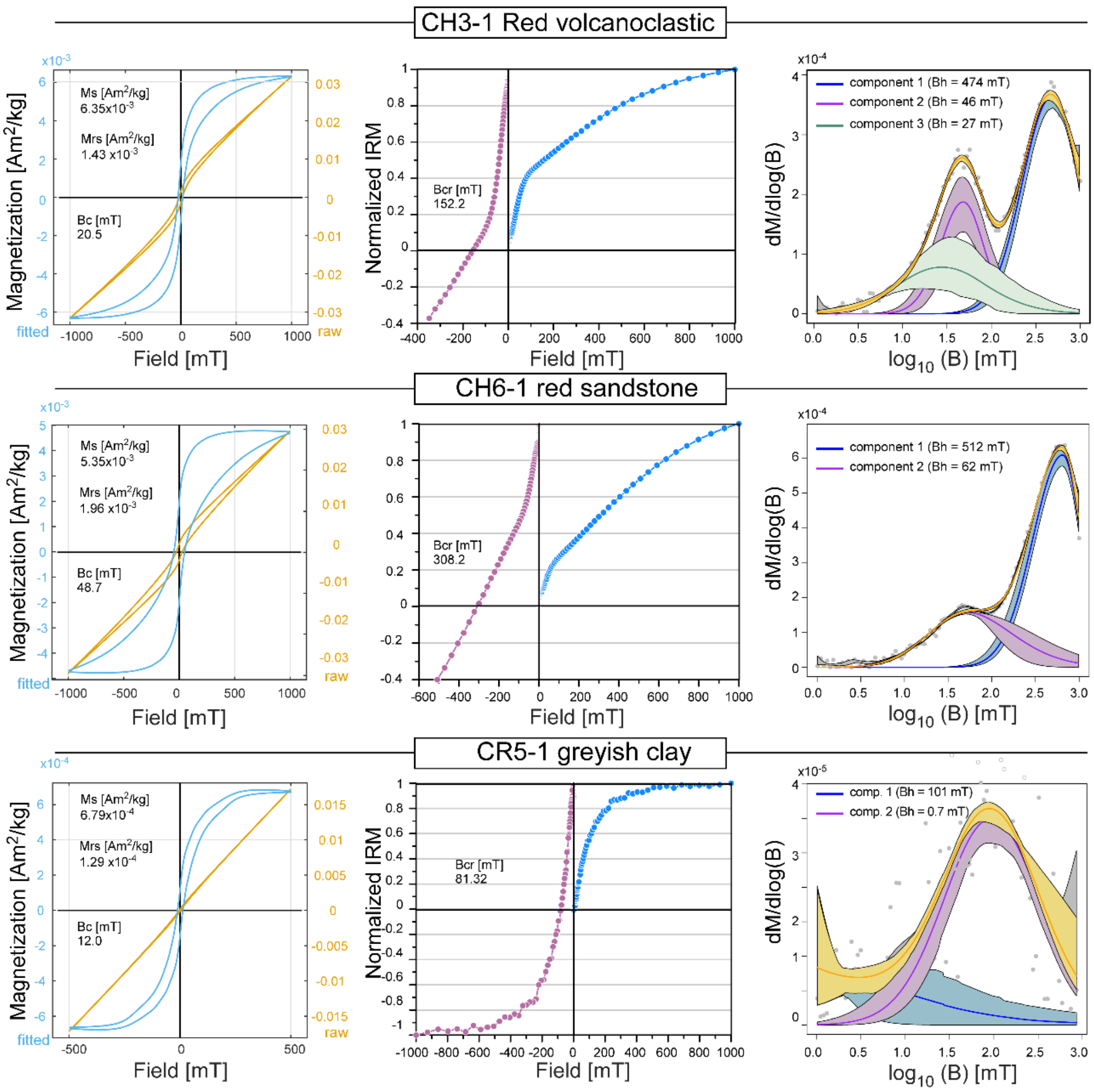

285 **Figure S2.**

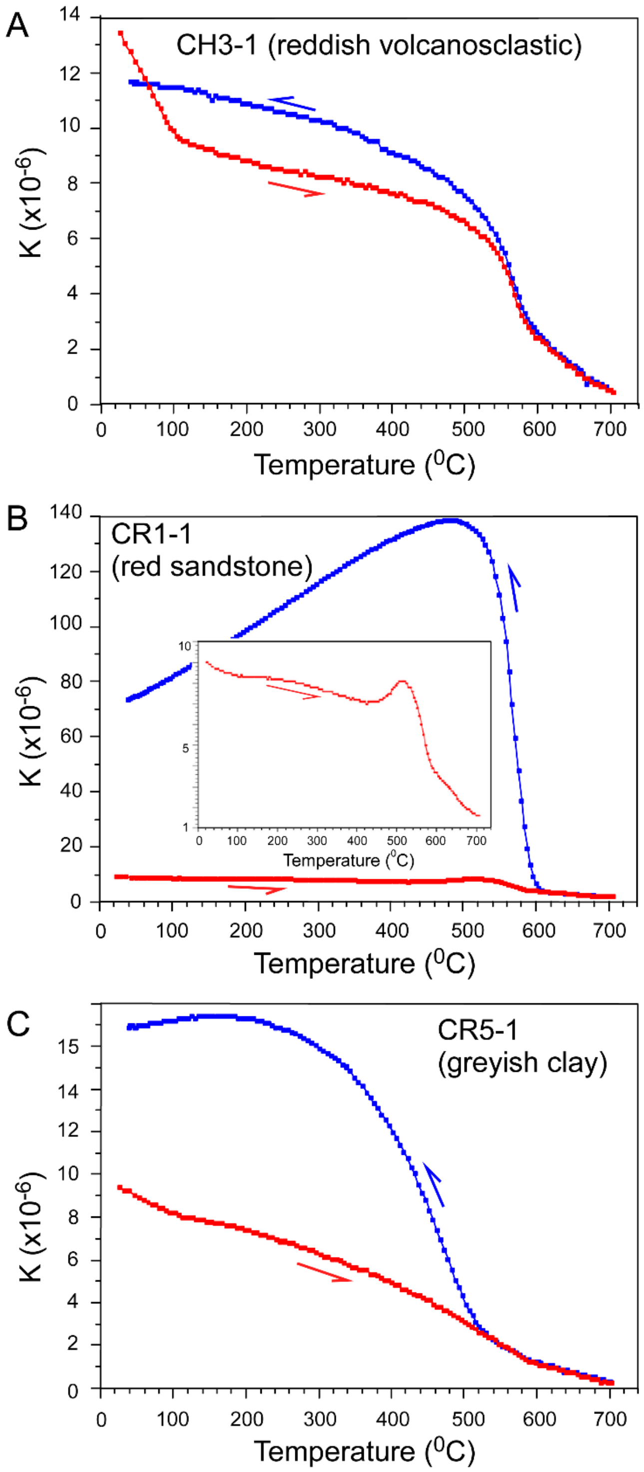

A
CH3-1 (reddish volcanosclastic)
K (x10-6)
Temperature (0C)
B
CR1-1
(red sandstone)
K (x10-6)
Temperature (0C)
Temperature (0C)
C
CR5-1
(greyish clay)
K (x10-6)
Temperature (0C)

Figure S3.

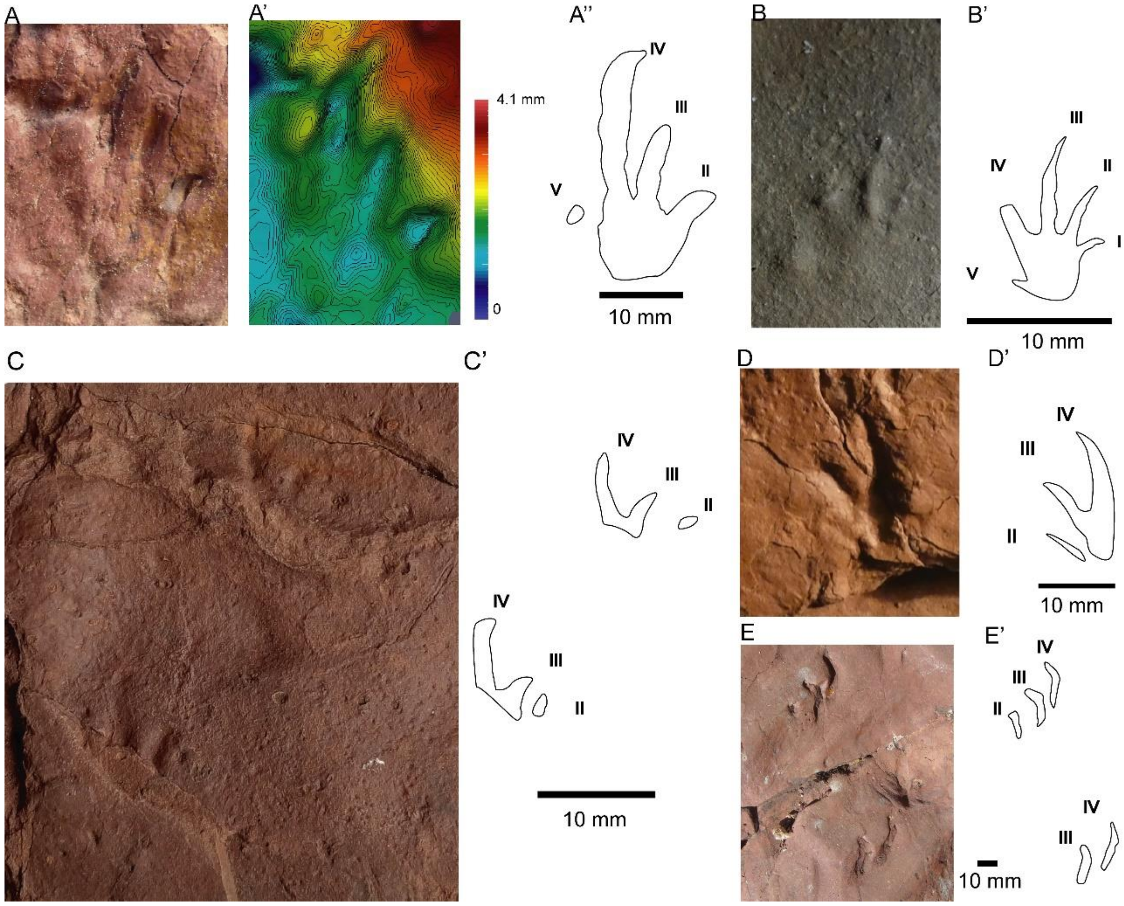
A
A'
4.1 mm
0
A''
IV
III
II
V
10 mm
B
B'
III
IV
II
I
V
10 mm
C
C'
IV
III
II
IV
III
II
10 mm
D
D'
IV
III
II
10 mm
E
E'
IV
III
II
IV
III
10 mm

Figure S4.

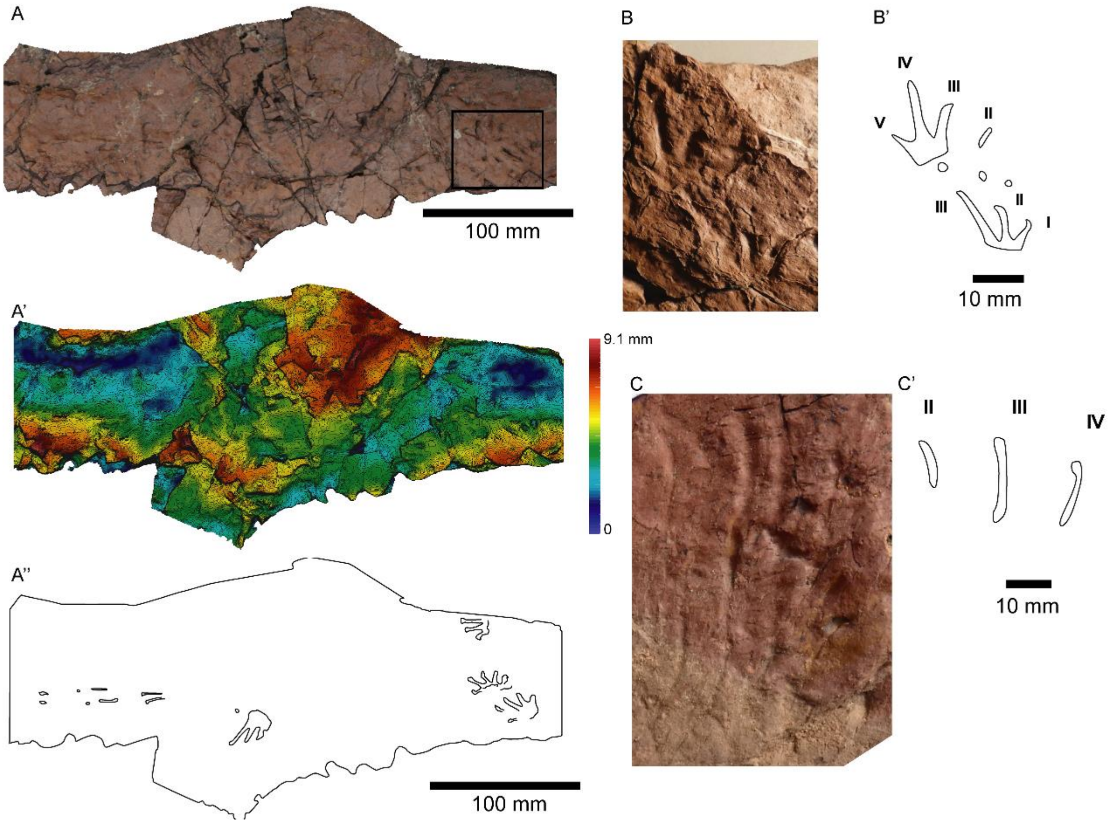

A
100 mm
A'
9.1 mm
0
A''
100 mm
B
B'
IV
III
V
II
III
II
I
10 mm
C
C'
II
III
IV
10 mm

Figure S5.

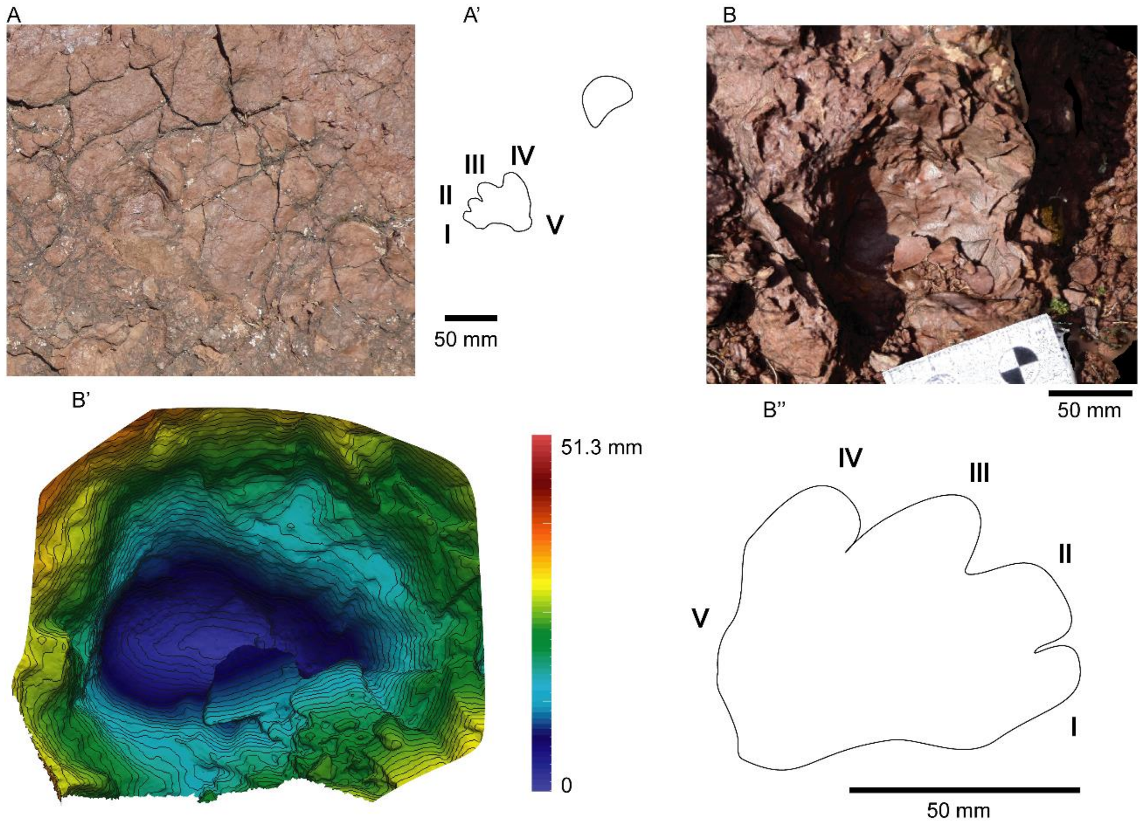

Figure S6.

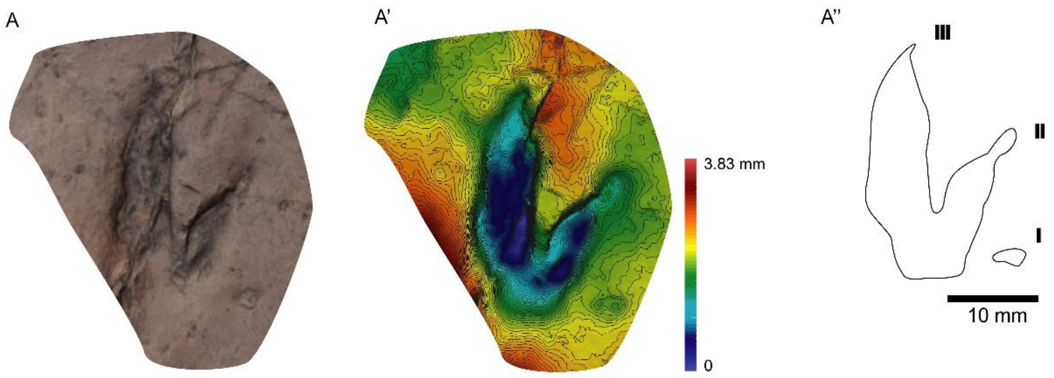

Figure S7.

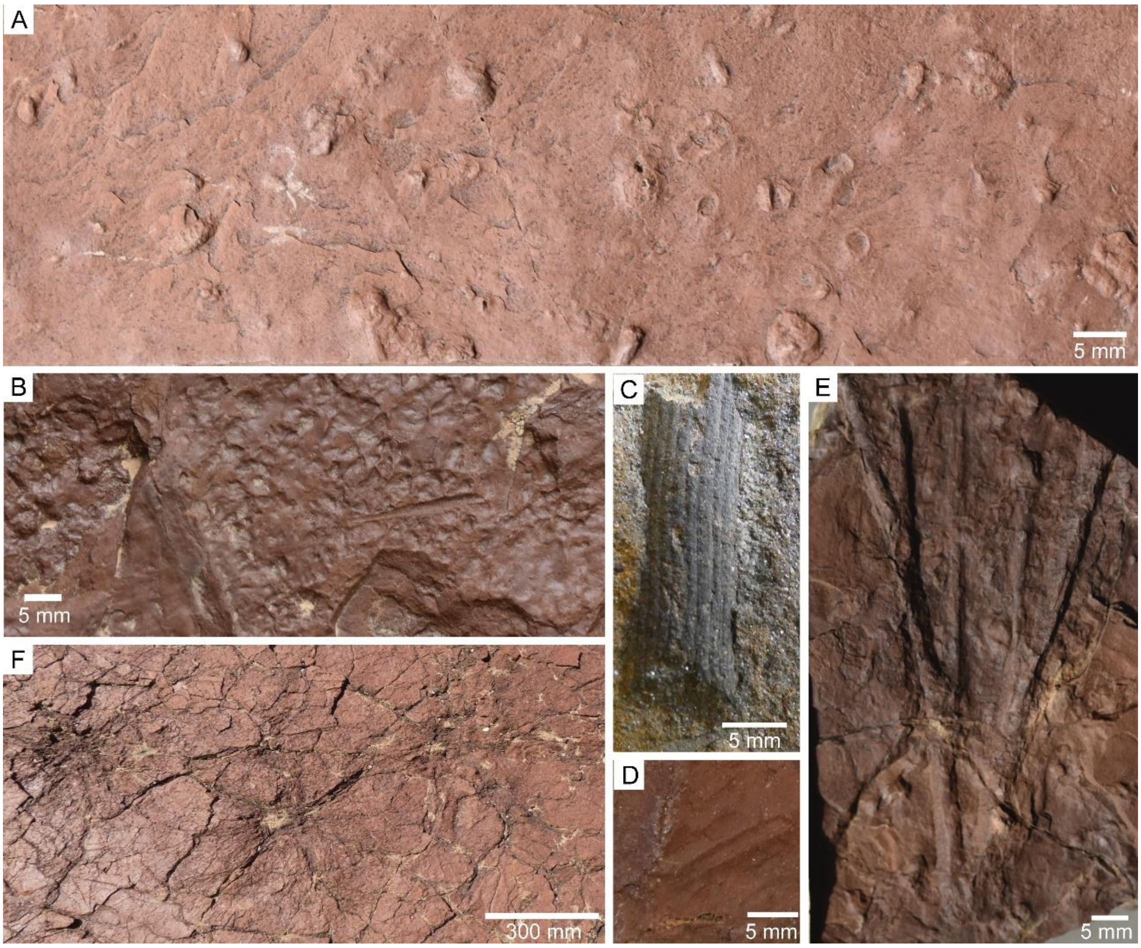

Figure S8.

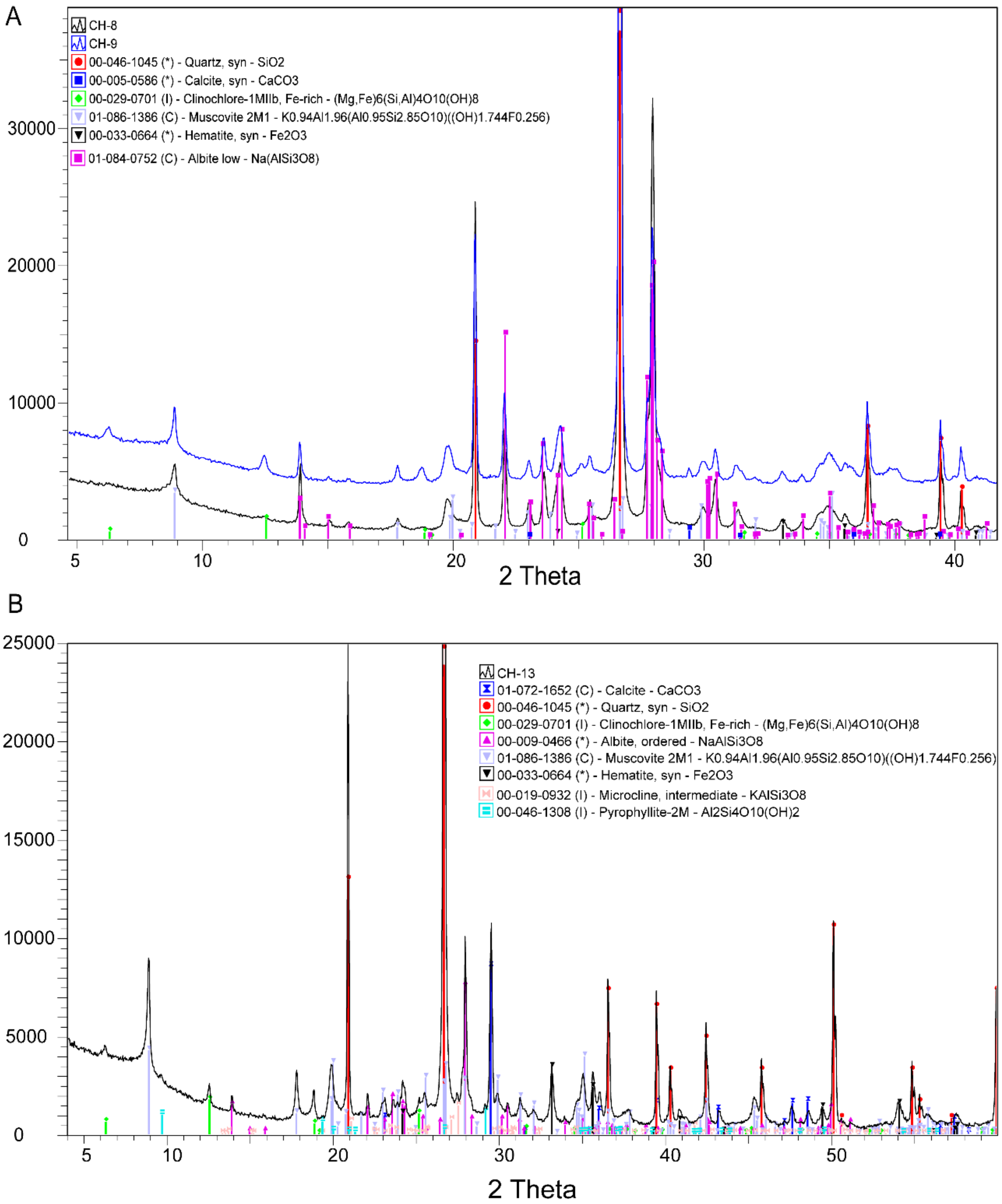
A
CH-8
CH-9
00-046-1045 (*) - Quartz, syn - SiO2
00-005-0586 (*) - Calcite, syn - CaCO3
00-029-0701 (I) - Clinochlore-1MIIb, Fe-rich - (Mg,Fe)6(Si,Al)4O10(OH)8
01-086-1386 (C) - Muscovite 2M1 - K0.94Al1.96(Al0.95Si2.85O10)((OH)1.744F0.256)
00-033-0664 (*) - Hematite, syn - Fe2O3
01-084-0752 (C) - Albite low - Na(AlSi3O8)
0
10000
20000
30000
5
10
20
30
40
2 Theta
B
CH-13
01-072-1652 (C) - Calcite - CaCO3
00-046-1045 (*) - Quartz, syn - SiO2
00-029-0701 (I) - Clinochlore-1MIIb, Fe-rich - (Mg,Fe)6(Si,Al)4O10(OH)8
00-009-0466 (*) - Albite, ordered - NaAlSi3O8
01-086-1386 (C) - Muscovite 2M1 - K0.94Al1.96(Al0.95Si2.85O10)((OH)1.744F0.256)
00-033-0664 (*) - Hematite, syn - Fe2O3
00-019-0932 (I) - Microcline, intermediate - KAlSi3O8
00-046-1308 (I) - Pyrophyllite-2M - Al2Si4O10(OH)2
0
5000
10000
15000
20000
25000
5
10
20
30
40
50
2 Theta

Figure S9.

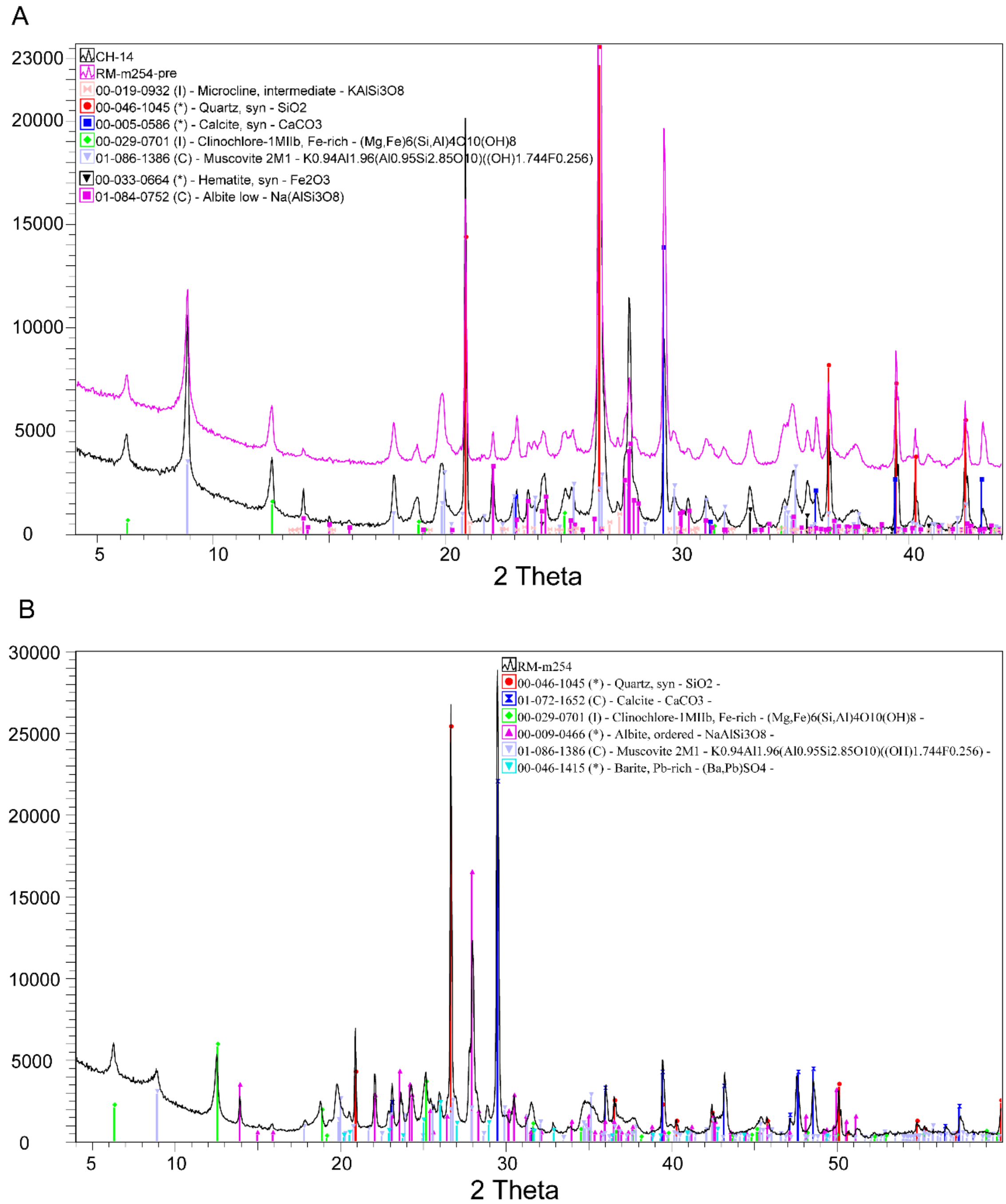
A
CH-14
RM-m254-pre
00-019-0932 (I) - Microcline, intermediate - KAlSi3O8
00-046-1045 (*) - Quartz, syn - SiO2
00-005-0586 (*) - Calcite, syn - CaCO3
00-029-0701 (I) - Clinochlore-1MIIb, Fe-rich - (Mg,Fe)6(Si,Al)4O10(OH)8
01-086-1386 (C) - Muscovite 2M1 - K0.94Al1.96(Al0.95Si2.85O10)((OH)1.744F0.256)
00-033-0664 (*) - Hematite, syn - Fe2O3
01-084-0752 (C) - Albite low - Na(AlSi3O8)
2 Theta
B
RM-m254
00-046-1045 (*) - Quartz, syn - SiO2 -
01-072-1652 (C) - Calcite - CaCO3 -
00-029-0701 (I) - Clinochlore-1MIIb, Fe-rich - (Mg,Fe)6(Si,Al)4O10(OH)8 -
00-009-0466 (*) - Albite, ordered - NaAlSi3O8 -
01-086-1386 (C) - Muscovite 2M1 - K0.94Al1.96(Al0.95Si2.85O10)((OH)1.744F0.256) -
00-046-1415 (*) - Barite, Pb-rich - (Ba,Pb)SO4 -
2 Theta

Figure S10.

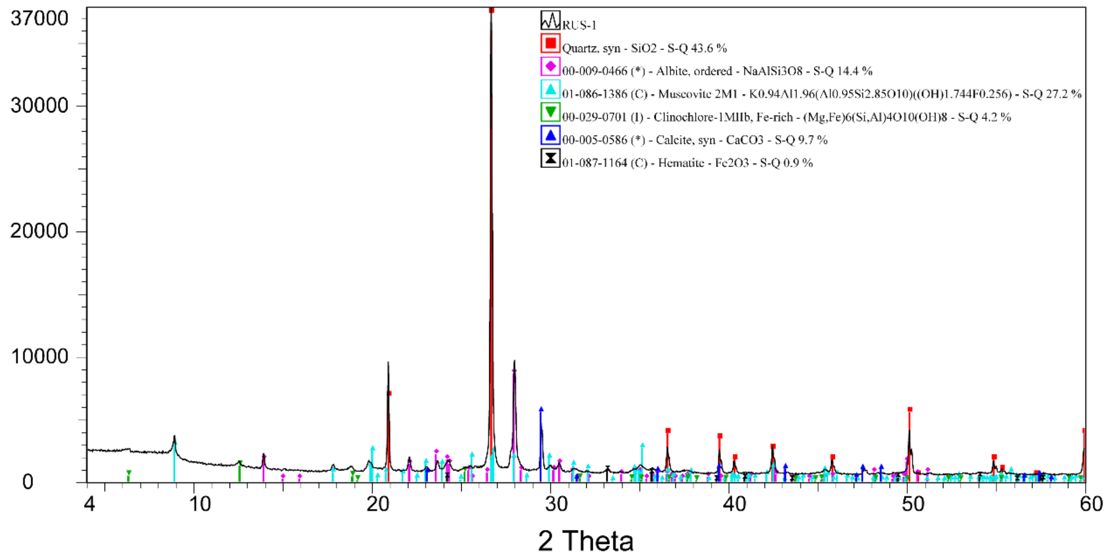
37000
30000
20000
10000
0
4
10
20
30
40
50
60
2 Theta
RUS-1
Quartz, syn - SiO2 - S-Q 43.6 %
00-009-0466 (*) - Albite, ordered - NaAlSi3O8 - S-Q 14.4 %
01-086-1386 (C) - Muscovite 2M1 - K0.94Al1.96(Al0.95Si2.85O10)((OH)1.744F0.256) - S-Q 27.2 %
00-029-0701 (I) - Clinochlore-1MIIb, Fe-rich - (Mg,Fe)6(Si,Al)4O10(OH)8 - S-Q 4.2 %
00-005-0586 (*) - Calcite, syn - CaCO3 - S-Q 9.7 %
01-087-1164 (C) - Hematite - Fe2O3 - S-Q 0.9 %

Figure S11.

Figures Captions S1–S11

Figure S1. Paleomagnetic sampling sites along the Castellar de n'Hug (CnH), Riera de Monell (RM) and Coll Roig (CR) sections simplified lithologic logs. Note the SG-SG2 and CP-CP16 sites from the LRU and URU units, they are located in nearby outcrops close to the CR section. The negative virtual geomagnetic pole (VGP) latitude that implies reverse polarity for all studied levels is depicted.

Figure S2. Rockmagnetic experiments, (A-C) Hysteresis loops (left diagrams), IRM acquisition curves and back-field IRM (central diagrams) and unmixed coercivity distributions (Maxbauer et al., 2016) (right diagrams) of representative lithologies. The model fit unmixed coercivity distributions were derived from back-field IRM acquisition data. Shaded area represents error envelopes of 95% confidence intervals.

Figure S3. Magnetic susceptibility (K) vs. temperature curves from representative samples. The heating (red) and cooling curves (blue) are also indicated by respective arrows.

Figure S4. *Dromopus* isp. tracks. **A.** IPS126632 with left ichnite in concave epirelief from the CnH section (**A**), detailed picture of the sample in concave epirelief, (**A'**) false colour depth map and contours, and (**A''**) interpretation. **B.** IPS88734 with right ichnite in convex hyporelief from the CR section (**B**) detailed picture and (**B'**) interpretation. **C.** IPS88733 with a right manus-pes set in concave epirelief from the CR section (**C**) detailed picture and (**C'**) interpretation. **D.** IPS88735 with right ichnite in concave epirelief surrounded by raindrop impressions from the RM section (**D**) detailed picture and (**D'**) interpretation. **E.** Right manus-pes set (CnH-121-1 and CnH-121-2) in concave epirelief from the CnH section (**E**) detailed picture and (**E'**) interpretation.

Figure S5. *Hyloidichnus* isp. tracks. **A.** Surface RM-177 with different ichnites in concave epirelief at 177 m of the base of the RM section (**A**), detailed picture of the surface, the square indicates the RM-177-1 and RM-177-2 manus-pes (Fig. 5D from the main text), (**A'**) false colour depth map and contours and (**A''**) interpretation. **B.** IPS88735 with a manus-pes set in concave epirelief recovered at 129 m of the base of RM section (**B**) detailed picture and (**B'**) interpretation of the impression. **C.** IPS126632 with a partial right ichnite with drag scratches in concave epirelief at 315 m in the CnH section CnH section (**C**) detailed picture and (**C'**) interpretation.

Figure S6. *Pachypes* cf. *dolomiticus* tracks. **A.** Mud-cracked surface with two ichnites (RM-209-1, 2) in concave epirelief from the RM section (**A**), picture, (**A'**) interpretation. **B**. Left partial manus track not recovered from in concave epirelief (CR-69-15) from the CR section (**B**), picture of the imprint, (**B'**) false colour depth map and contours, and (**B''**) interpretation of the track.

Figure S7. Indeterminate morphotype. Left pes imprint of an indeterminate tetrapod ichnogenus from Coll Roig section (CR-15-3). The footprint is in concave epirelief and includes false-colour depth maps with contours (A') and interpretive outlines (A'').

Figure S8.A. Slab (IPS128896) with invertebrate traces interpreted as *Rusophycus* from the upper URU deposits of the Castellar de n'Hug sub-basin. **B**. Globular structures possibly corresponding to pellets associated with notostracan traces (IPS128896) from the upper URU deposits of RM section. **C.** Partial remain of a horsetail (IPS88725) preserved in a sandstone of the TU recovered near to the CnH section. **D.** Plant impression (IPS128890) recovered from the lower URU deposits at the CnH section. **E.** Plant remain identified as a fern with *Rusophycus* traces (IPS128905), recovered from the upper URU of RM section. **F.** Mud-cracked surface of the upper URU at 190 metres from the base of the CR section with trunk marks,

Figure S9. A. Graphic of the XRD scan results of the samples CH-8 (black line) and CH-9 (blue line) attributed, respectively, to volcanic material and to fluvial sediments of the LRU at 369 and 230 m of the CnH section. **B.** Graphic of the XRD scan of the sample CH-13, which corresponds to the first deposits of the lower URU deposited after the last volcanic materials at 633 m of the CnH section.

Figure S10. A. Graphic of the XRD scan of the CH-14 (lower URU of Coll Roig, black line) and RM-m254-pre (upper URU of Riera de Monell section, pink line), which corresponds to fluvial sediments of the Upper Red Unit at 11 m of the CR section and 254 m of the RM section. **B.** Graphic of the XRD scan results of the sample RM-m254 attributed to a reduced organic-matter-rich fluvial deposit of the upper URU at 254 m of the CR section.

Figure S11. Graphic of the XRD scan results of the sample RUS-1 attributed to the first deposits of the lower URU deposited after the last volcanic materials at the RM section.

Table S1. Geomagnetic data of the samples recovered in the Permian deposits of the Castellar de n'Hug sub-basin.

Sample	Level (m)	Declination	Inclination	Coordinates	core azimuth	core dip	bedding strike	bedding dip	MAD	anchored	number steps	steps
Castellar de n'Hug (CnH) section												
CH2	179	189,39	16,71	tectonic	197	28	107	28	3,6	TRUE	5	580 610 640 660 680
CH3.2-1A	345,2	168,27	-25,17	tectonic	197	28	107	28	1,5	TRUE	13	250 300 350 400 450 500 600 800 1000 300 400 500 580
CH3A	345	191,49	3,39	tectonic	55	45	107	28	0,7	TRUE	5	580 610 640 660 680
CH5-1A	351	145,04	-9,63	tectonic	197	28	107	28	5,9	TRUE	3	610 660 680
CH6-1A	353	182,97	8,73	tectonic	197	28	107	28	2,3	TRUE	5	580 610 640 660 680
CH7-1A	375	169,16	12,42	tectonic	175	60	85	60	6,6	TRUE	6	500 580 610 640 660 680
Pardinella de Gavarrós												
CP10-1A		161,02	-48,64	tectonic	190	48	100	48	9,1	FALSE	7	500 540 580 610 640 660 680
CP11-1A		168,76	-13,83	tectonic	190	48	100	48	9,1	FALSE	5	540 580 610 640 660
CP1-1A		168,69	-25,99	tectonic	196	50	106	50	4,4	TRUE	7	340 380 420 460 500 580 640
CP12-1A		153,98	2,02	tectonic	190	48	100	48	3,8	TRUE	6	540 580 610 640 660 680
CP13-1A		158,18	-4,42	tectonic	190	48	100	48	5,4	TRUE	6	540 580 610 640 660 680
CP14-1A		165,1	1,45	tectonic	190	48	100	48	3,9	TRUE	3	640 660 680

CP15-1A		167,24	11,52	tectonic	190	48	100	48	1,3	TRUE	3	640 660 680
CP16-1A		186,28	-18,07	tectonic	190	48	100	48	2,2	TRUE	9	350 450 500 540 580 610 640 660 680
CP17-1A		181,09	39,92	tectonic	190	48	100	48	13,5	TRUE	2	660 680
CP18-1A		163,81	5,53	tectonic	190	48	100	48	3,6	TRUE	2	660 680
CP19-1A		159,31	-0,9	tectonic	190	48	100	48	2,6	TRUE	8	450 500 540 580 610 640 660 680
CP21-1A		150,22	-8,05	tectonic	190	48	100	48	8,5	TRUE	5	580 610 640 660 680
CP2-1B		178,04	31,12	tectonic	196	50	106	50	5,2	TRUE	5	460 500 580 640 680
CP5-1A		173,5	-23,87	tectonic	190	48	100	48	3,7	FALSE	4	610 640 660 680
CP6-1A		172,48	-7,41	tectonic	190	0	100	48	1,8	TRUE	6	540 580 610 640 660 680
CP7-1A		200,99	-18,23	tectonic	190	48	100	48	2,7	TRUE	6	540 580 610 640 660 680
CP8-1A		176,61	-17,29	tectonic	190	48	100	48	2,9	TRUE	6	540 580 610 640 660 680
CP9-1A		174,59	-16,11	tectonic	190	48	100	48	2,7	TRUE	6	540 580 610 640 660 680
Coll Roig (CR) section												
CR1A	59	171,21	-17,98	tectonic	196	50	106	50	1,6	TRUE	4	610 640 660 680
CR2.5A	100	232,62	-12,4	tectonic	196	50	106	50	2,1	TRUE	4	610 640 660 680
CR3A	115	165,83	-12,94	tectonic	196	50	106	50	1,5	TRUE	4	610 640 660 680

CR4A	244	184,77	-14,91	tectonic	196	50	106	50	2,1	TRUE	3	640 660 680
CR5A	246	194,59	-27,66	tectonic	196	50	106	50	2,6	TRUE	4	300 400 500 580
CR7-1A	246	148,98	-15,38	tectonic	196	50	106	50	3,7	TRUE	6	250 350 350 450 500 540
CR6A	246,2	189,45	22,01	tectonic	196	50	106	50	3,1	TRUE	6	500 580 610 640 660 680
CR9-1A	248	193,85	3,14	tectonic	196	50	106	50	3,4	TRUE	6	540 580 610 640 660 680
CR10-1A	253	176,65	-10,36	tectonic	196	50	106	50	4,4	TRUE	9	350 450 500 540 580 610 640 660 680
CR11-1A	254	191,34	3	tectonic	196	50	106	50	1,5	TRUE	5	580 610 640 660 680
CR12-1A	255	133,98	-27,16	tectonic	196	50	106	50	3	TRUE	3	640 660 680
CR13-1A	258	194,26	-1,32	tectonic	196	50	106	50	1,4	TRUE	2	660 680
CR14-1A	261	145,63	-40,21	tectonic	196	5	106	50	1	TRUE	3	640 660 680
CR15-1A	264	130,48	-35,65	tectonic	196	5	106	50	3,2	TRUE	6	540 580 610 640 660 680
CR16-1A	267	130,1	-7,61	tectonic	196	50	106	50	3,7	TRUE	4	610 640 660 680
Riera de Monell (RM) section												
RM1A	254	159,53	-13,18	tectonic	182	52	92	52	15,9	FALSE	6	500 600 300 400 500 580
RM2A	254,2	151,5	-3,44	tectonic	182	52	92	52	1,7	TRUE	5	580 610 640 660 680
Solell de la Gallarda												

SG1-1A	188,31	-5,12	tectoni c	180	70	90	70	2,1	TRUE	3	640 660 680
SG2-1A	182,44	29,71	tectoni c	180	70	90	70	5,4	TRUE	3	640 660 680

Table S2. Measurements of the tetrapod footprints described in the Permian deposits of the Castellar de n'Hug sub-basin. Preservation levels are assigned following the procedures of Marchetti et al. (2019a). Abbreviation: FL, foot length; FW, foot width; psL, palm/sole length; psW, palm/sole width; I-V, digit number; L, length of the digit; di, divergence. Length measurements in mm, angular measures in degrees.

Ichnotaxon	Specimen numer	Trackway number	Manus/pes	Section	Unit	Preservation	FL	FW	psL	psW	I L	II L	III L	IV L	V L	di I/II	di II/III	di III/IV	di IV/V	di I/V
Batrachichnus salamandroides	IPS16631	-	-	CnH	LRU	1	-	-	-	-	-	-	-	-	-	22.62	21.3	-	-	-
Batrachichnus salamandroides	IPS88731	1	-	CR	lURU	1	10.56	9.07	-	-	-	6.4	7.18	5.62	-	15.75	18.67	-	-	-
Batrachichnus salamandroides	IPS88731	2	Pes	CR	lURU	1	12.9	-	-	-	4.3	7.11	7.78	-	-	16.56	20.71	-	-	-
Batrachichnus salamandroides	IPS88731	3	Manus	CR	lURU	1	11.2	10.93	5.03	7.01	3.03	6.01	5.68	3.35	-	20.73	16.87	14.6	-	-
Batrachichnus salamandroides	IPS88731	-	Pes	CR	lURU	1	2.79	2.84	-	-	0.93	1.17	1.38	1.27	0.78	30.17	16.76	30.78	32.15	-
Batrachichnus salamandroides	IPS88731	-	Manus	CR	lURU	1	2.31	2.16	-	-	0.92	1.21	1.33	1.06	-	44.77	35.97	26.07	-	-
Batrachichnus salamandroides	IPS88734	-	-	CR	lURU	1	-	-	-	-	-	-	-	-	-	26.92	31.5	-	-	-

Batrachichnus salamandroides	IPS88734	-	Manus	CR	lURU	2	4.29	5.07	-	-	1.94	2.33	2.4	2,00	-	30.64	21.16	30.12	-	-
***Dromopus* isp.**	CnH-121-1	1	Pes	CnH	LRU	2	-	-	-	-	-	-	18.4	31.5	-	-	-	18,00	-	-
***Dromopus* isp.**	CnH-121-2	2	Manus	CnH	LRU	2	-	-	-	-	-	11.5	22.3	27.6	-	-	19,00	13,00	-	-
***Dromopus* isp.**	IPS126632		-	CnH	LRU	2	21.28	15.22	4.9	6.9		7.36	9.98	16.25	7.1	-	27,00	16,00	50,00	-
***Dromopus* isp.**	IPS88735	-	-	RM	uURU	1.5	-	-	-	-	-	5.44	8.02	14.09	-	-	14.05	24.9	-	-
***Dromopus* isp.**	IPS88733	1	Pes	CR	lURU	1.5	9.55	7.4	-	-	-	2.35	3.28	7.62	-	-	12.6	26.4	-	-
***Dromopus* isp.**	IPS88733	2	Manus	CR	lURU	2	8.31	5.9	-	-	-	1.88	3.6	7.8	-	-	42.0	28.3	-	-
***Dromopus* isp.**	IPS88733	-	-	CR	lURU	2	13.7	8.78	-	-	3.32	5.76	7.31	9.62	4.66	-	16.2	23.4	38.8	105.6
***Dromopus* isp.**	IPS88734	-	-	CR	lURU	1.5	-	10.1	7.5	5.7	2.8	3.5	7.0	-	-	40.68	16.1	22.02	38.14	104.3
***Dromopus* isp.**	CR-15-1	-	-	CR	lURU	2	13.82	13.54	2.93	3.05	-	4.27	6.63	9.6	3.99	-	39.39	37.15	82.68	-
***Dromopus* isp.**	CR-15-2	-	-	CR	lURU	1.5	-	-	-	-	-	-	6.41	12.85	-	-	-	37.86	-	-
***Dromopus* isp.**	CR-15-3	-	-	CR	lURU	1.5	-	-	-	-	-	-	7.75	10.76	3.7	-	-	35.59	48.12	-
***Dromopus* isp.**	CR-69-1	-	-	CR	uURU	1.5	-	-	-	-	-	-	7.84	12.02	-	-	-	32.64	-	-
***Hyloidichnus* isp.**	IPS135414	2	Pes	CnH	LRU	2	35.94	43.15	11.11	19.85	8.01	21.33	22.64	23.74	15.24	36.76	29.67	19.97	57.16	132.16
***Hyloidichnus* isp.**	IPS135414	1	Manus	CnH	LRU	2	-	-	-	-	-	19.01	21.38	-	-	-	34.37	22.82	-	-
***Hyloidichnus* isp.**	IPS126632	-	-	CnH	LRU	1.5	-	-	-	-	-	14.53	19.53	18.65	-	-	-	-	-	-
***Hyloidichnus* isp.**	RM-177-14	1	Pes	RM	uURU	2	26.83	27.74	8.46	10.13	6.81	13.72	17.62	18.62	7.1	12.22	44.83	29.49	28.8	109.87

***Hyloidichnus* isp.**	RM-177-15	2	Manus	RM	uURU	2	18,00	26.82	5.19	11.39	6.65	7.3	11.85	12.46	5.4	19.03	52.04	22,55	62.99	124.78
***Hyloidichnus* isp.**	IPS88735	-	Pes	RM	uURU	1.5	19.68	22.68	6.47	9.17	-	8.22	8.93	12.58	6.14	-	-	29.15	45.05	-
***Hyloidichnus* isp.**	IPS88735	-	Manus	RM	uURU	1.5	-	-	-	-	-	-	8.18	6.98	6.03	-	-	33.30	46.86	-
Brontopus antecursor	RM-17-4	4	Manus	RM	uURU	2.5	117.31	96.33	58.51	54.98	15.4	31.11	35.56	-	-	20.03	23.34	33.29	-	-
Brontopus antecursor	RM-17-5	5	Pes	RM	uURU	2.5	243.59	132.65	195.84	106.17	66.89	71.39	76.17	72.68	62.13	48.76	29.11	38.9	20.04	131.59
Brontopus antecursor	RM-17-6	6	Manus	RM	uURU	2.5	145.36	82.21	99.35	58.82	23.59	32.95	36.19	45.96	-	27.8	20.15	24.1	-	-
Brontopus antecursor	RM-17-7	7	Pes	RM	uURU	2.5	268.45	115.12	196.67	115.12	33.98	52.26	60.23	70.66	-	30.2	19.78	15.96	21.23	-
Brontopus antecursor	RM-17-8	8	Manus	RM	uURU	2.5	132.45	117.26	-	-	-	-	-	-	-	40.41	33.92	22.25	20.15	92.12
Brontopus antecursor	RM-17-9	9	Pes	RM	uURU	2.5	242.51	105.17	198.18	89.69	-	-	-	-	-	-	-	-	-	-
Brontopus antecursor	RM-17-10	10	Manus	RM	uURU	2.5	148.87	105.51	51.48	68.83	-	-	-	-	-	-	-	-	-	-
Brontopus antecursor	CR-69-2	-	Pes	CR	uURU	2.5	178.93	113.14	119.11	113.14	39.72	48.42	49.31	47.00	-	48.48	19.65	22.56	28.3	94.29
Brontopus antecursor	CR-69-3	-	Manus	CR	uURU	2.5	82.32	99.85	67.66	99.85	-	22.7	39.48	38.86	20.69	-	18.43	15.43	14.97	75.32
Brontopus antecursor	CR-69-4	-	Manus	CR	uURU	2.5	93.45	96.57	60.00	96.57	-	33.11	37.47	35.72	-	-	-	23.72	24.57	-
Brontopus antecursor	CR-69-14	-	Pes	CR	uURU	2.5	113.32	65.73	97.49	65.73	10.36	11.03	13.54	16.94	8.98	19.2	17.54	12..93	12.92	74.85
Pachypes	RM-209-2	-	-	RM	uURU	2	93.3	95.7	54.57	67.6	17.8	26.84	32.16	43.78	-	33.17	34.27	35.44	51.66	122.75
Pachypes	CR-69-15	-	-	CR	uURU	1	60.4	78.28	38.6	60.22	-	-	-	-	-	30.2	25.66	38.86	-	-

Indeterminate morphotype	CR-15-4	-	-	CR	lURU	1	28.80	-	7.75	12.16	5.48	13.10	20.95	17.84	-	60.65	26.68	36.6	-	-

Table S3. Parameters of the tetrapod trackways observed in the Permian of the Castellar de n'Hug sub-basin.

Trackway parameters	***Brontopus antecursor* trackway (RM-177)**
Stride manus (mm)	964.82
Stride pes (mm)	971.05
Pace manus (mm)	558.21
Pace pes (mm)	555.28
Pace angulation manus (degrees)	119.84
Pace angulation pes (degrees)	115.00
Width pace manus (mm)	326.33
Width pace pes (mm)	382.42
Manus-Pes distance (mm)	290.41
Div. Manus midline (degrees)	6.1
Div. Pes midline (degrees)	21.10
Div. Manus-pes digit III (degrees)	12.21
Glenoacetabular distance (mm)	796.414

Table S4. Brief description and stratigraphic position of the studied thin section samples.

Thin sectic sample	Sectior	Metre	Metre cor	DRX	Unit	Description
CH-6	CnH	136,2	136,2	Yes	LRU	Consolidated sandstone.
CH-1	CnH	155	155	No	LRU	Sample matrix-rich with plagioclase crystals with angular shape.
CH-2	CnH	155	155	No	LRU	Well-sorted sample with fissures refilled of calcite. The thin section view is not resolutive.
CH-4	CnH	180	180	No	LRU	Sample without matrix.
CH-5	CnH	180	180	No	LRU	Fluvial sedimentary sample.
CH-3	CnH	199	199	No	LRU	Consolidated sandstone with abundant quarz, some grains of plagioclase and mica. There are low presence of matrix.
CH-9	CnH	270,3	270,3	Yes	LRU	Well sorted consolidated sandstone with abundant quarz grains moderately rounded. There are low quantity of plagioclase.
CH-8	CnH	369,7	369,7	Yes	LRU	Seem to be volcanic matrix with no classified angulous grains. Albite crystals are abundant It resembles a lot to samples 8 and 9, however is not the thin section view is not resolutive.
CH-13	CnH	633,5	633,5	Yes	LRU-lU	Absent matrix and abundante albite.
CH-10	CnH	639	639	No	lURU	Absent matrix and abundante albite.
CH-18	CnH	667	668	No	lURU	Consolidated fluvial sandston with edaphic bioturbations.
CH-15	CnH	694	694	No	lURU	Consolidated fluvial sandston with edaphic bioturbations.
CH-11	RM	1	602	No	LRU	Very altered volcanic palaeosol with coated grains.
CH-16	RM	10	612	No	lURU	Very altered volcanic palaeosol with coated grains.
CH-12	RM	11	613	No	lURU	Very altered volcanic palaeosol with root bioturbation and coated grains.
CH-17	CR	8	617	No	lURU	Fluvial sedimentary sample with pedogenetic activity and coated grains.
CH-14	CR	11	620	Yes	lURU	Consolidated fluvial sandstone with edaphic bioturbations.
RM-223	RM	223	825	Yes	uURU	Very altered fluvial sample with tractive structures and abundant organic matter.
RM-254	RM	254	856	Yes	uURU	Very altered fluvial sample with pedogenetic activity, abundant organic matter and presenc clorite.
RM-246	CR	246	854	Yes	uURU	Very altered fluvial sample with pedogenetic activity and abundant organic matter.
CH-7	Pardinella (out of successic				uURU	Fluvial sandstone with very fine grain-size.

Stratigraphical section of Castellar de n’Hug (CnH)

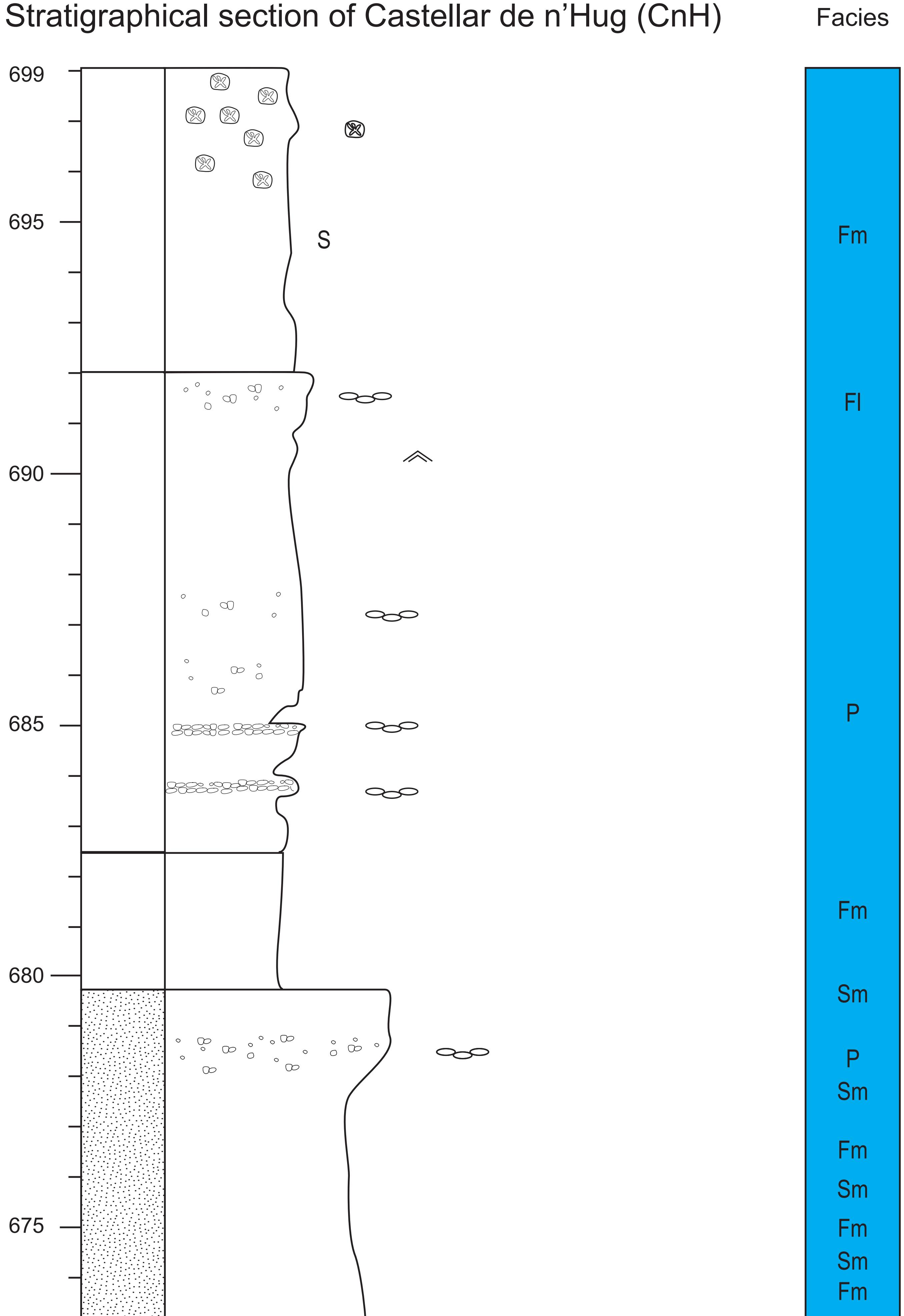

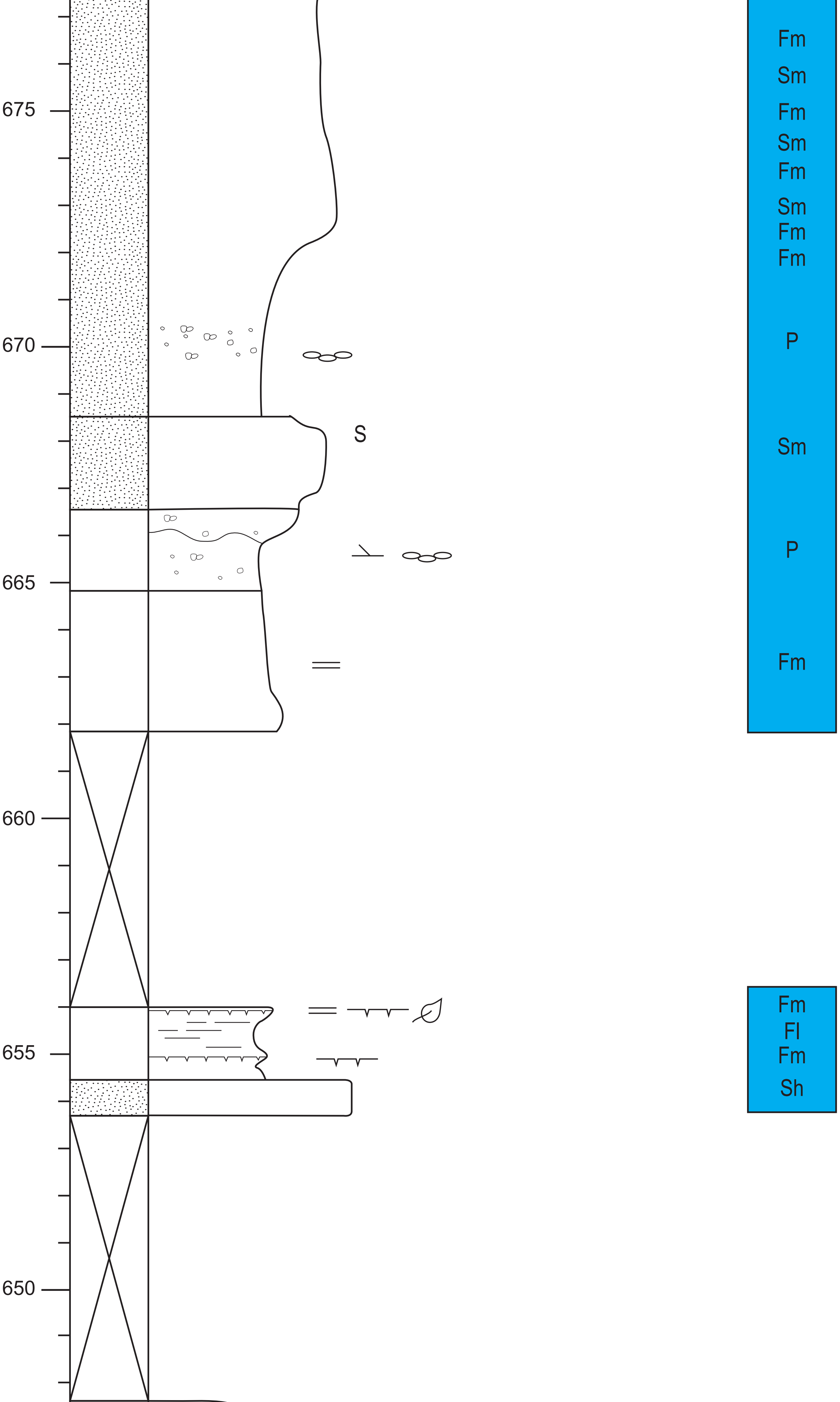

675
670
665
660
655
650
S
Fm
Sm
Fm
Sm
Fm
Sm
Fm
Fm
P
Sm
P
Fm
Fm
Fl
Fm
Sh

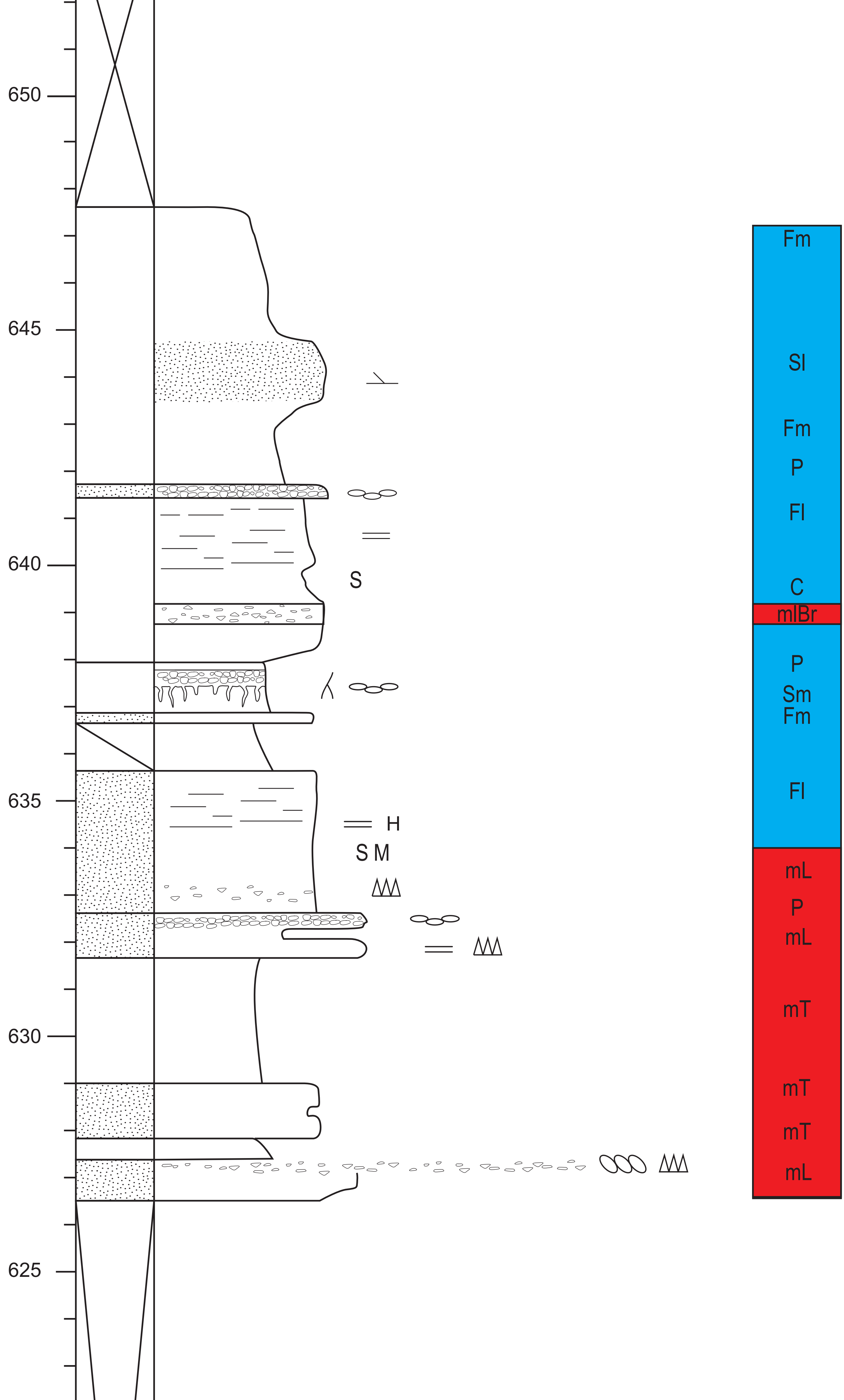

650
645
640
635
630
625
S
H
S M
Fm
Sl
Fm
P
Fl
C
mlBr
P
Sm
Fm
Fl
mL
P
mL
mT
mT
mT
mL

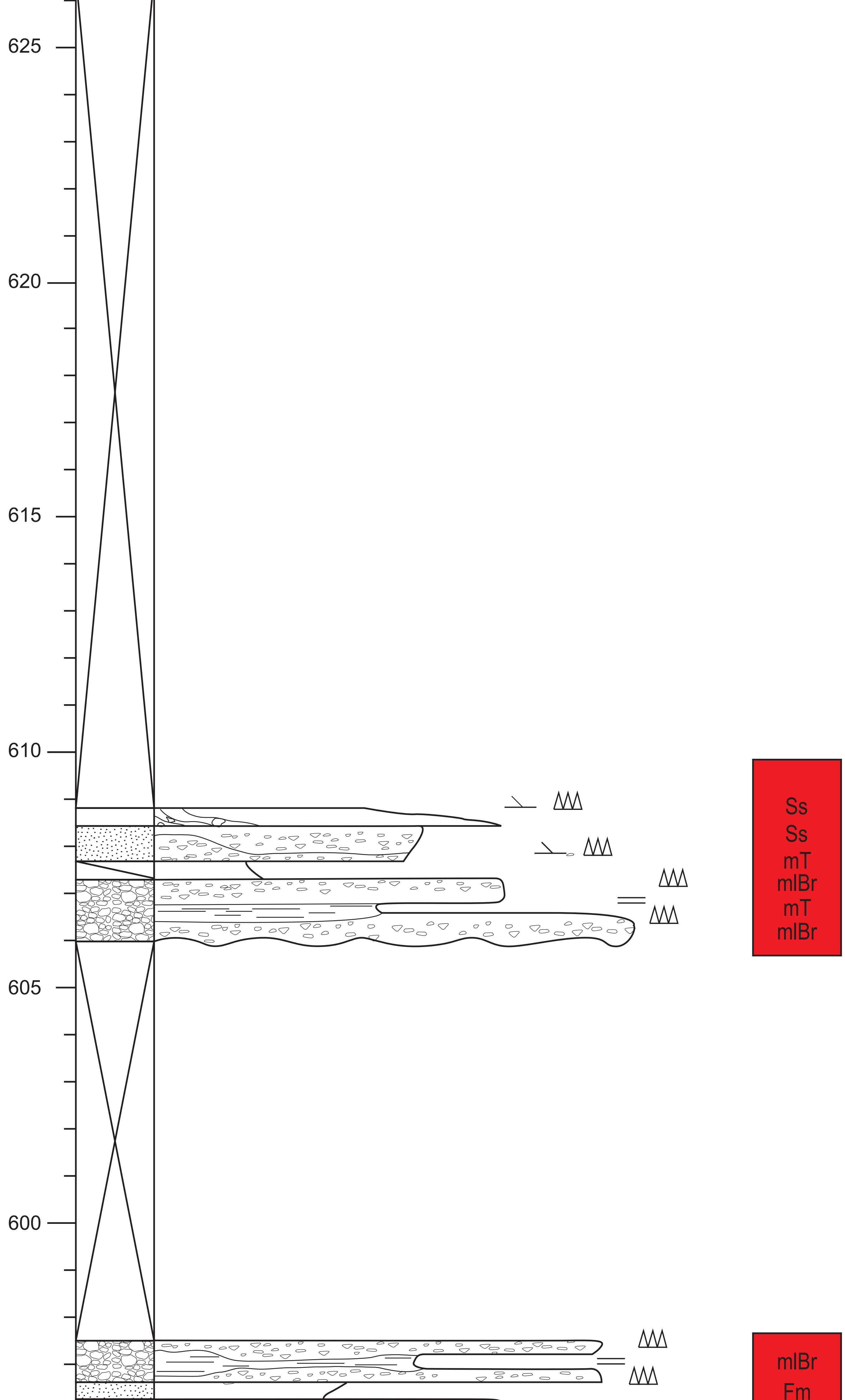
625
620
615
610
605
600
Ss
Ss
mT
mlBr
mT
mlBr
mlBr
Fm

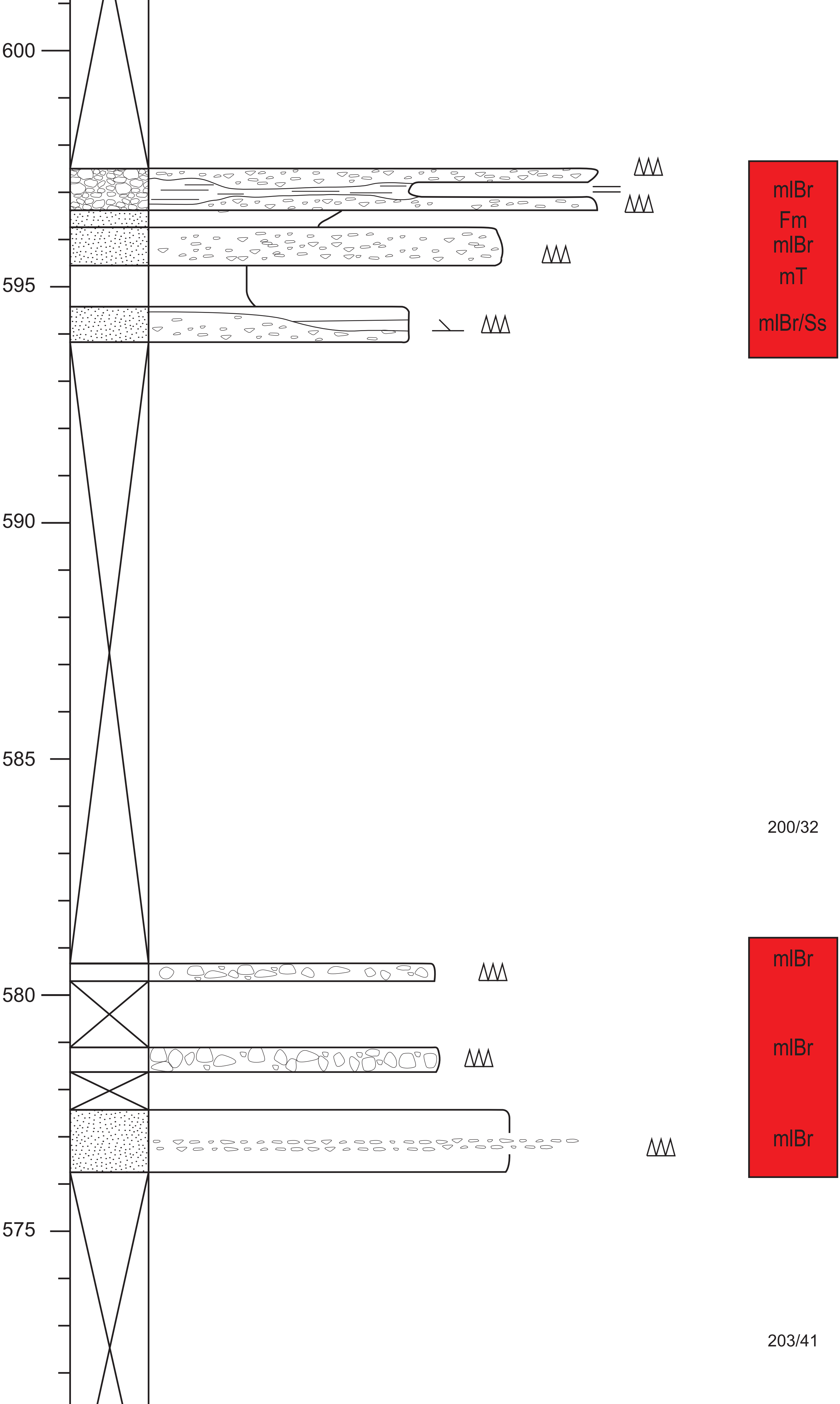

600
595
590
585
580
575
mlBr
Fm
mlBr
mT
mlBr/Ss
200/32
mlBr
mlBr
mlBr
203/41

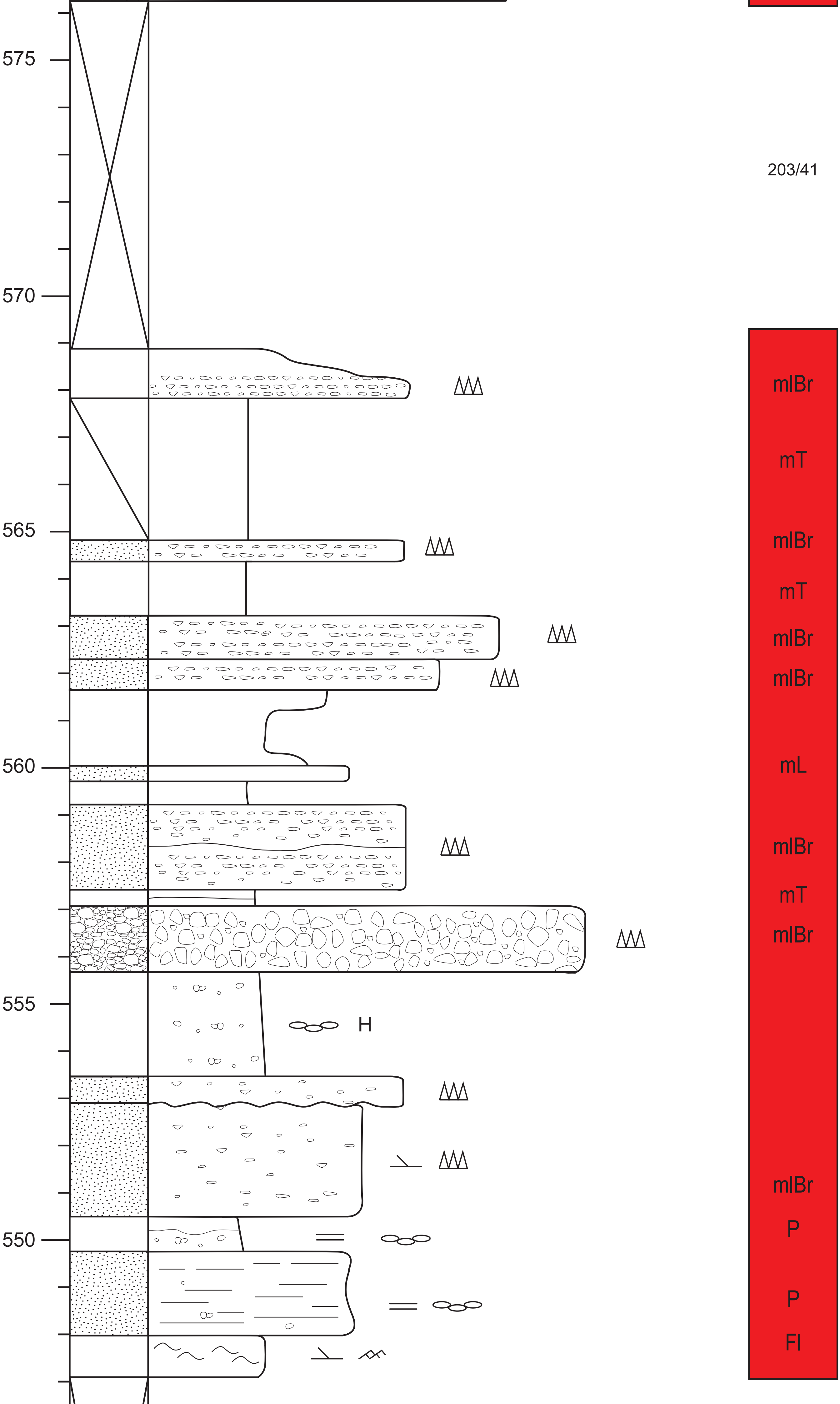
575
570
565
560
555
550
H
203/41
mlBr
mT
mlBr
mT
mlBr
mlBr
mL
mlBr
mT
mlBr
mlBr
P
P
Fl

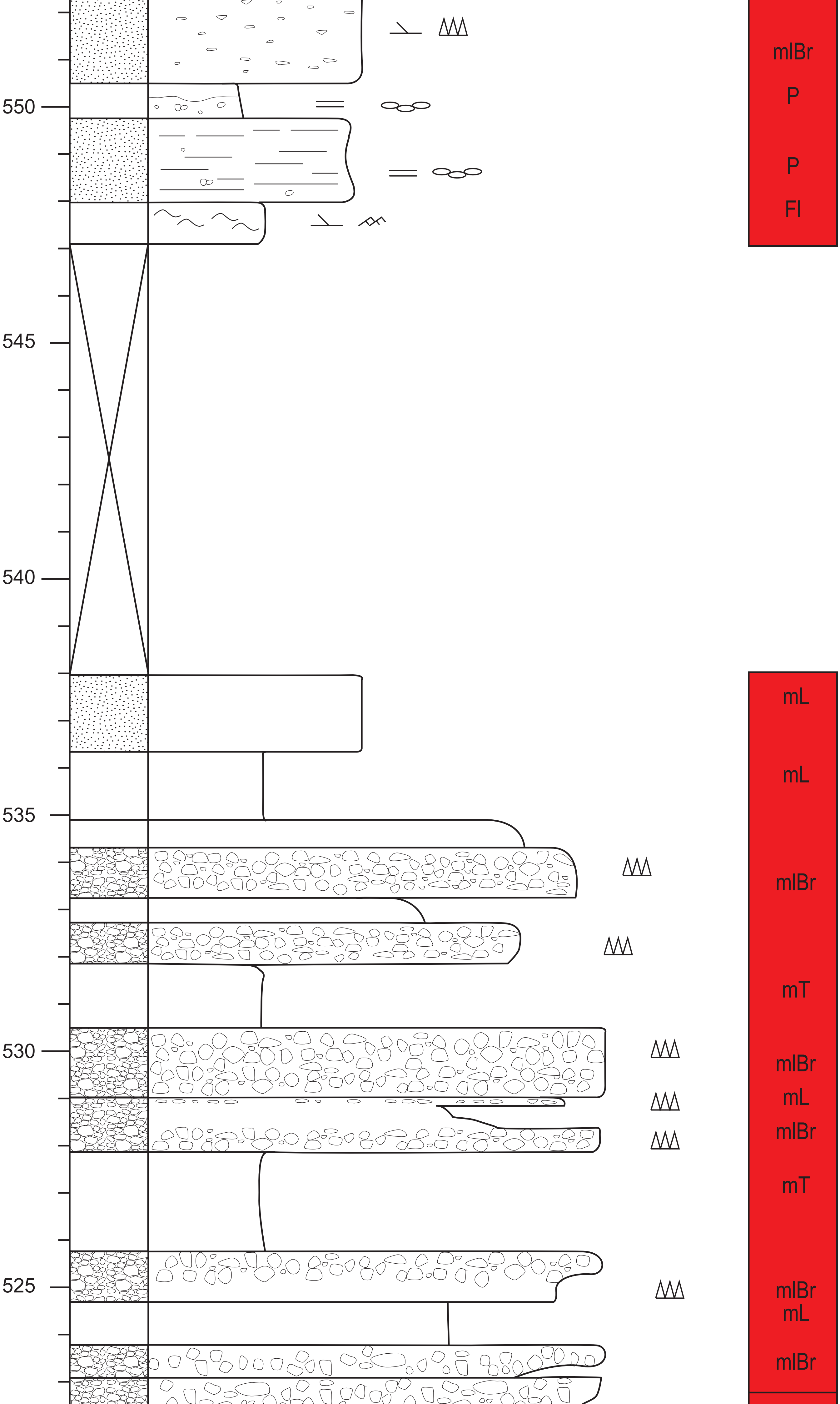

550
545
540
535
530
525
mlBr
P
P
Fl
mL
mL
mlBr
mT
mlBr
mL
mlBr
mT
mlBr
mL
mlBr

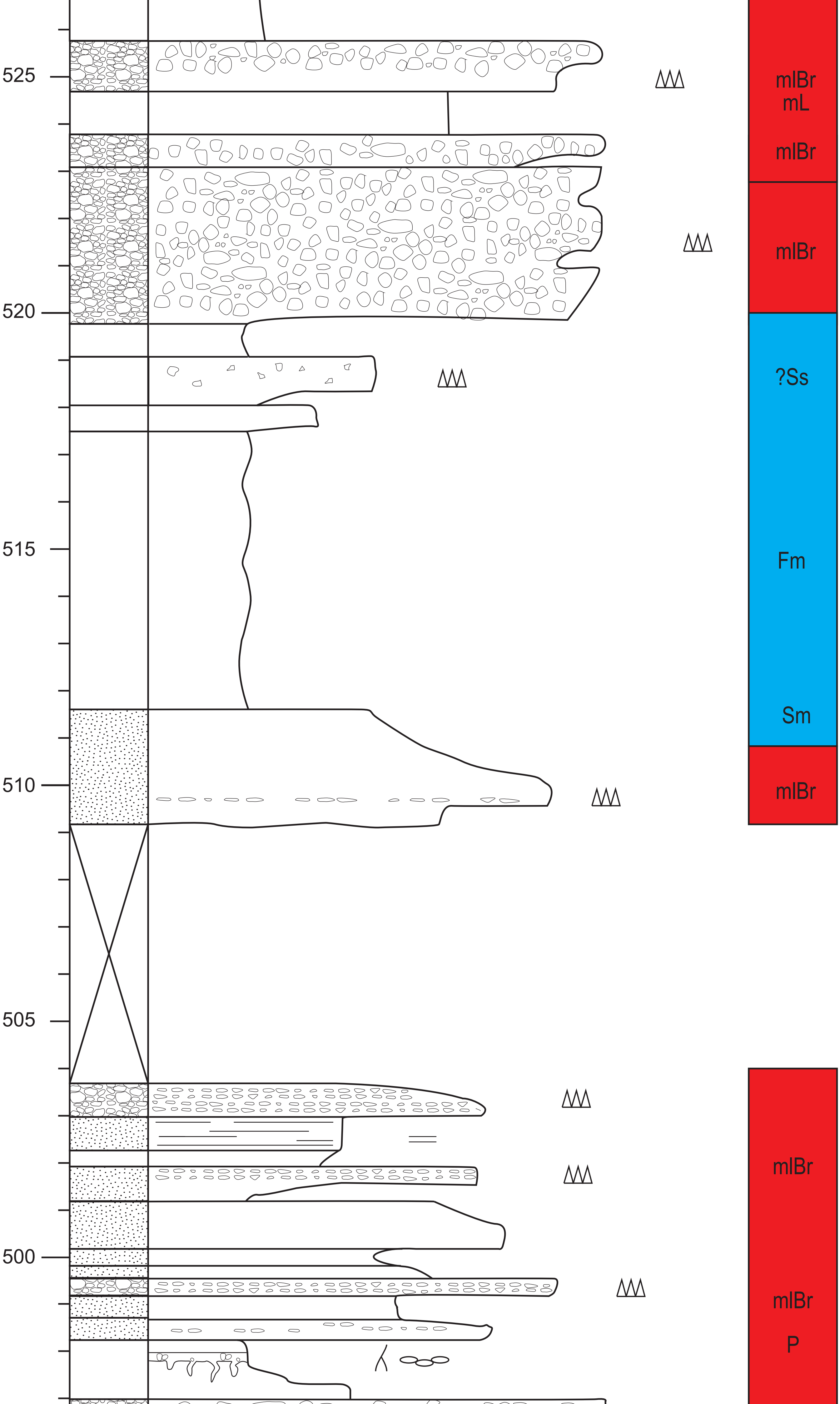

525
520
515
510
505
500
mlBr
mL
mlBr
mlBr
?Ss
Fm
Sm
mlBr
mlBr
mlBr
P

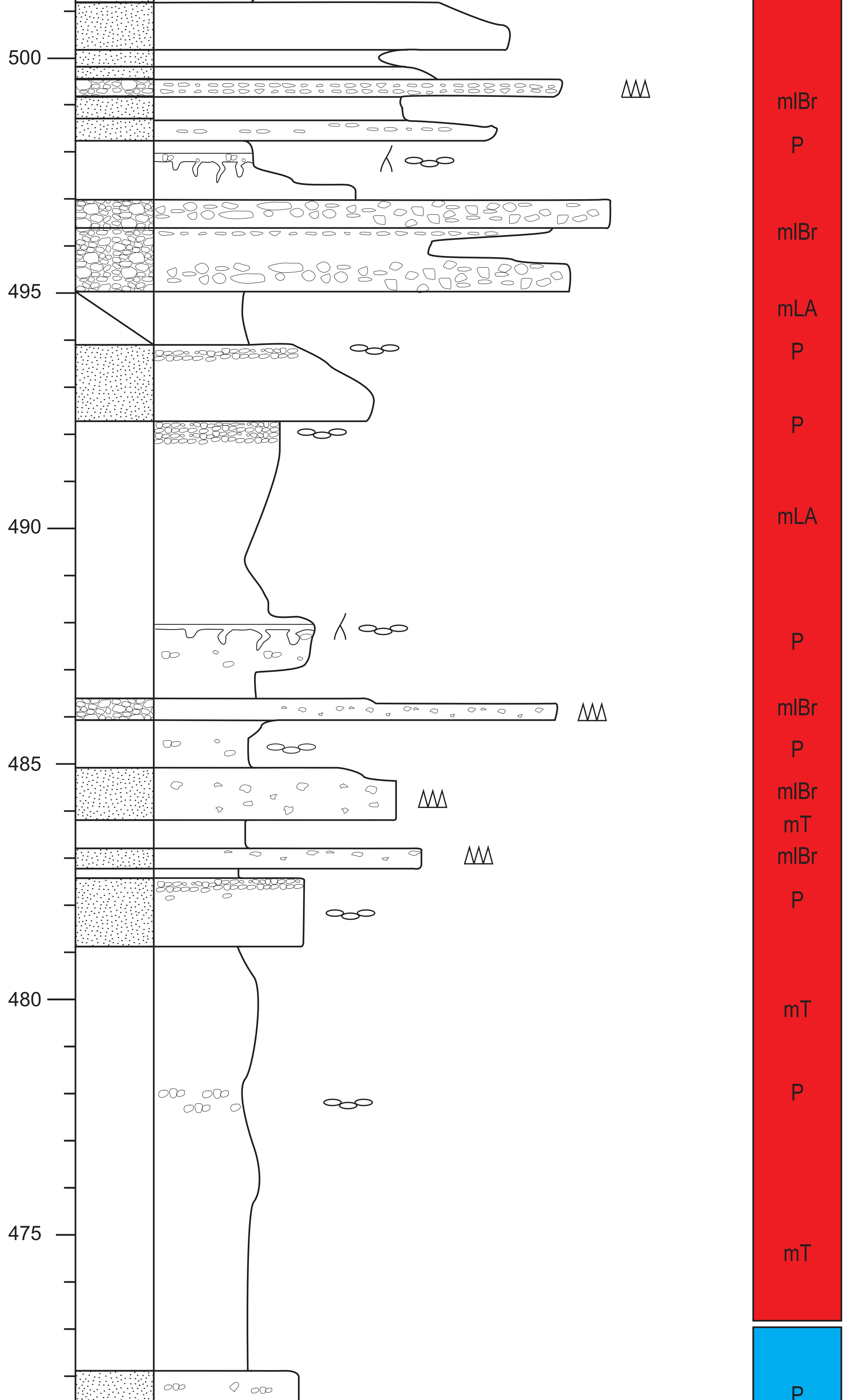
500
495
490
485
480
475
mlBr
P
mlBr
mLA
P
P
mLA
P
mlBr
P
mlBr
mT
mlBr
P
mT
P
mT
P

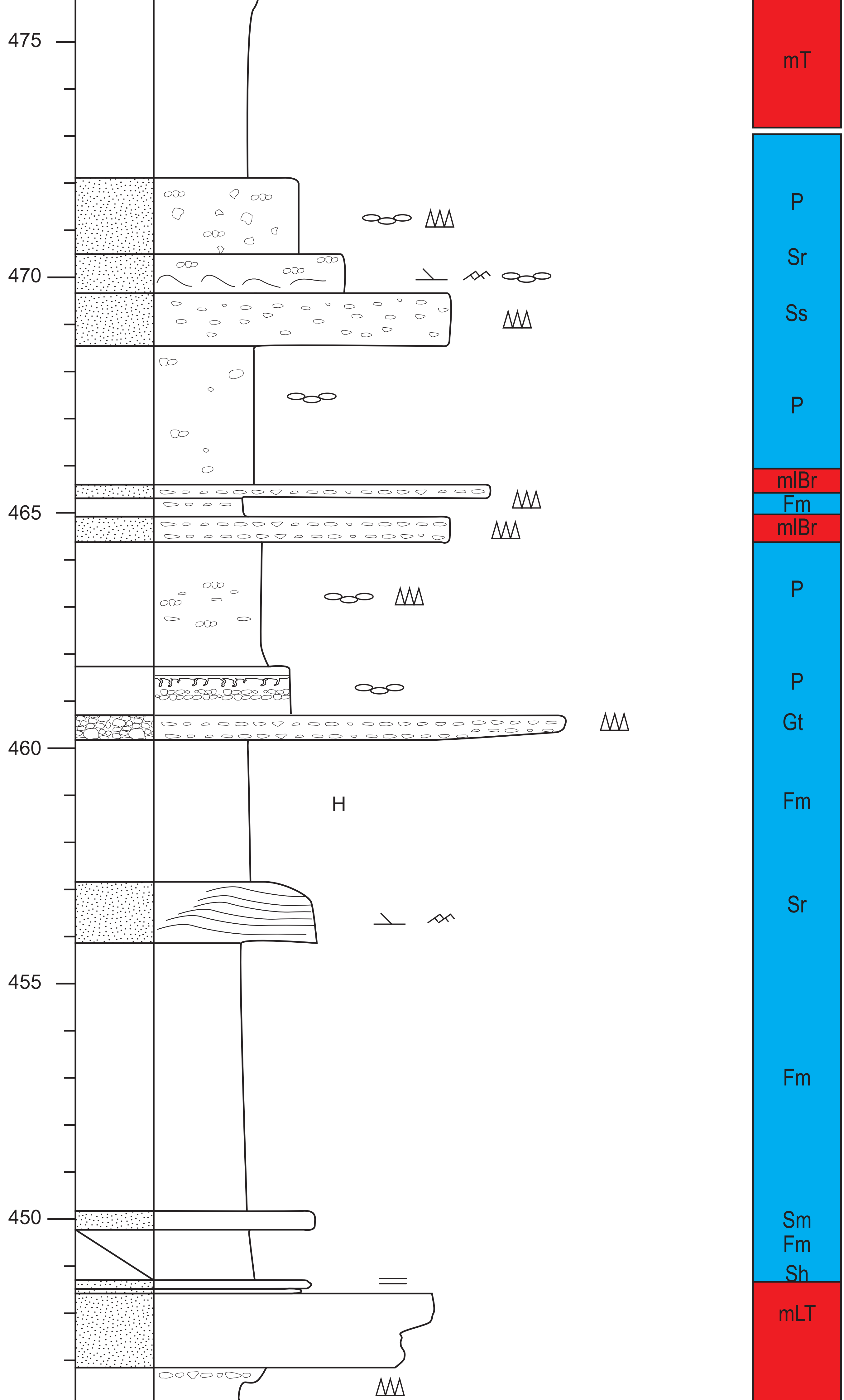

475
470
465
460
455
450
H
mT
P
Sr
Ss
P
mlBr
Fm
mlBr
P
P
Gt
Fm
Sr
Fm
Sm
Fm
Sh
mLT

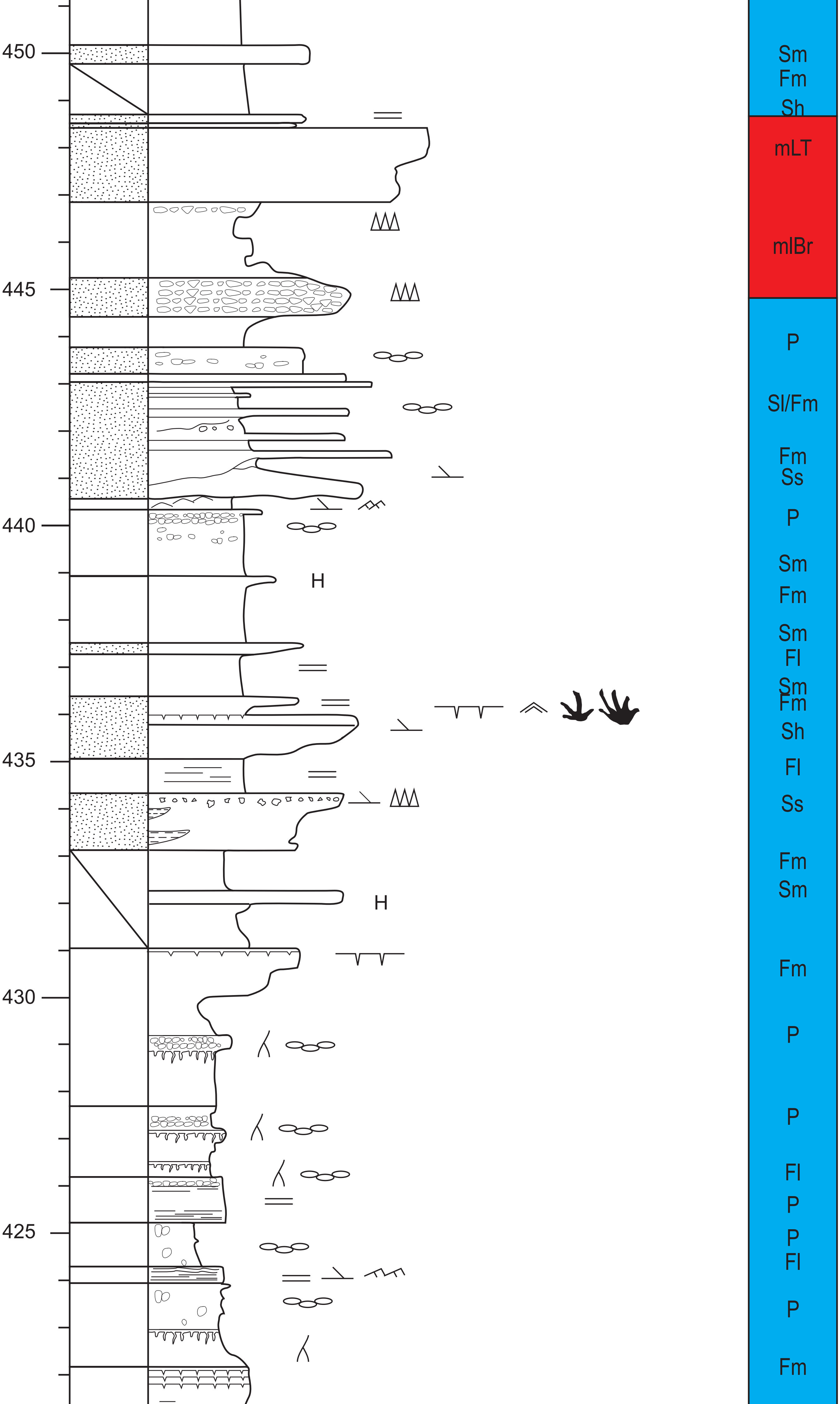

450
445
440
435
430
425
H
H
Sm
Fm
Sh
mLT
mlBr
P
Sl/Fm
Fm
Ss
P
Sm
Fm
Sm
Fl
Sm
Fm
Sh
Fl
Ss
Fm
Sm
Fm
P
P
Fl
P
P
Fl
P
Fm

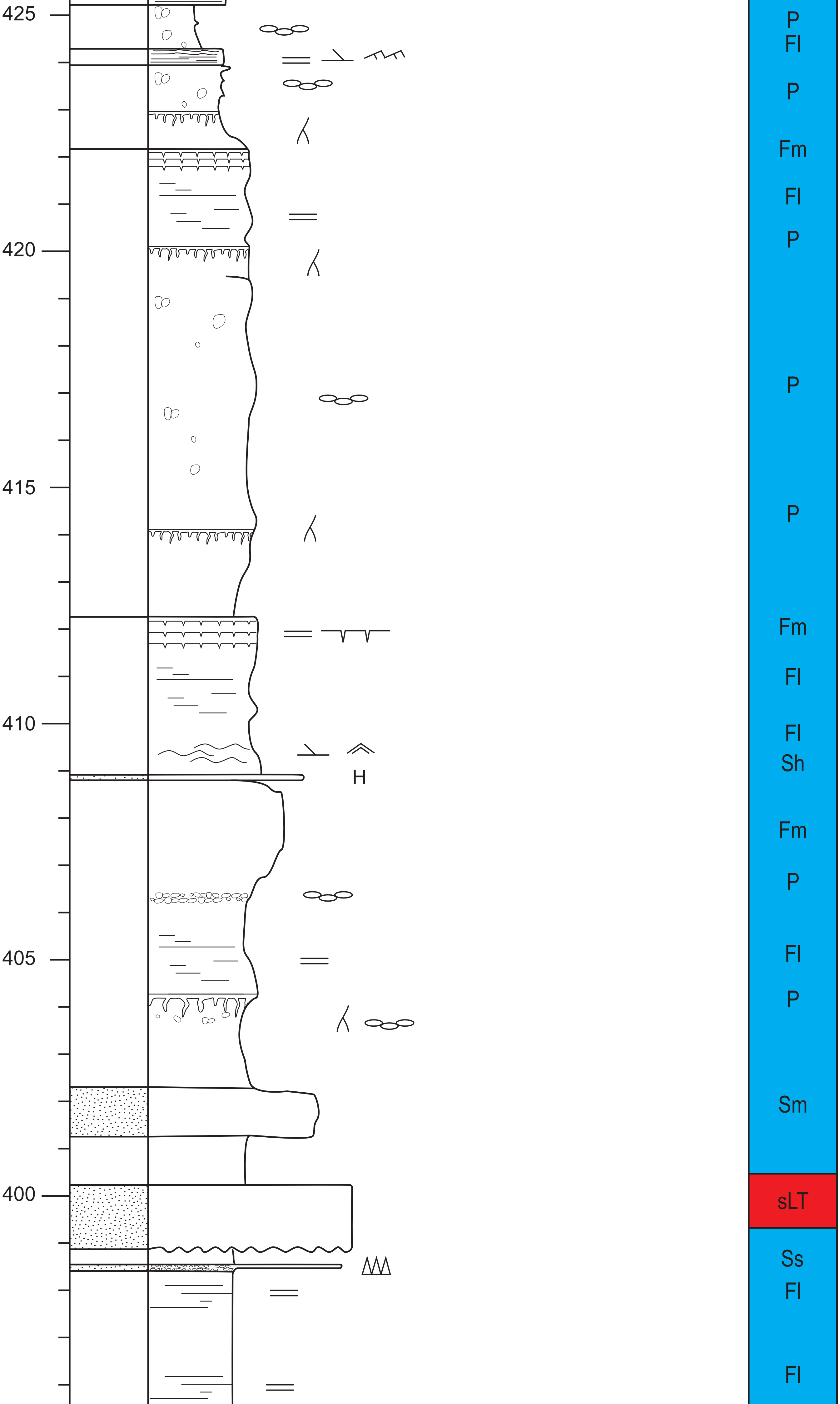

425
420
415
410
405
400
H
P
Fl
P
Fm
Fl
P
P
P
Fm
Fl
Fl
Sh
Fm
P
Fl
P
Sm
sLT
Ss
Fl
Fl

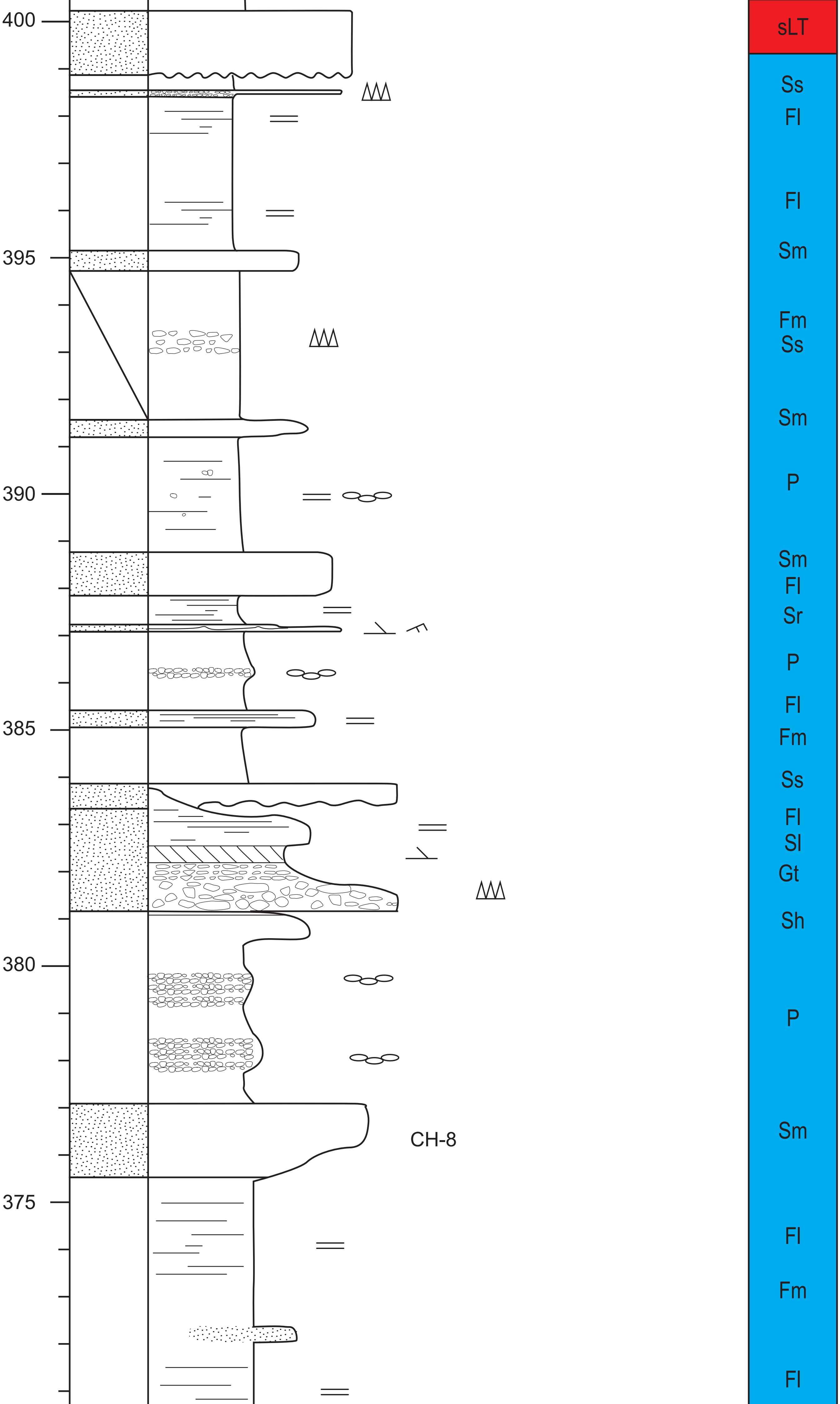

400
395
390
385
380
375
CH-8
sLT
Ss
Fl
Fl
Sm
Fm
Ss
Sm
P
Sm
Fl
Sr
P
Fl
Fm
Ss
Fl
Sl
Gt
Sh
P
Sm
Fl
Fm
Fl

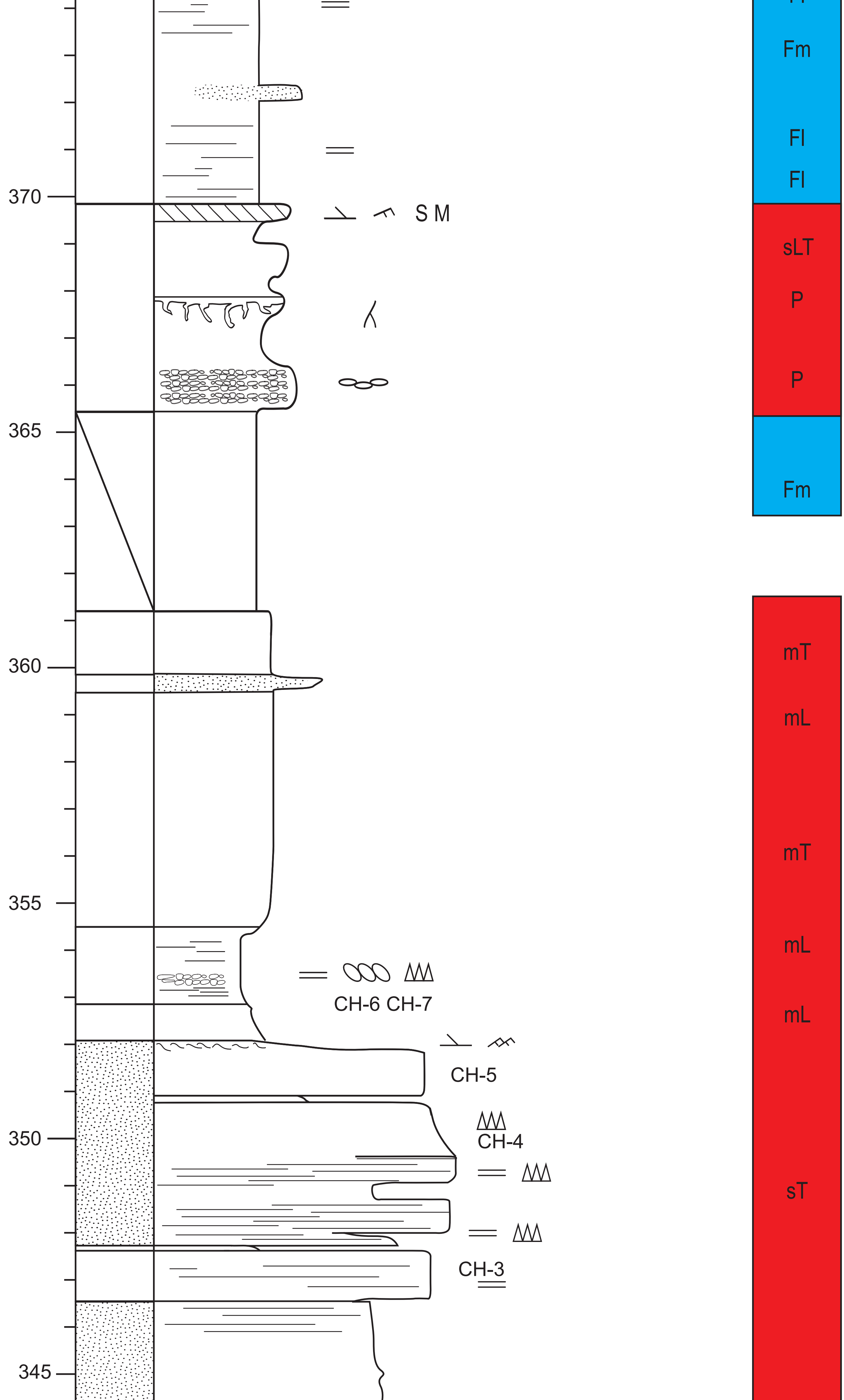

370
365
360
355
350
345
S M
CH-6 CH-7
CH-5
CH-4
CH-3
Fm
Fl
Fl
sLT
P
P
Fm
mT
mL
mT
mL
mL
sT

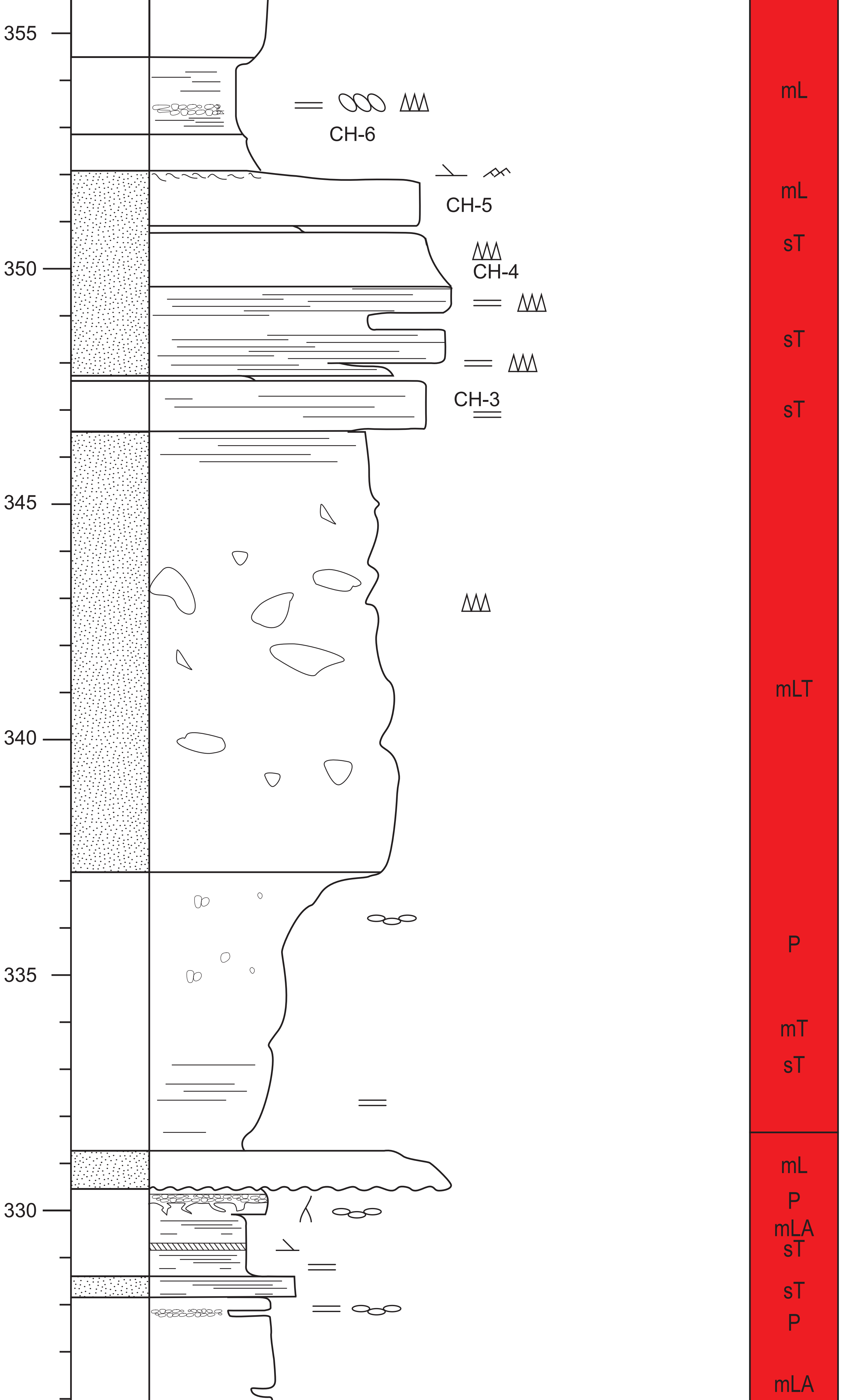
355
350
345
340
335
330
CH-6
CH-5
CH-4
CH-3
mL
mL
sT
sT
sT
mLT
P
mT
sT
mL
P
mLA
sT
sT
P
mLA

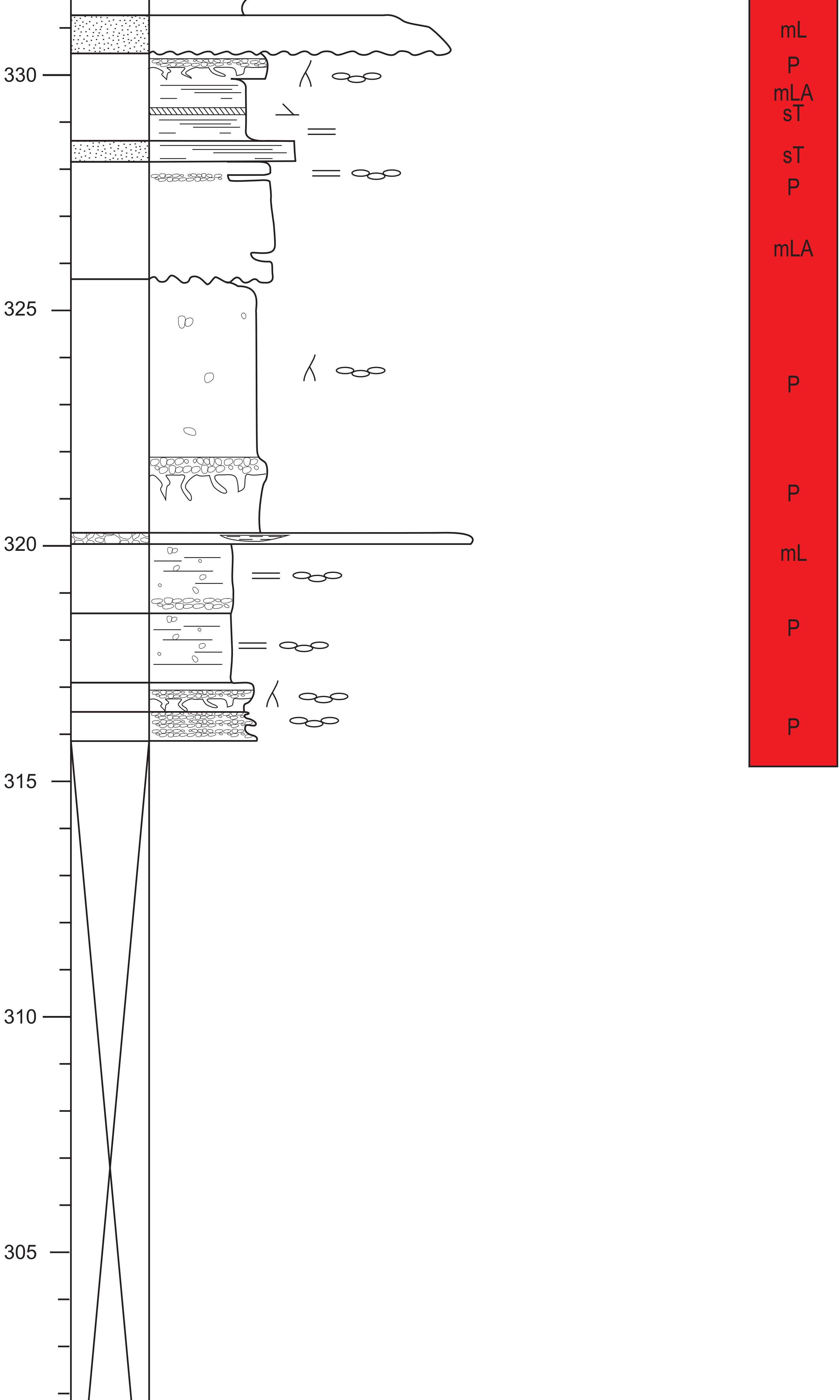
330
325
320
315
310
305
mL
P
mLA
sT
sT
P
mLA
P
P
mL
P
P

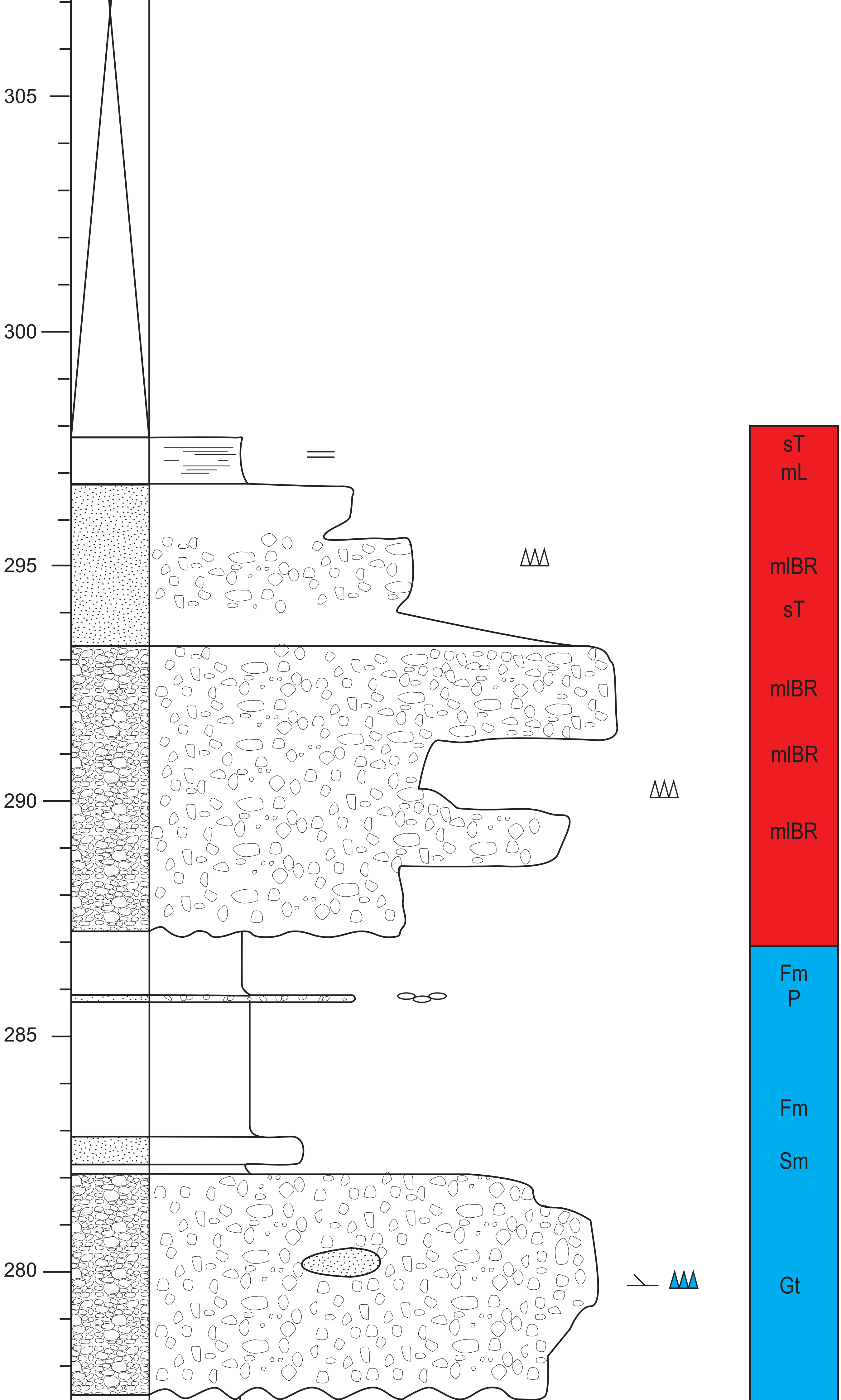
305
300
295
290
285
280
sT
mL
mlBR
sT
mlBR
mlBR
mlBR
Fm
P
Fm
Sm
Gt

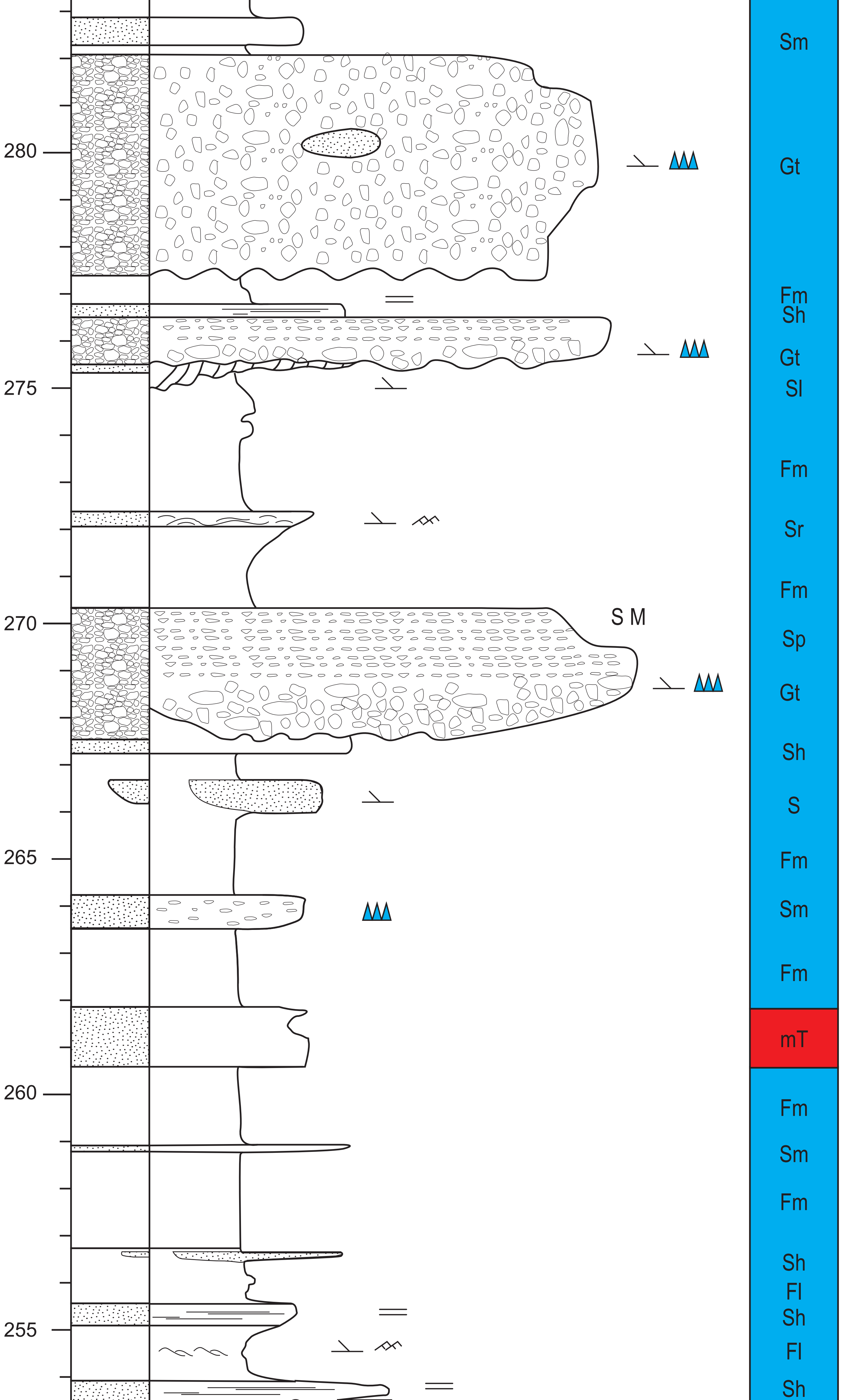

280
275
270
265
260
255
S M
Sm
Gt
Fm
Sh
Gt
Sl
Fm
Sr
Fm
Sp
Gt
Sh
S
Fm
Sm
Fm
mT
Fm
Sm
Fm
Sh
Fl
Sh
Fl
Sh

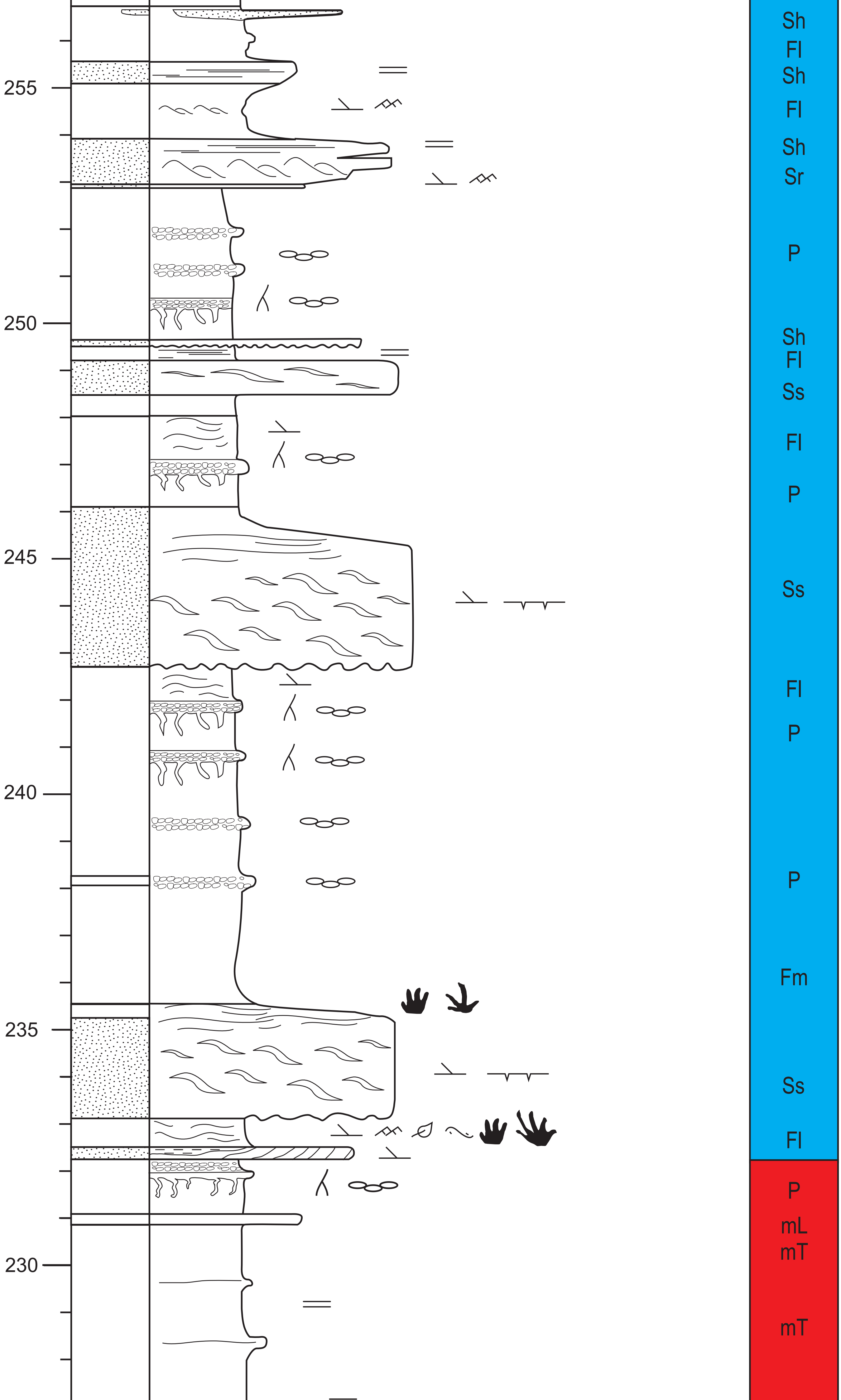

255
250
245
240
235
230
Sh
Fl
Sh
Fl
Sh
Sr
P
Sh
Fl
Ss
Fl
P
Ss
Fl
P
P
Fm
Ss
Fl
P
mL
mT
mT

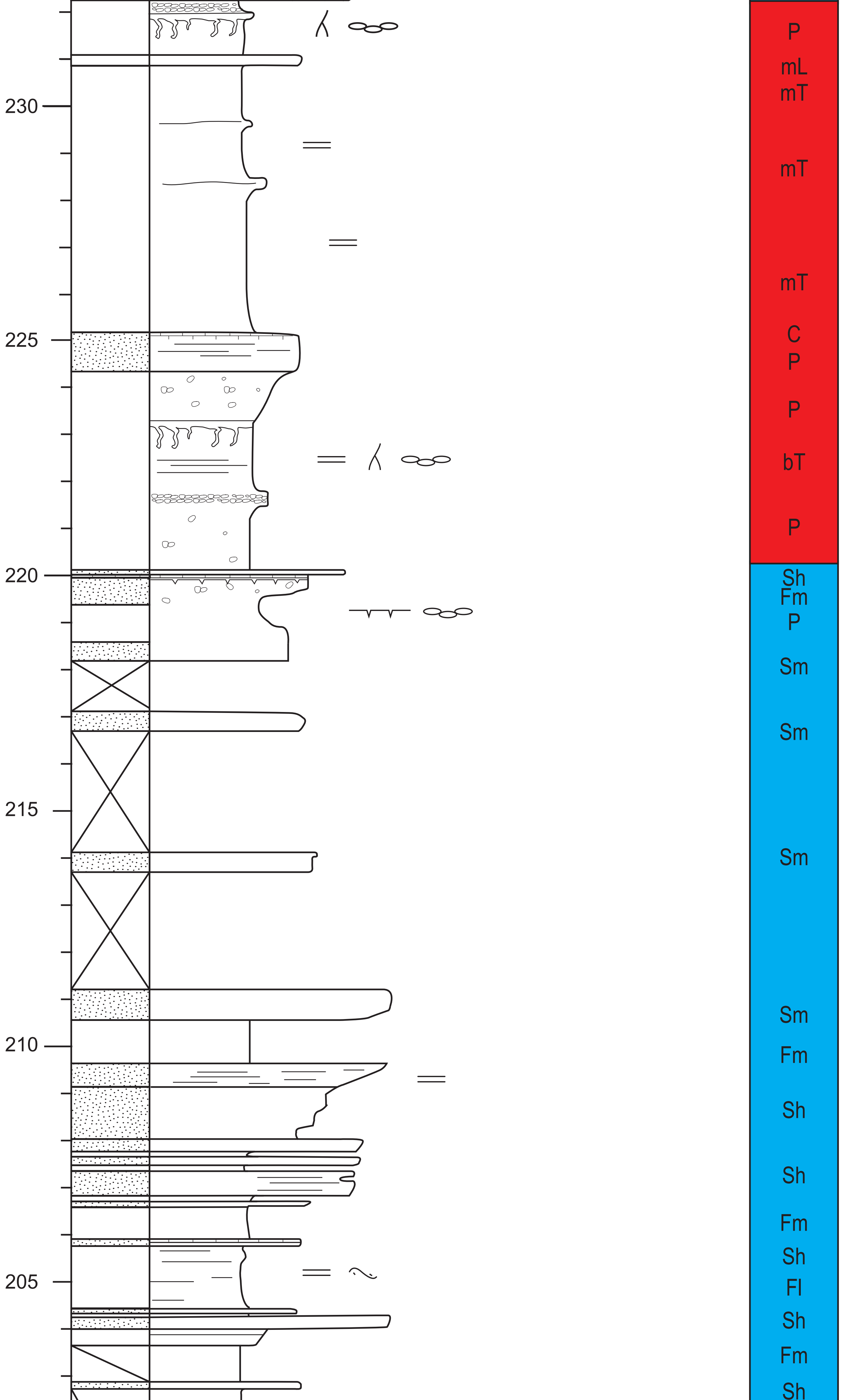

230
225
220
215
210
205
P
mL
mT
mT
mT
C
P
P
bT
P
Sh
Fm
P
Sm
Sm
Sm
Sm
Fm
Sh
Sh
Fm
Sh
Fl
Sh
Fm
Sh

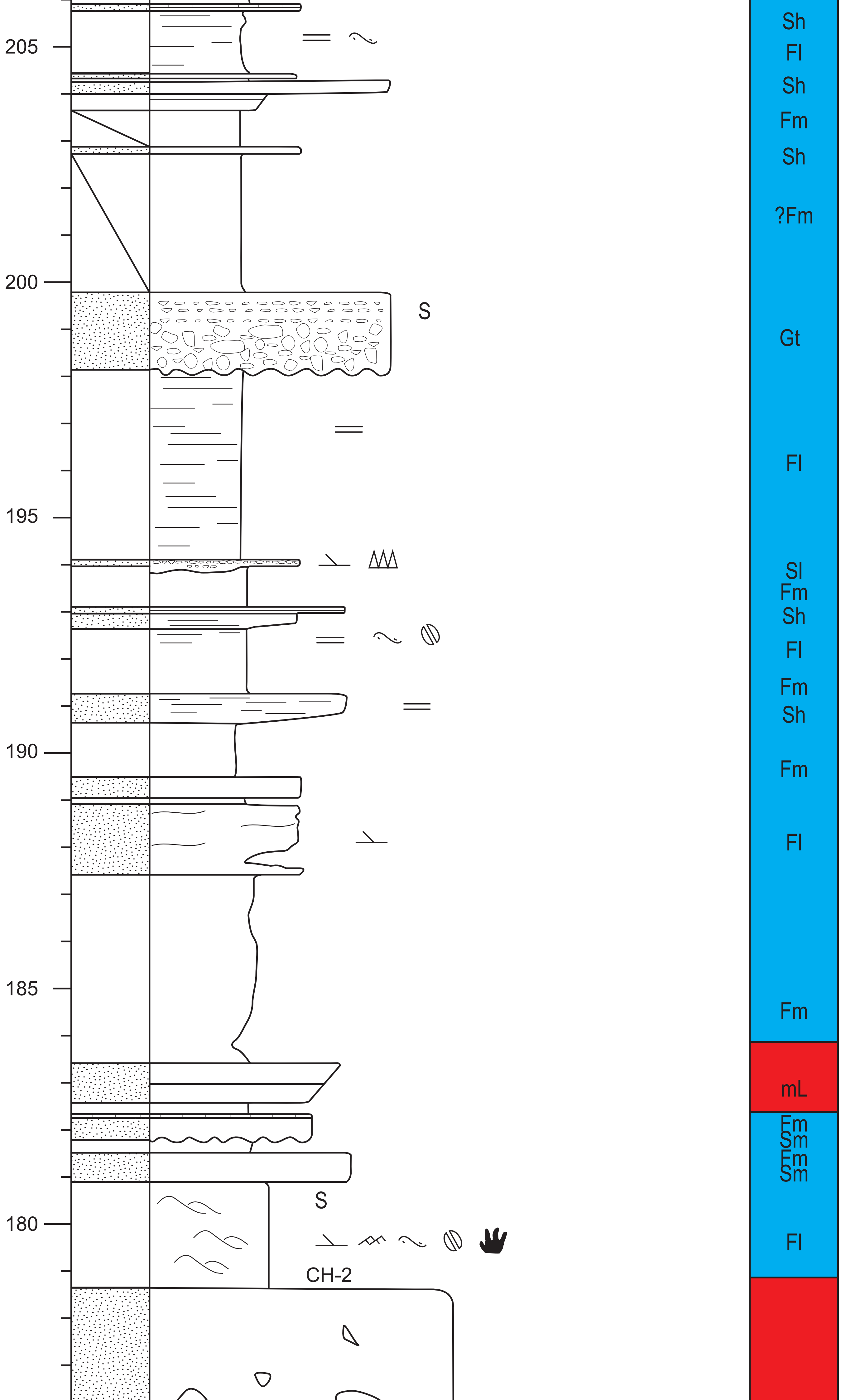
205
200
195
190
185
180
S
S
CH-2
Sh
Fl
Sh
Fm
Sh
?Fm
Gt
Fl
Sl
Fm
Sh
Fl
Fm
Sh
Fm
Fl
Fm
mL
Fm
Sm
Fm
Sm
Fl

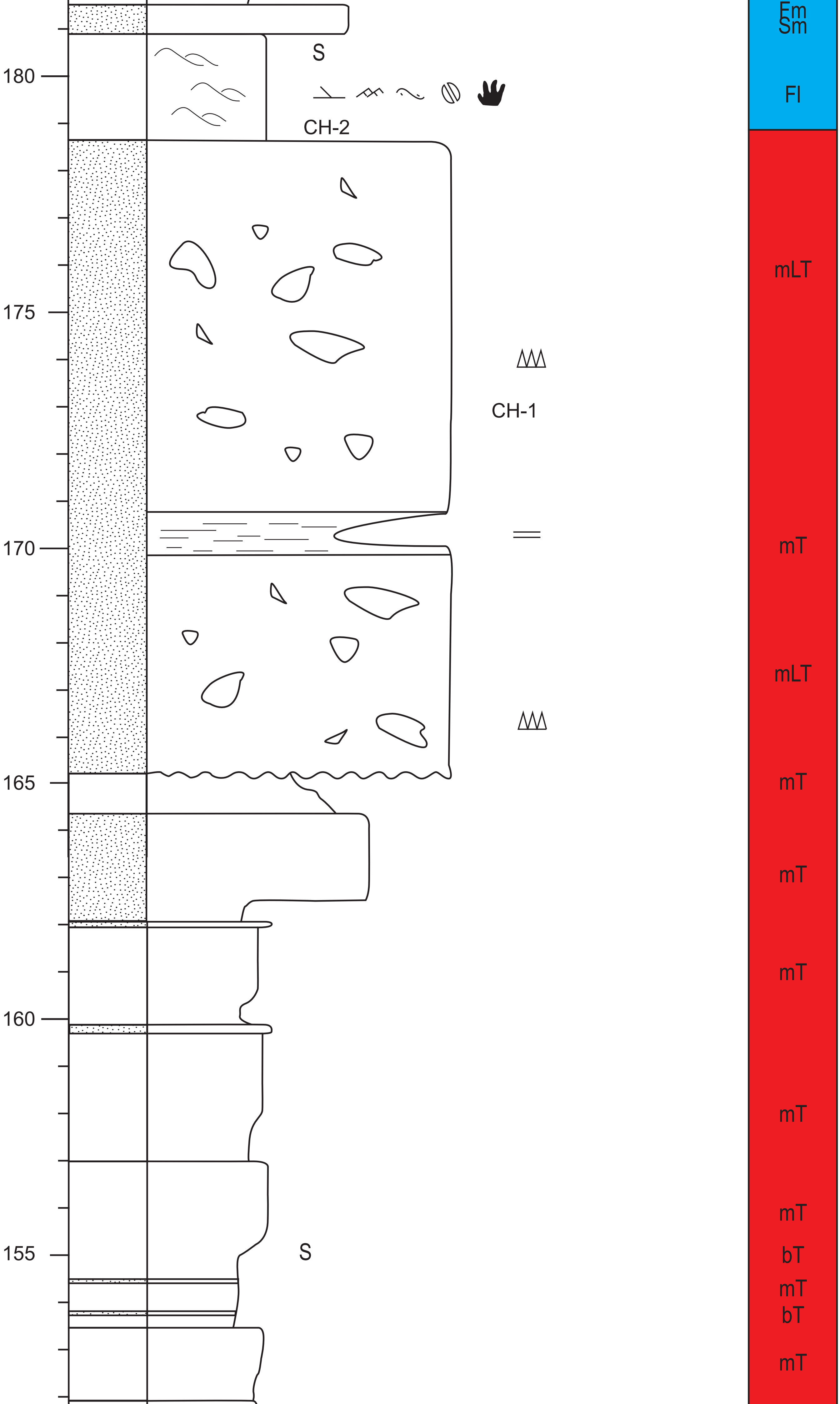

180
175
170
165
160
155
S
CH-2
CH-1
S
Fm
Sm
Fl
mLT
mT
mLT
mT
mT
mT
mT
mT
bT
mT
bT
mT

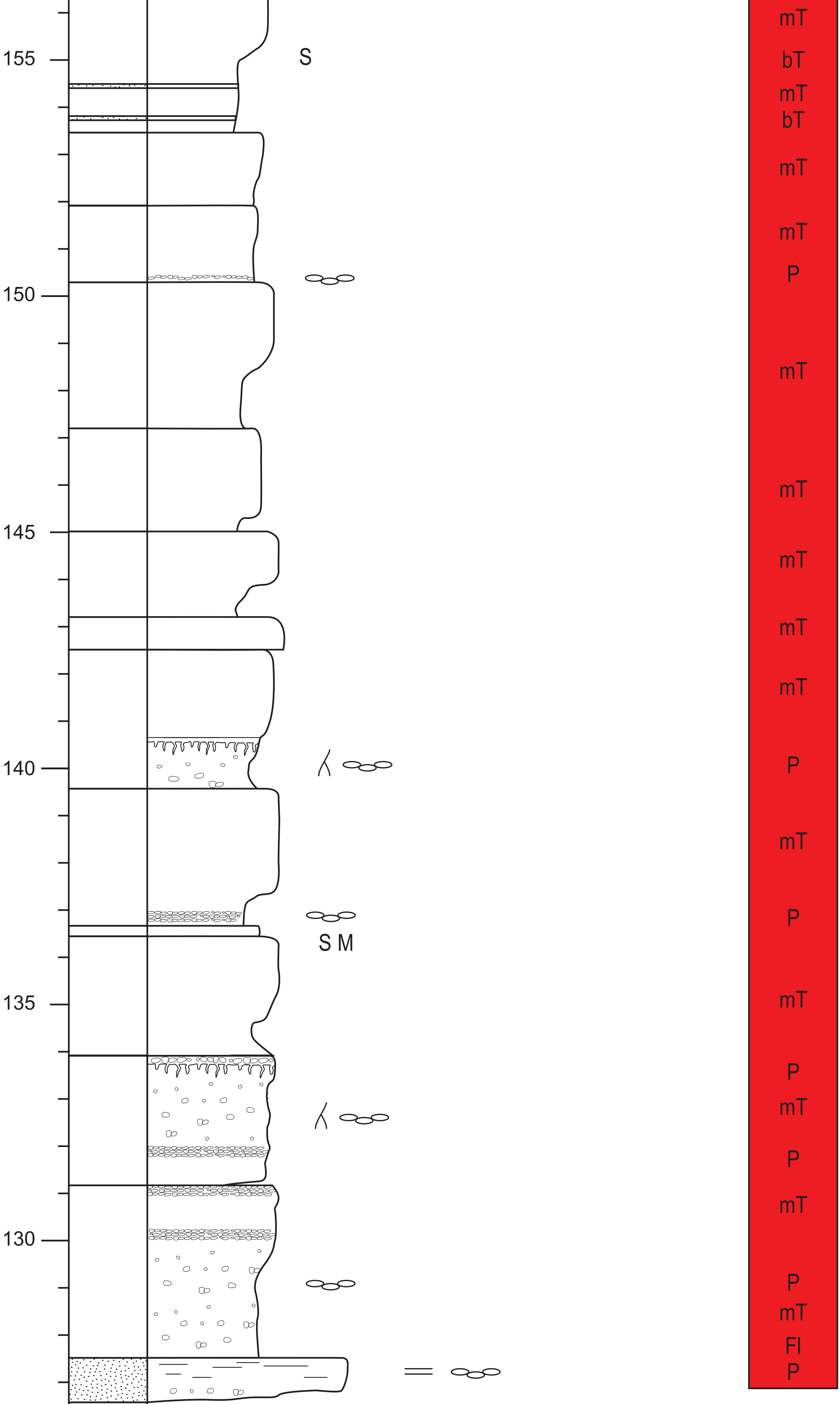
155
150
145
140
135
130
S
S M
mT
bT
mT
bT
mT
mT
P
mT
mT
mT
mT
mT
P
mT
P
mT
P
mT
P
mT
P
mT
Fl
P

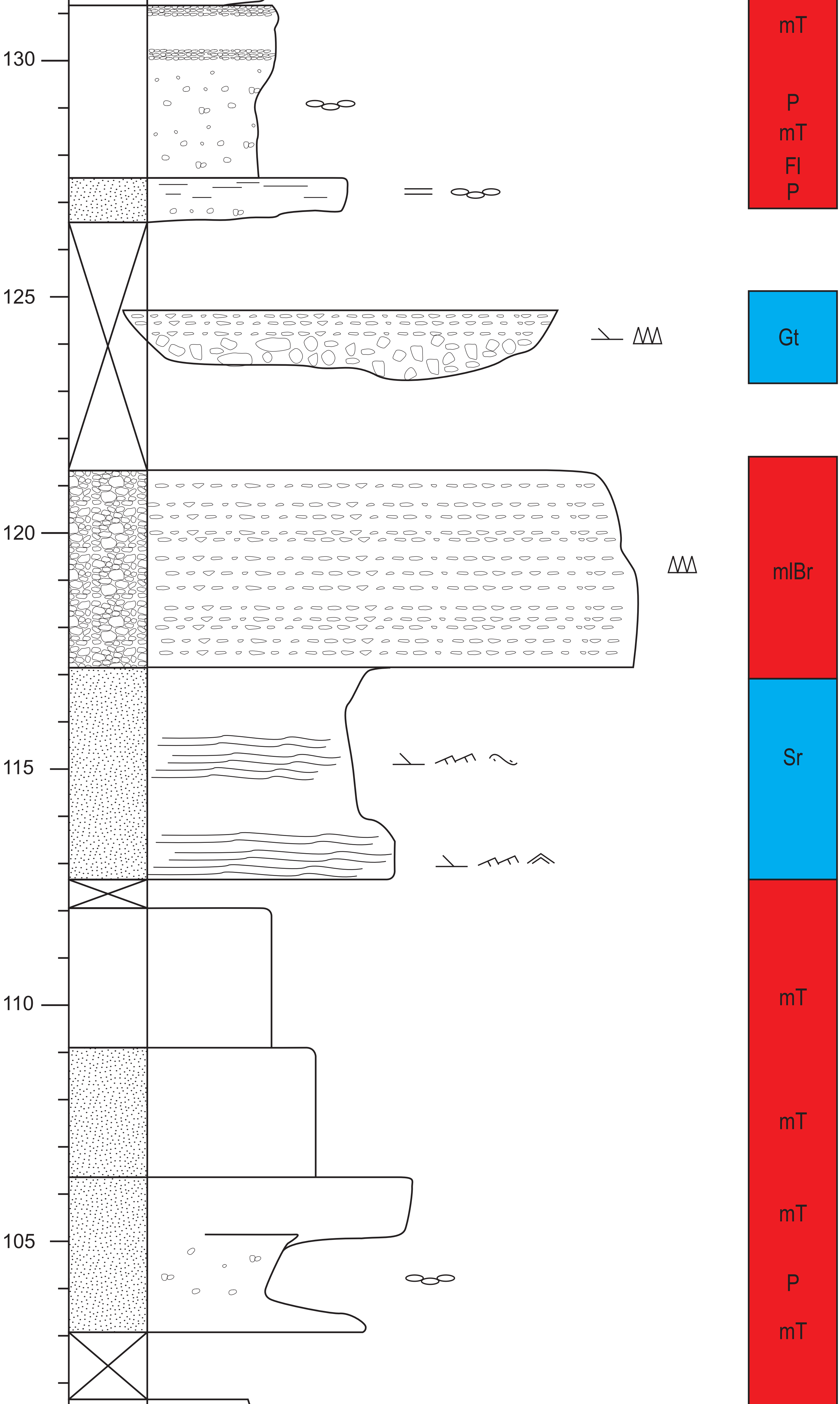
130
125
120
115
110
105
mT
P
mT
Fl
P
Gt
mlBr
Sr
mT
mT
mT
P
mT

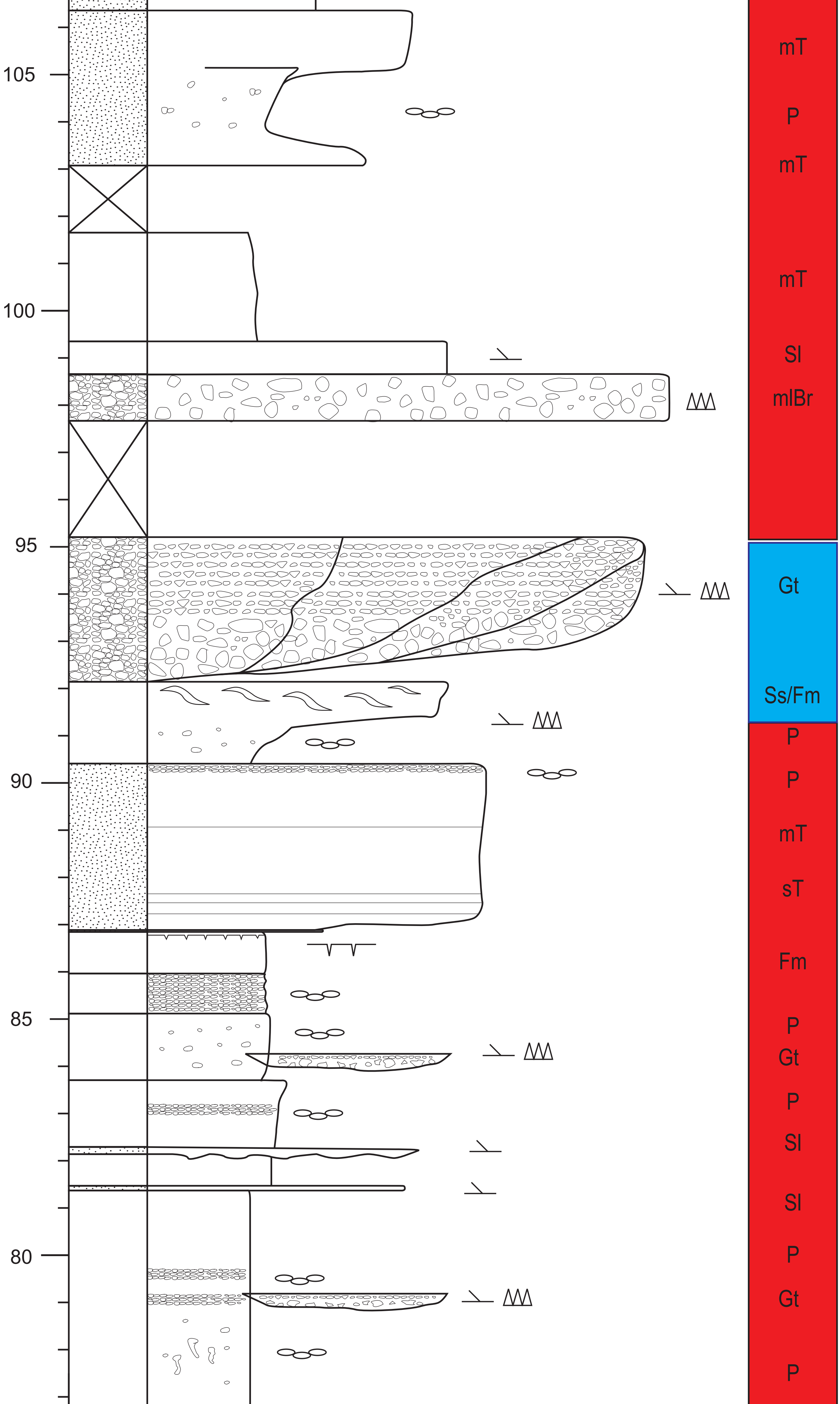
105
100
95
90
85
80
mT
P
mT
mT
Sl
mlBr
Gt
Ss/Fm
P
P
mT
sT
Fm
P
Gt
P
Sl
Sl
P
Gt
P

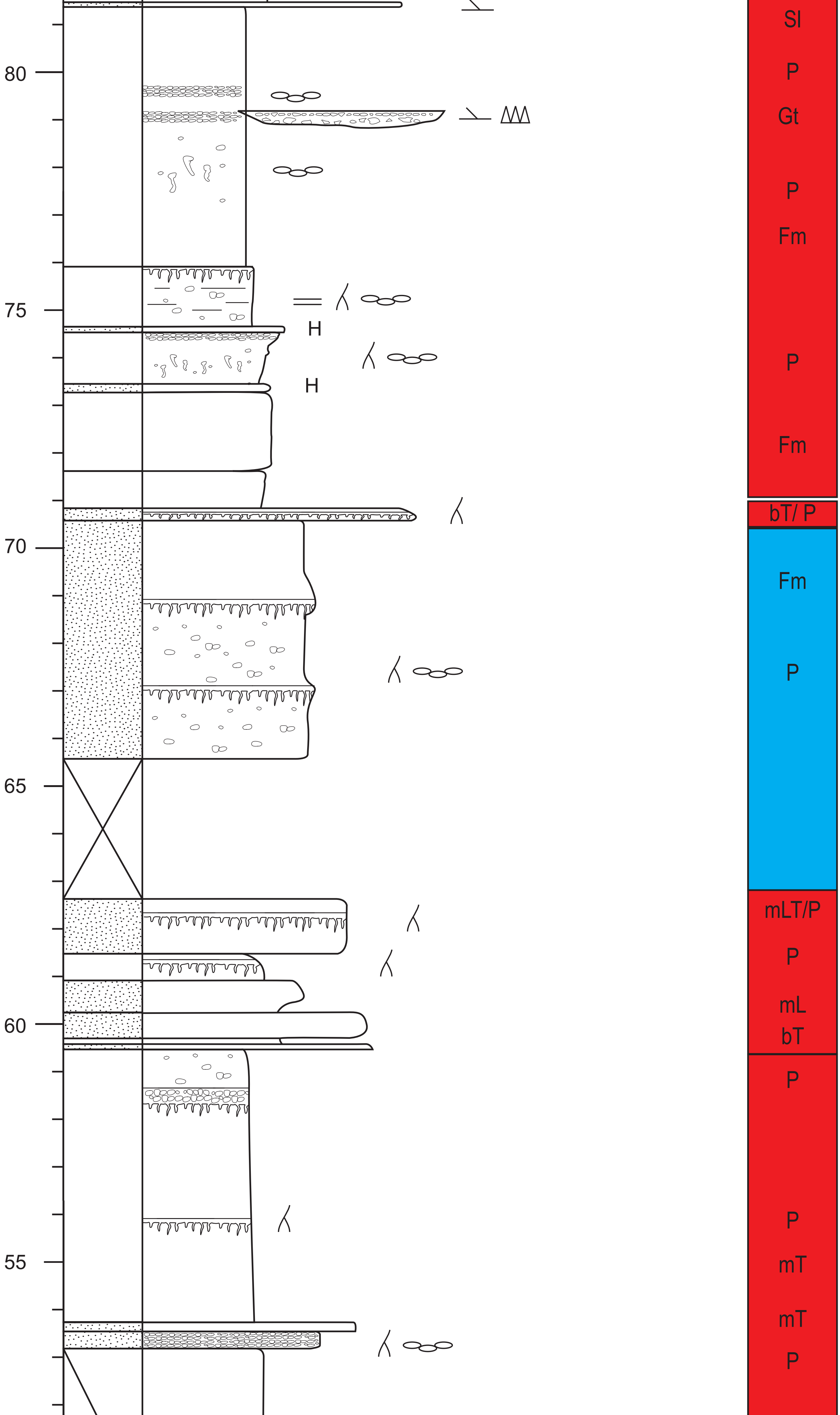

80
75
70
65
60
55
H
H
Sl
P
Gt
P
Fm
P
Fm
bT/ P
Fm
P
mLT/P
P
mL
bT
P
P
mT
mT
P

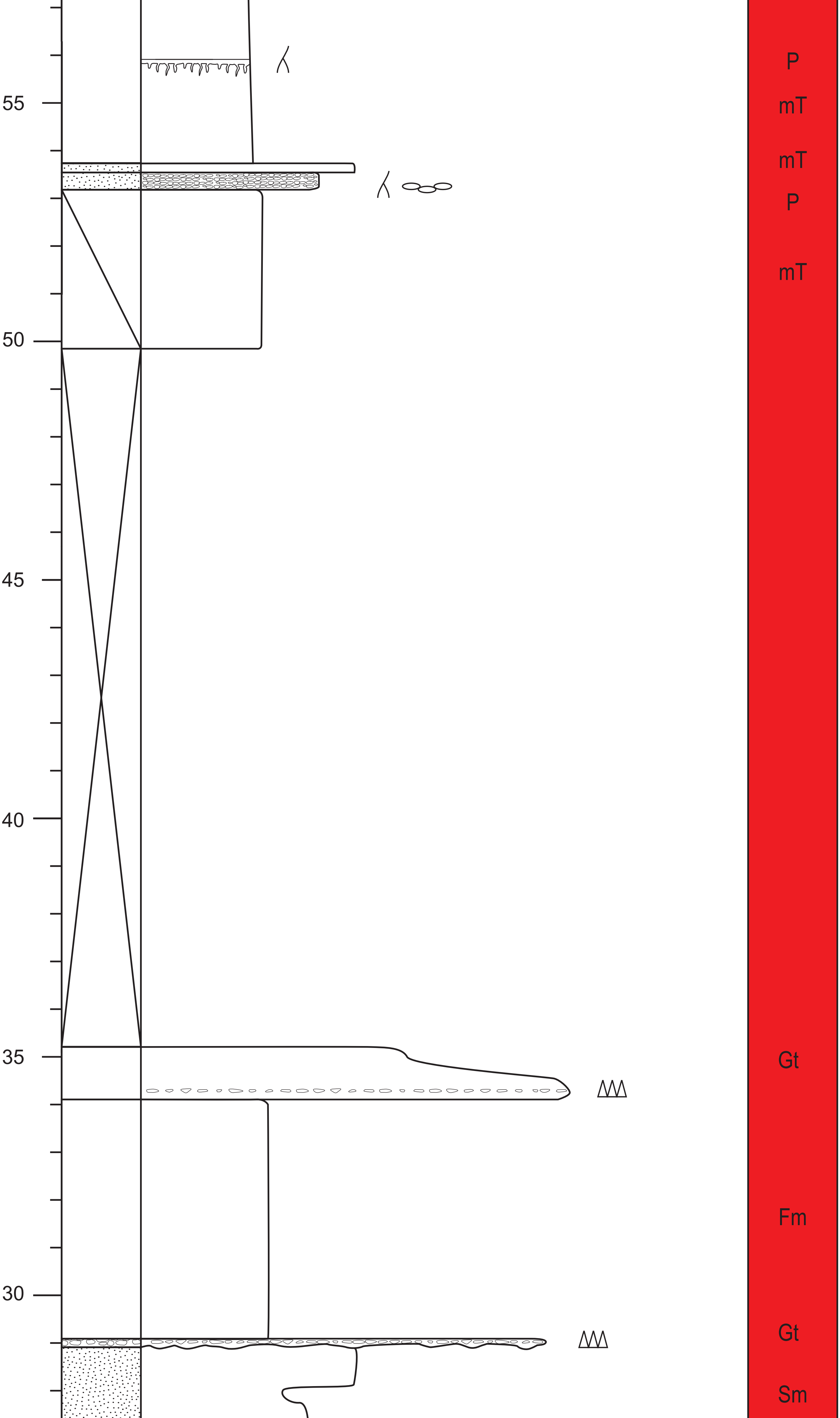
55
50
45
40
35
30
P
mT
mT
P
mT
Gt
Fm
Gt
Sm

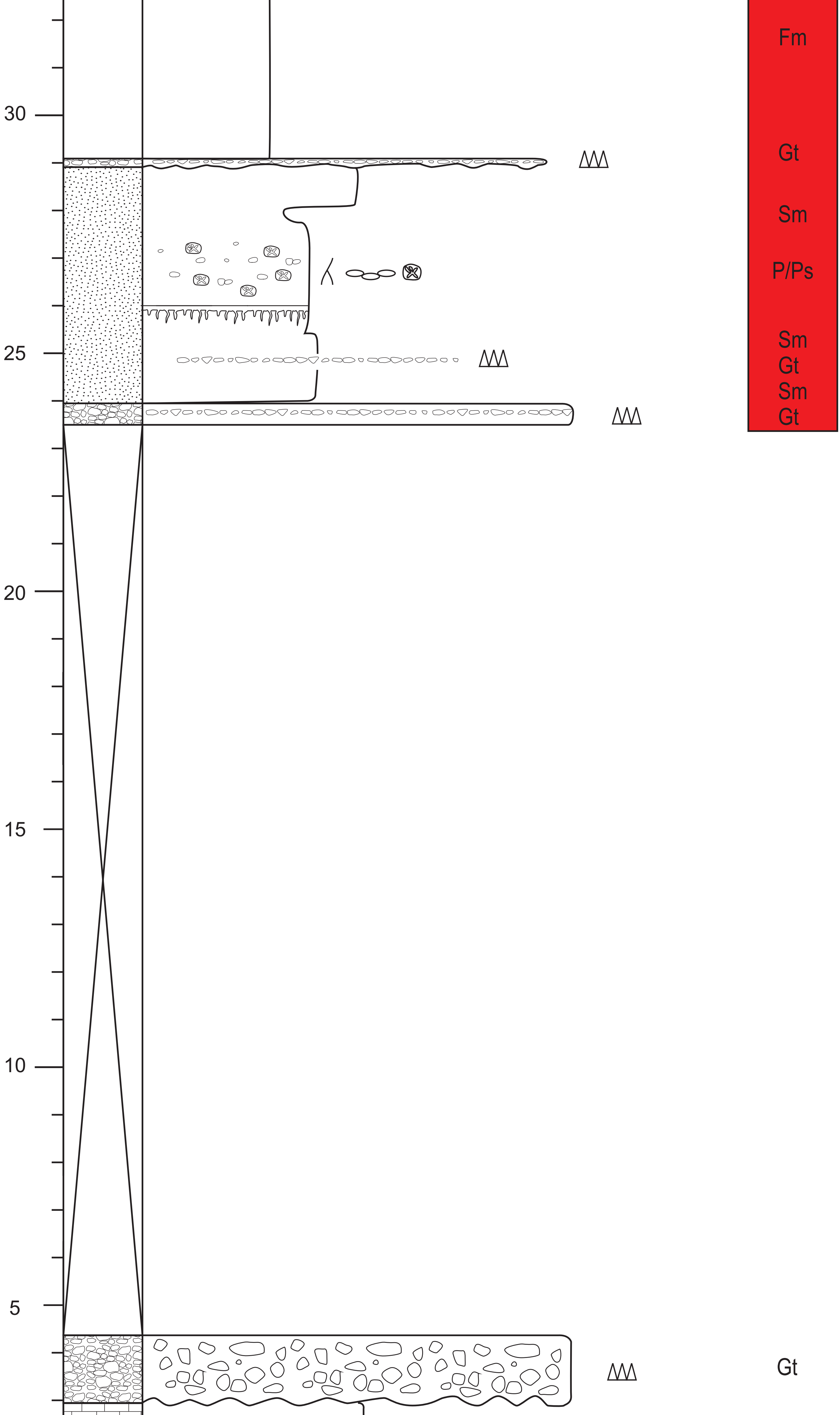

30
25
20
15
10
5
Fm
Gt
Sm
P/Ps
Sm
Gt
Sm
Gt
Gt

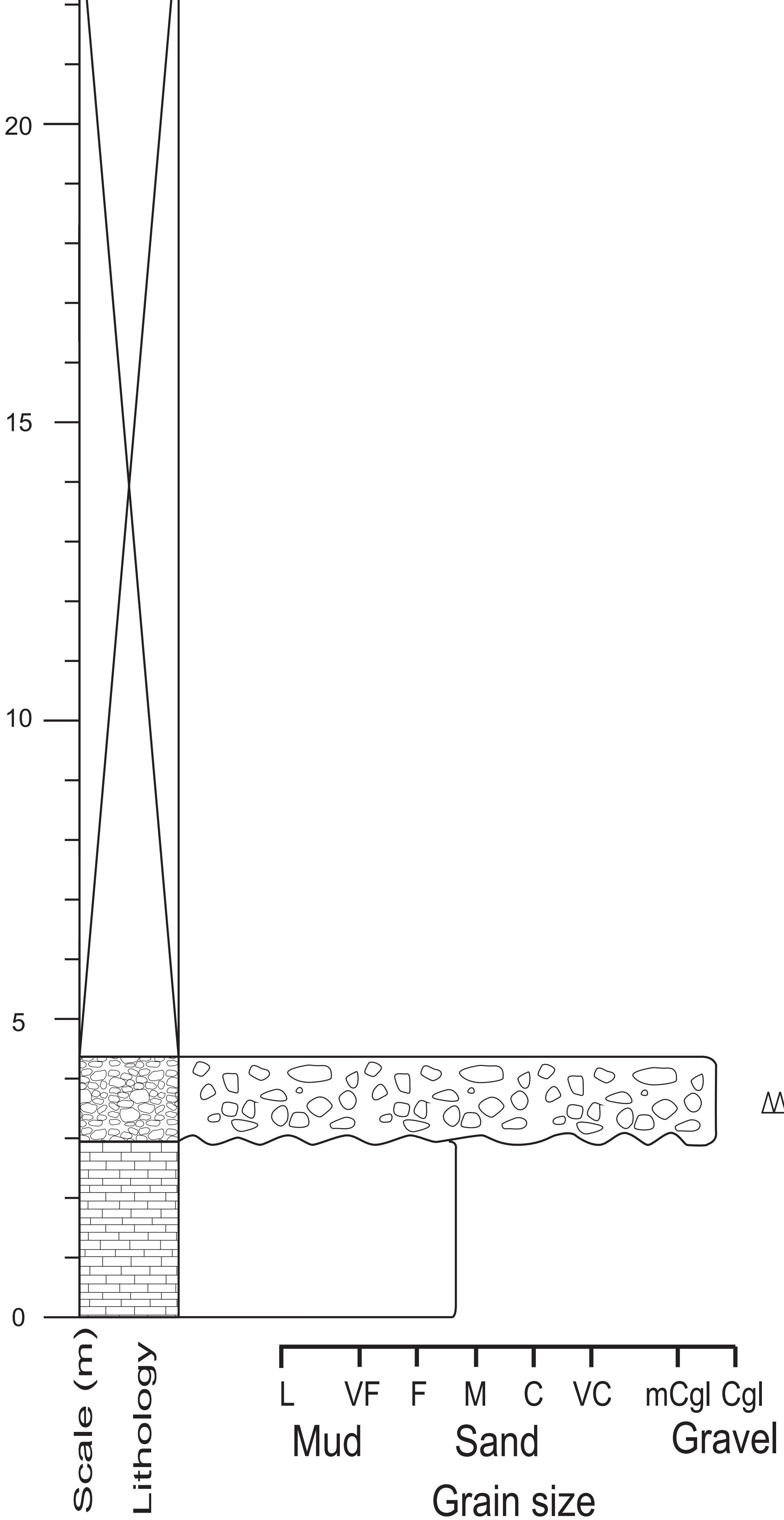

20
15
10
5
0
Gt
Scale (m)
Lithology
L
VF
F
M
C
VC
mCgl
Cgl
Mud
Sand
Gravel
Grain size

Stratigraphical section of Riera de Monell

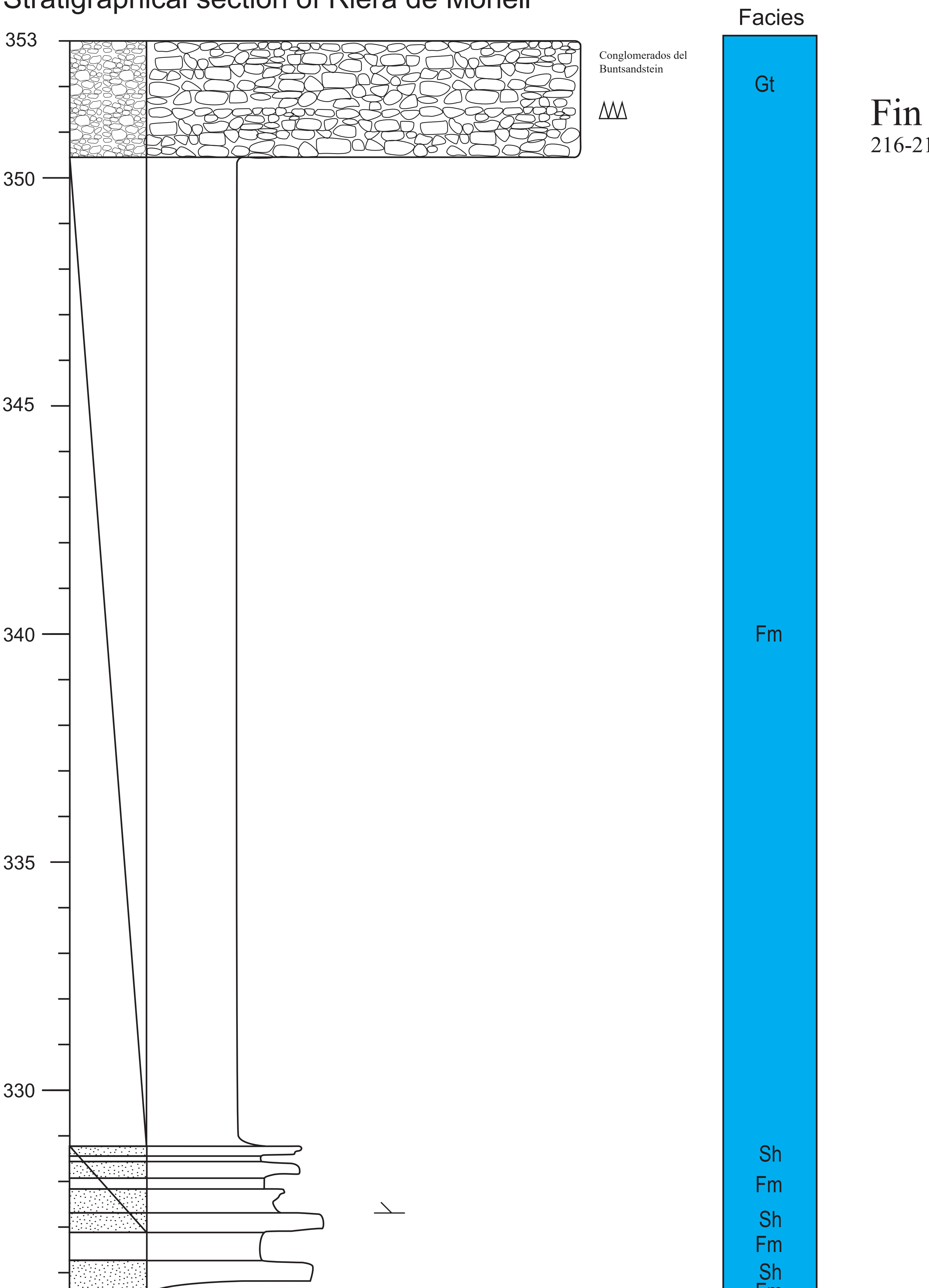

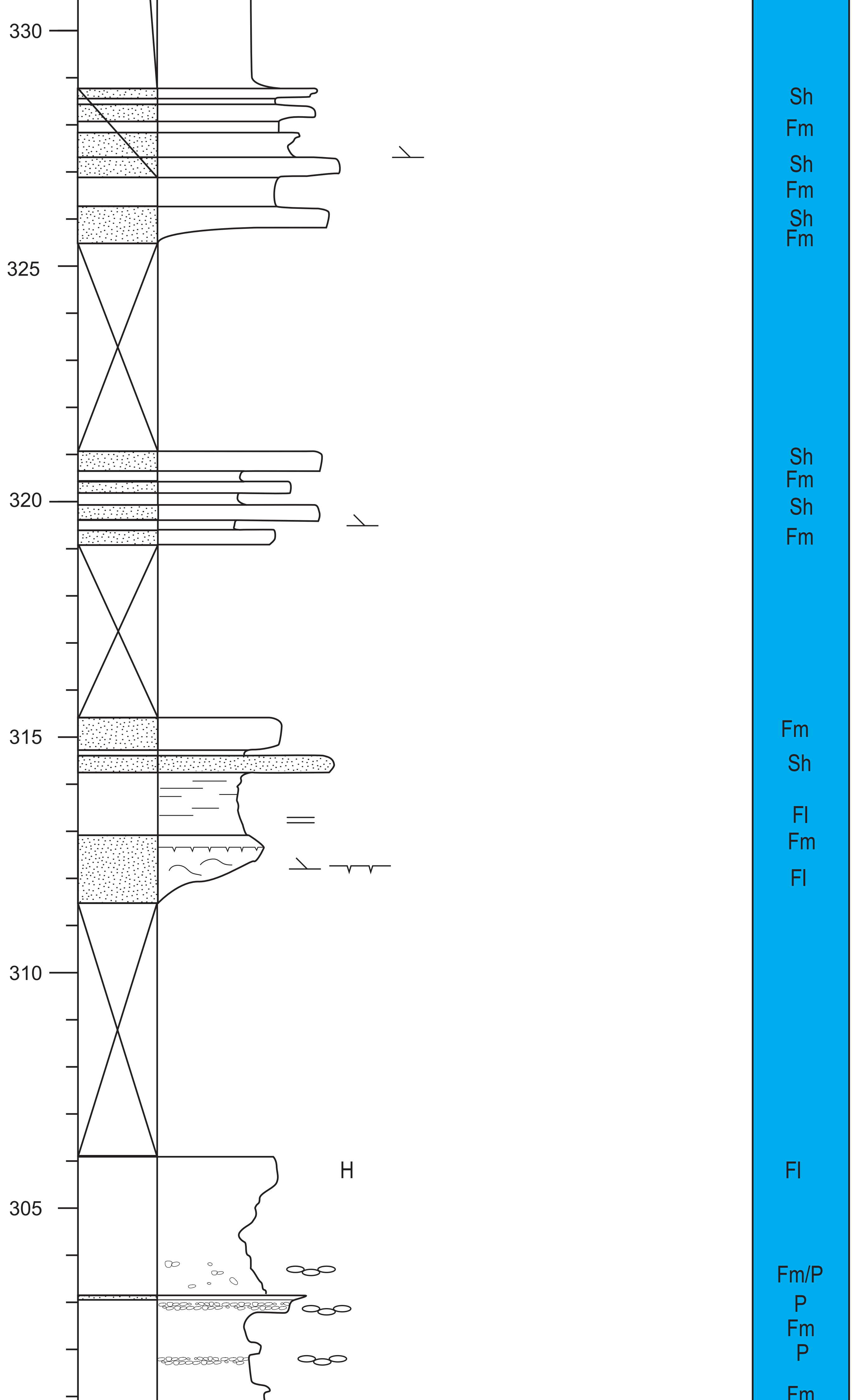
330
325
320
315
310
305
H
Sh
Fm
Sh
Fm
Sh
Fm
Sh
Fm
Sh
Fm
Fm
Sh
Fl
Fm
Fl
Fl
Fm/P
P
Fm
P
Fm

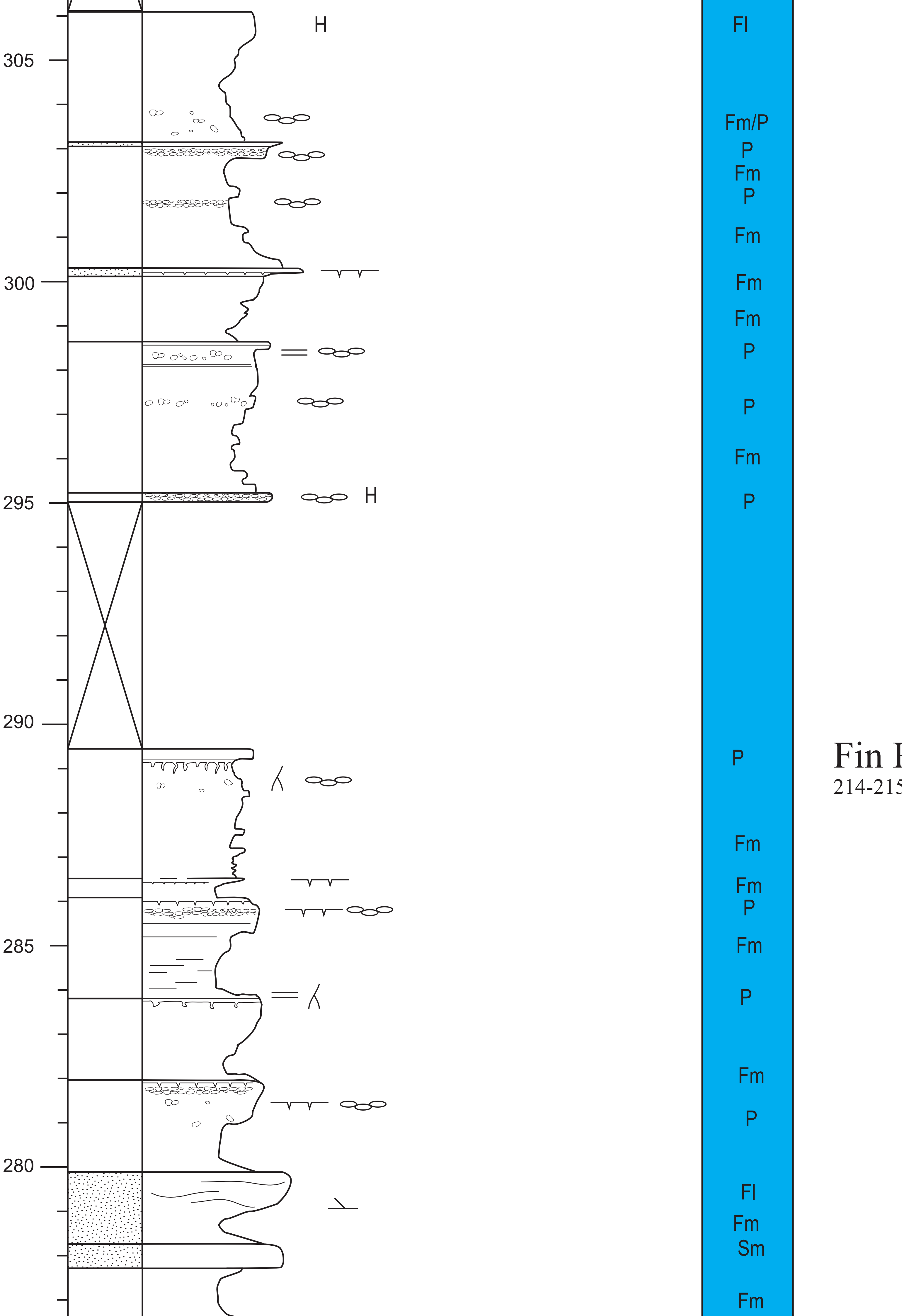
305
300
295
290
285
280
H
H
Fl
Fm/P
P
Fm
P
Fm
Fm
Fm
P
P
Fm
P
P
Fm
Fm
P
Fm
P
Fm
P
Fl
Fm
Sm
Fm
Fin
214-215

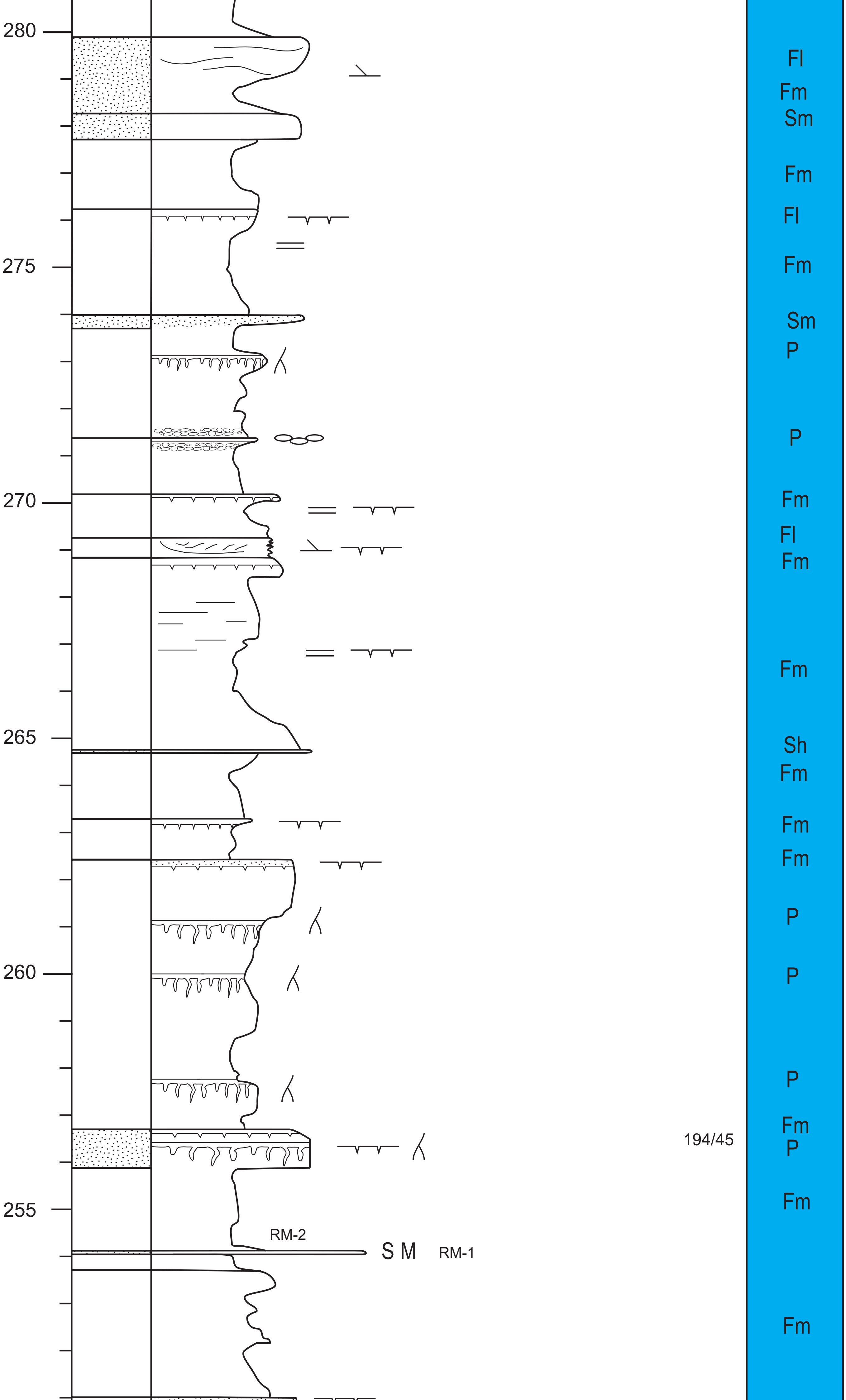
280
275
270
265
260
255
RM-2
S M
RM-1
194/45
Fl
Fm
Sm
Fm
Fl
Fm
Sm
P
P
Fm
Fl
Fm
Fm
Sh
Fm
Fm
Fm
P
P
P
Fm
P
Fm
Fm

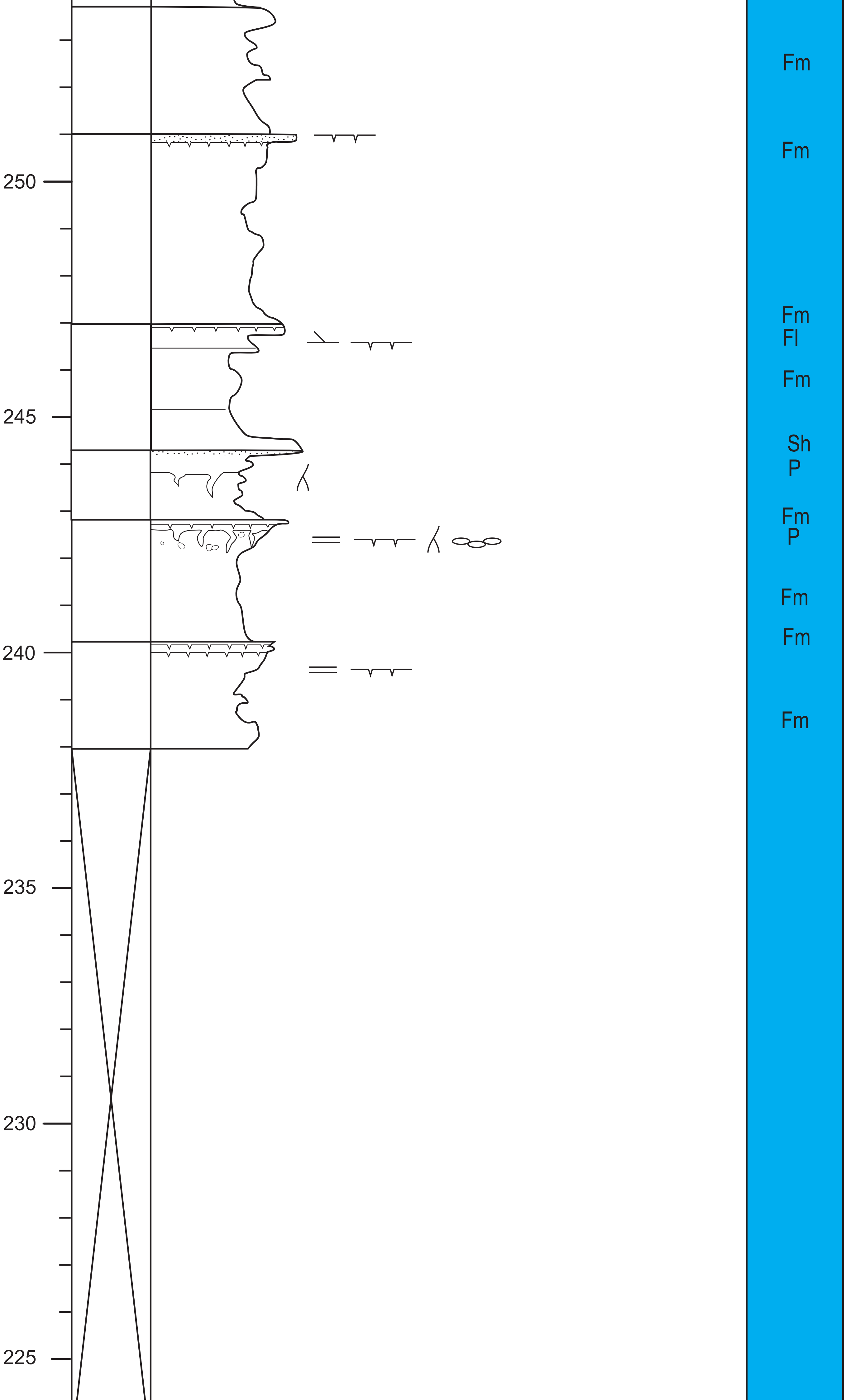

Fin R
212-213)

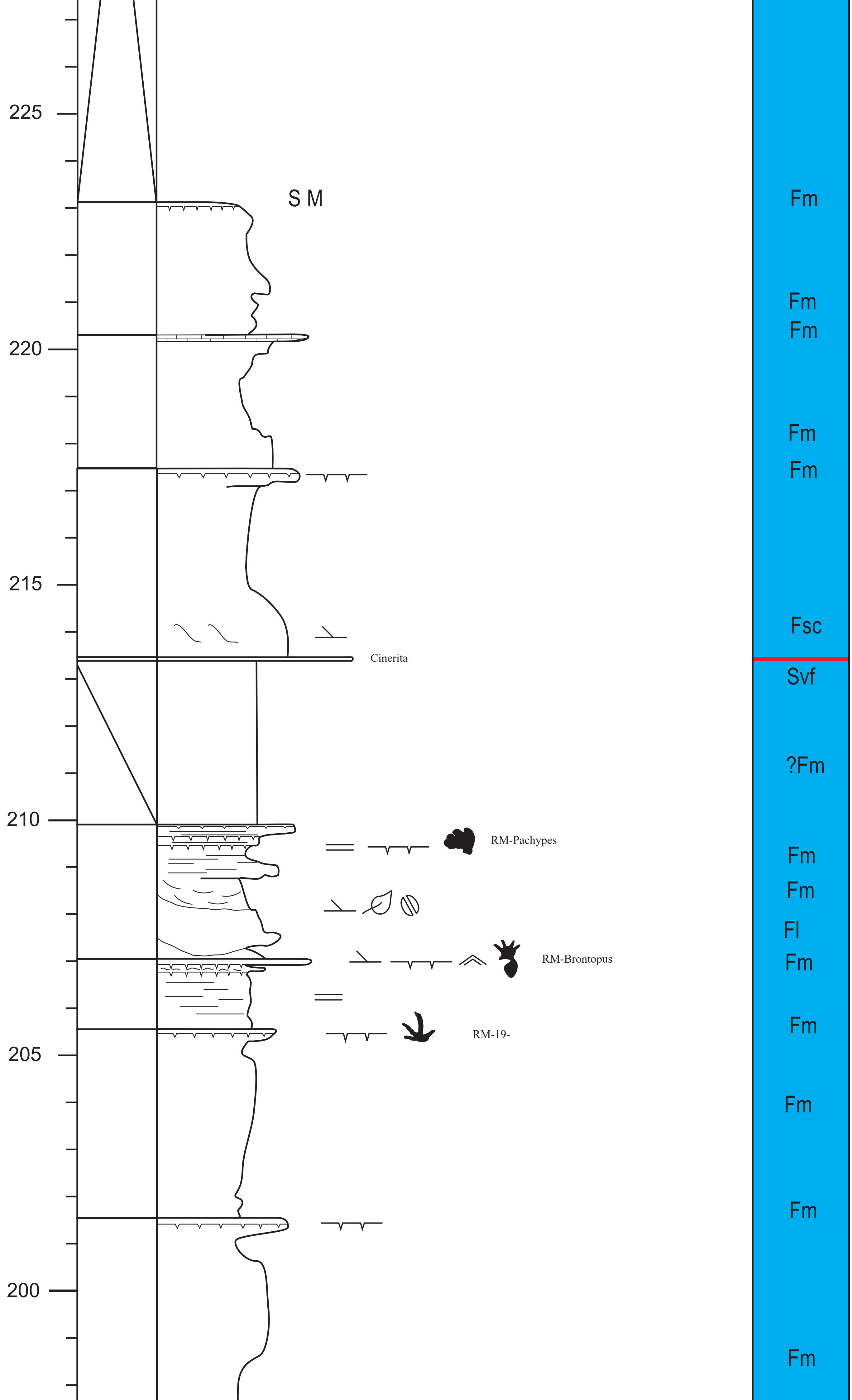

225
220
215
210
205
200
S M
Cinerita
RM-Pachypes
RM-Brontopus
RM-19-
Fm
Fm
Fm
Fm
Fm
Fsc
Svf
?Fm
Fm
Fm
Fl
Fm
Fm
Fm
Fm
Fm

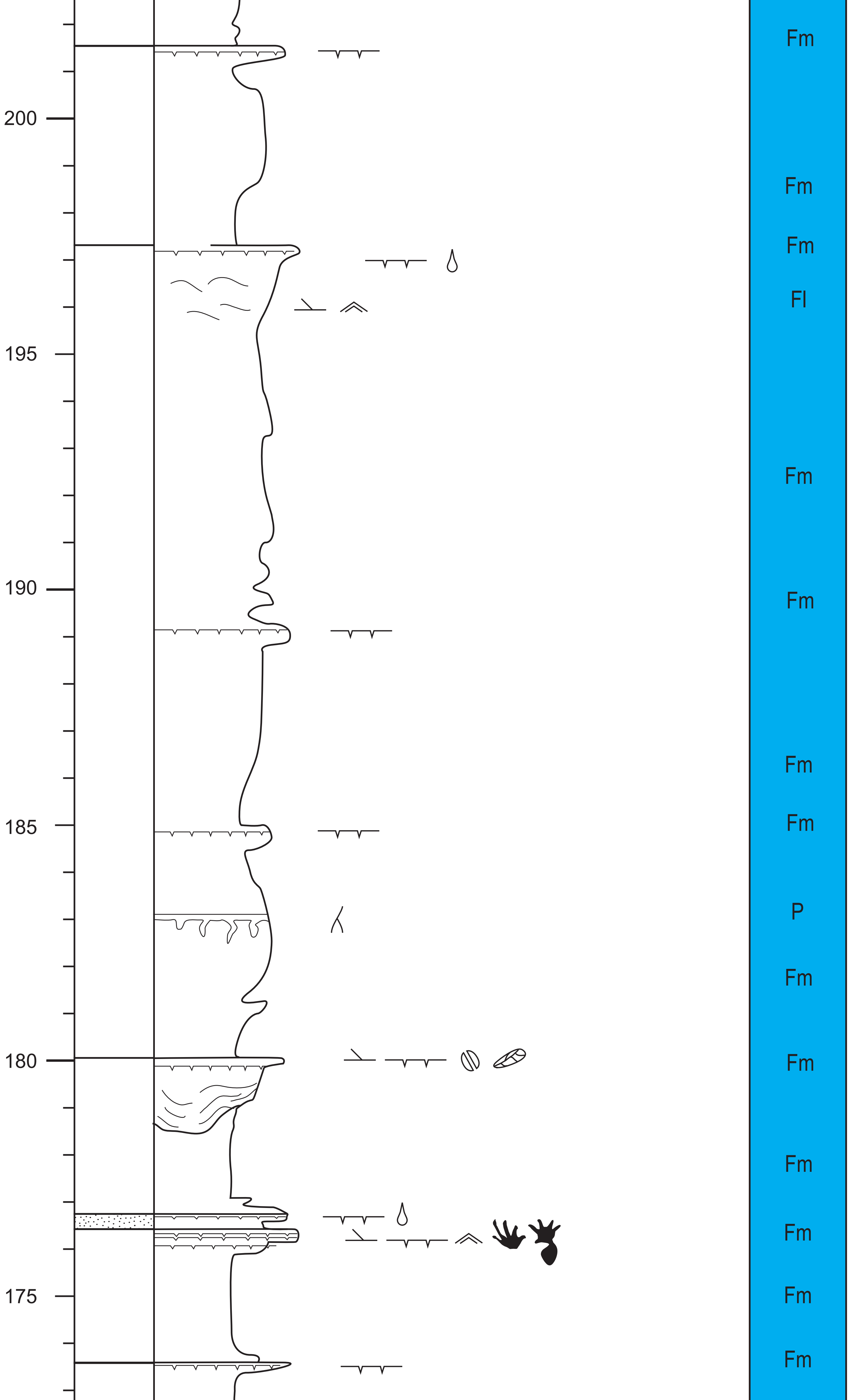

Fm
200
Fm
Fm
Fl
195
Fm
190
Fm
Fm
185
Fm
P
Fm
180
Fm
Fm
Fm
175
Fm
Fm

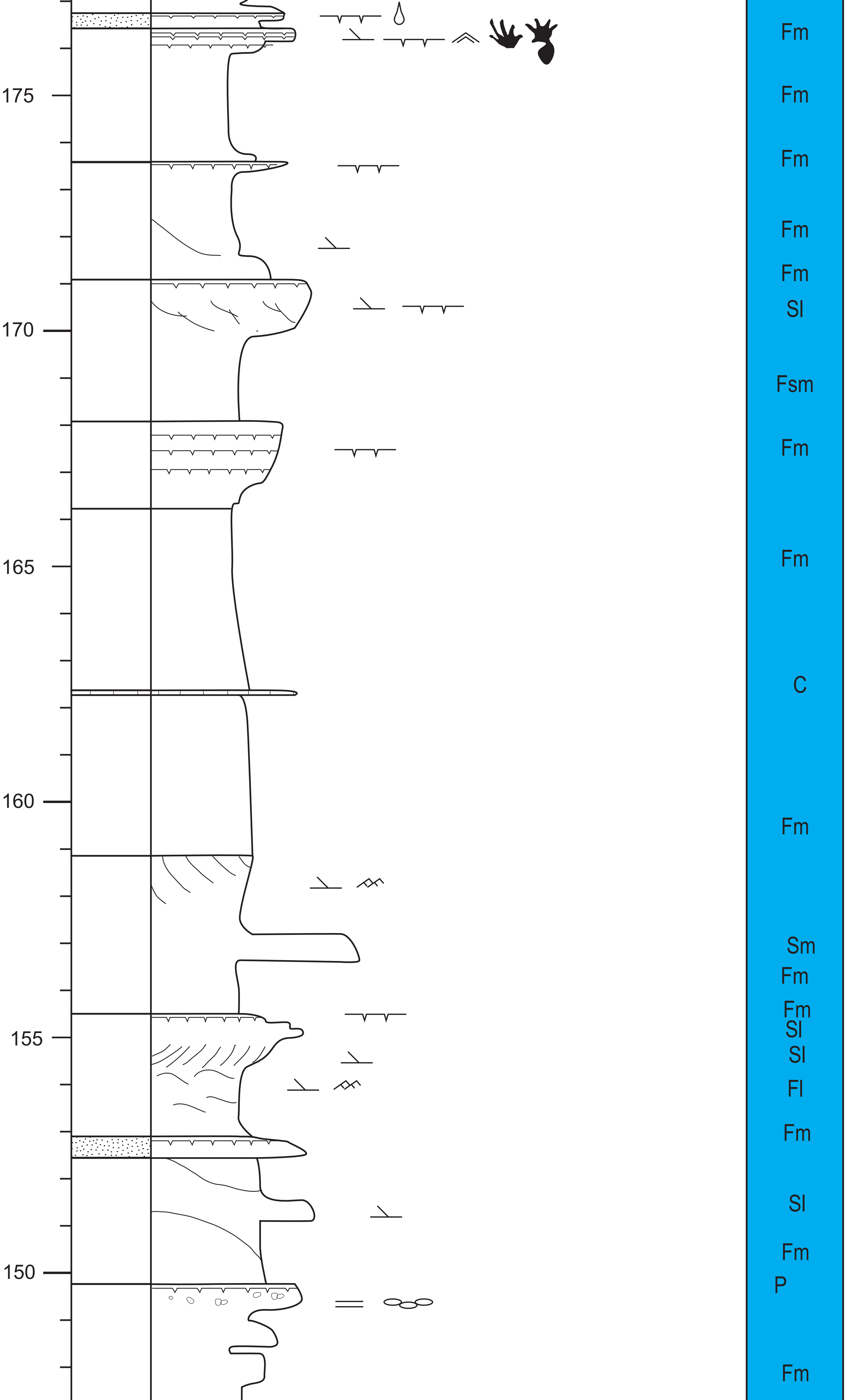
175
170
165
160
155
150
Fm
Fm
Fm
Fm
Fm
Sl
Fsm
Fm
Fm
C
Fm
Sm
Fm
Fm
Sl
Sl
Fl
Fm
Sl
Fm
P
Fm

Fin R

210-211)

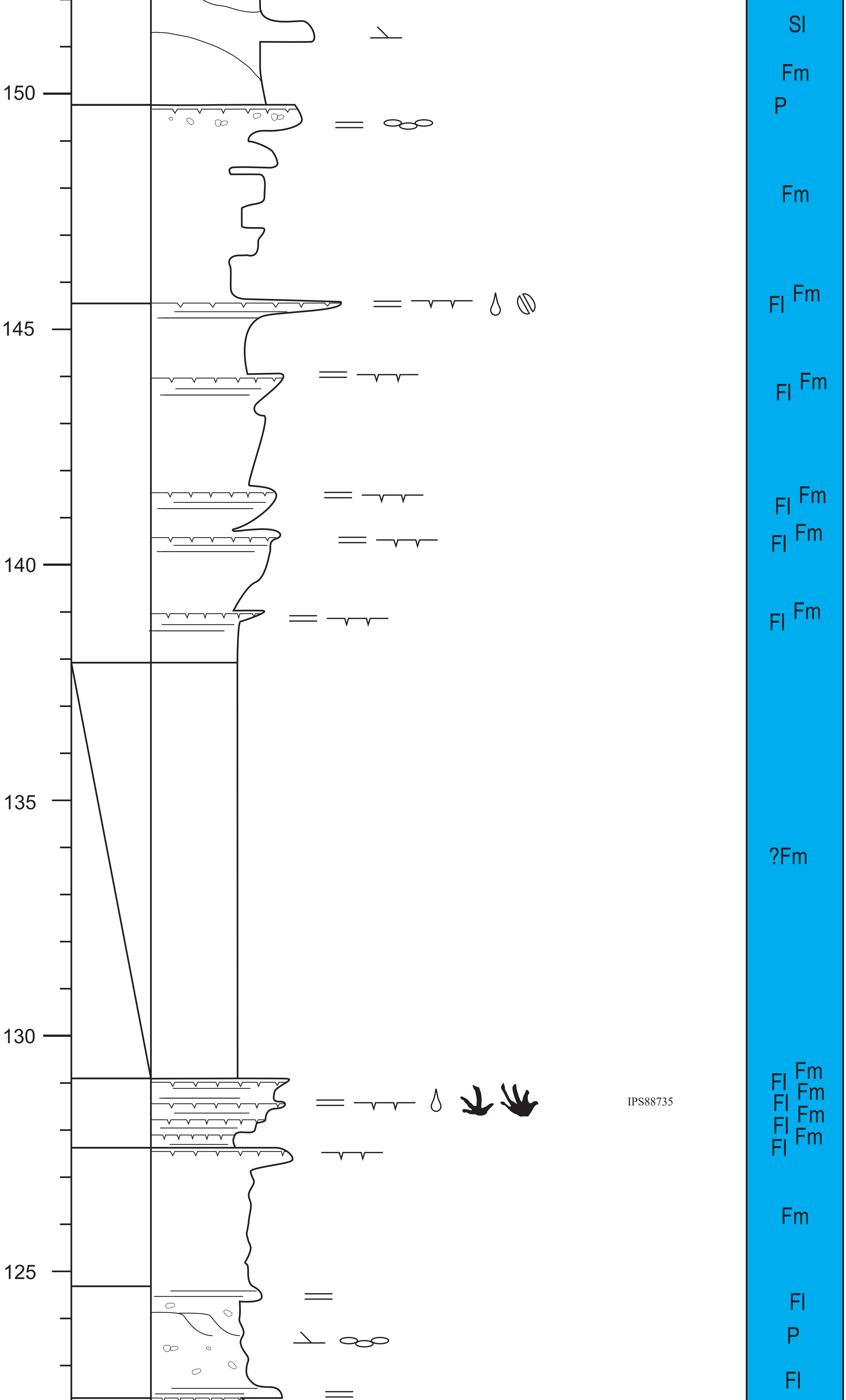
150
145
140
135
130
125
IPS88735
Sl
Fm
P
Fm
Fl Fm
Fl Fm
Fl Fm
Fl Fm
Fl Fm
?Fm
Fl Fm
Fl Fm
Fl Fm
Fl Fm
Fm
Fl
P
Fl

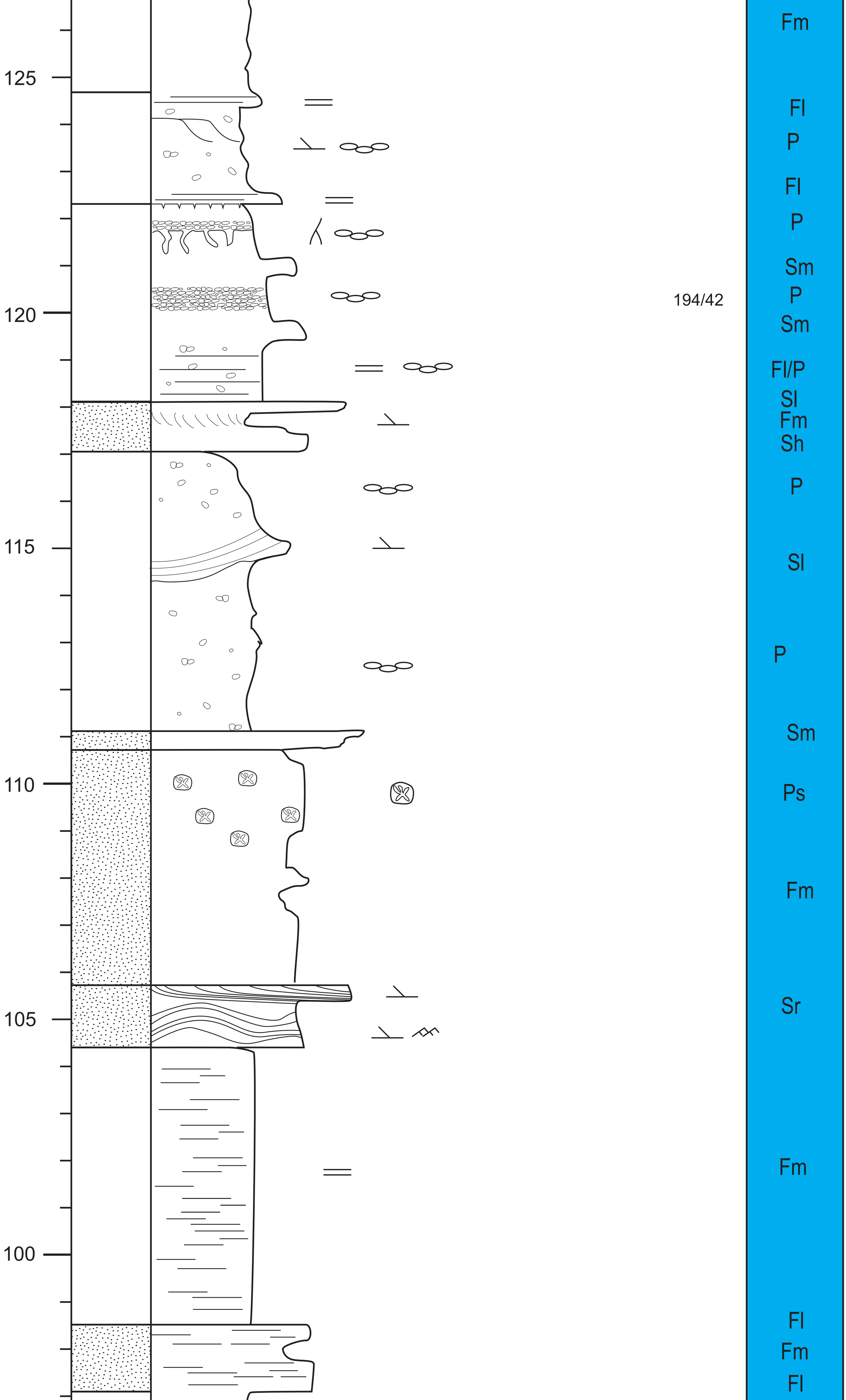

125
120
115
110
105
100
194/42
Fm
Fl
P
Fl
P
Sm
P
Sm
Fl/P
Sl
Fm
Sh
P
Sl
P
Sm
Ps
Fm
Sr
Fm
Fl
Fm
Fl

Fin
(pgs 17

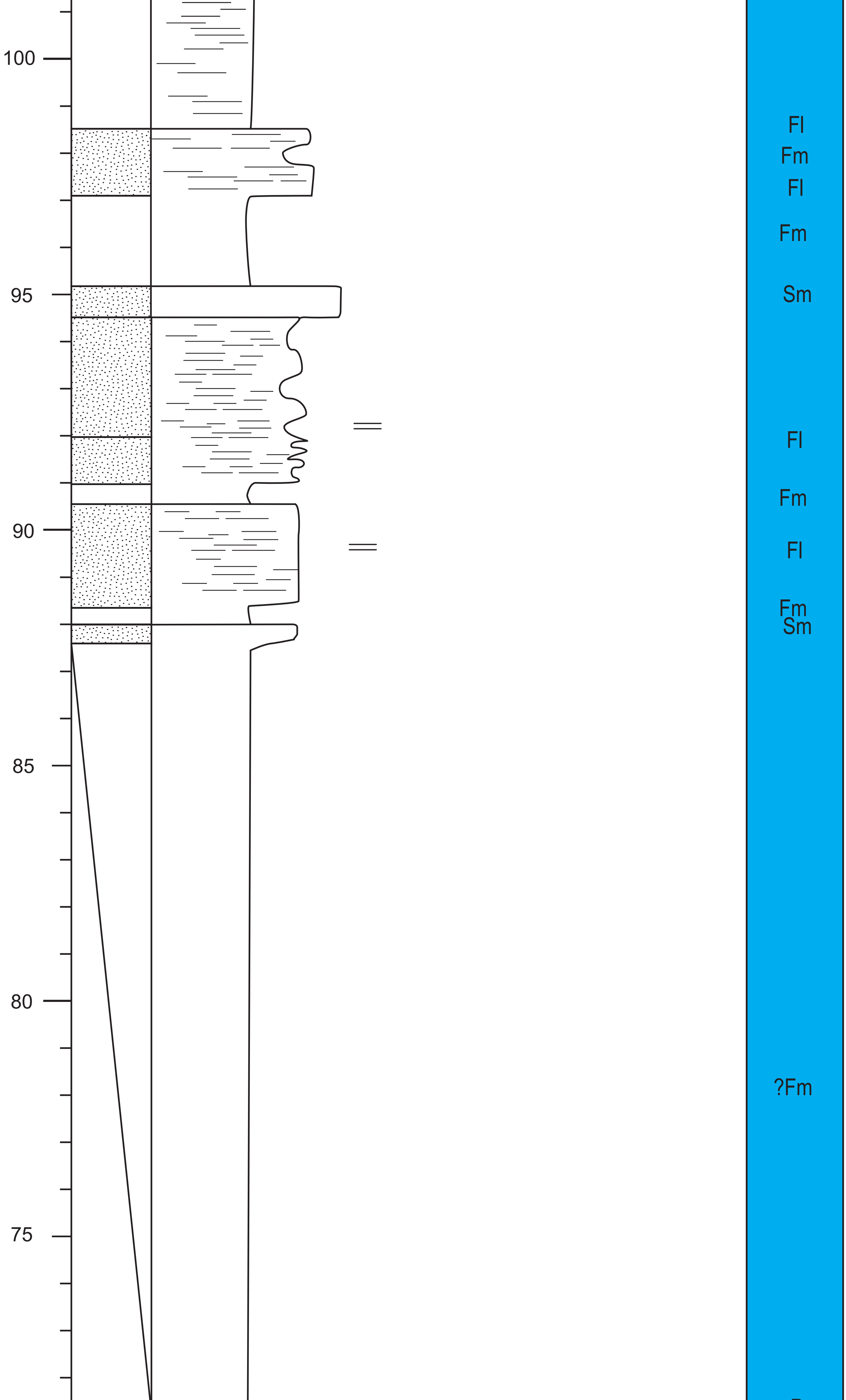
100
95
90
85
80
75
Fl
Fm
Fl
Fm
Sm
Fl
Fm
Fl
Fm
Sm
?Fm

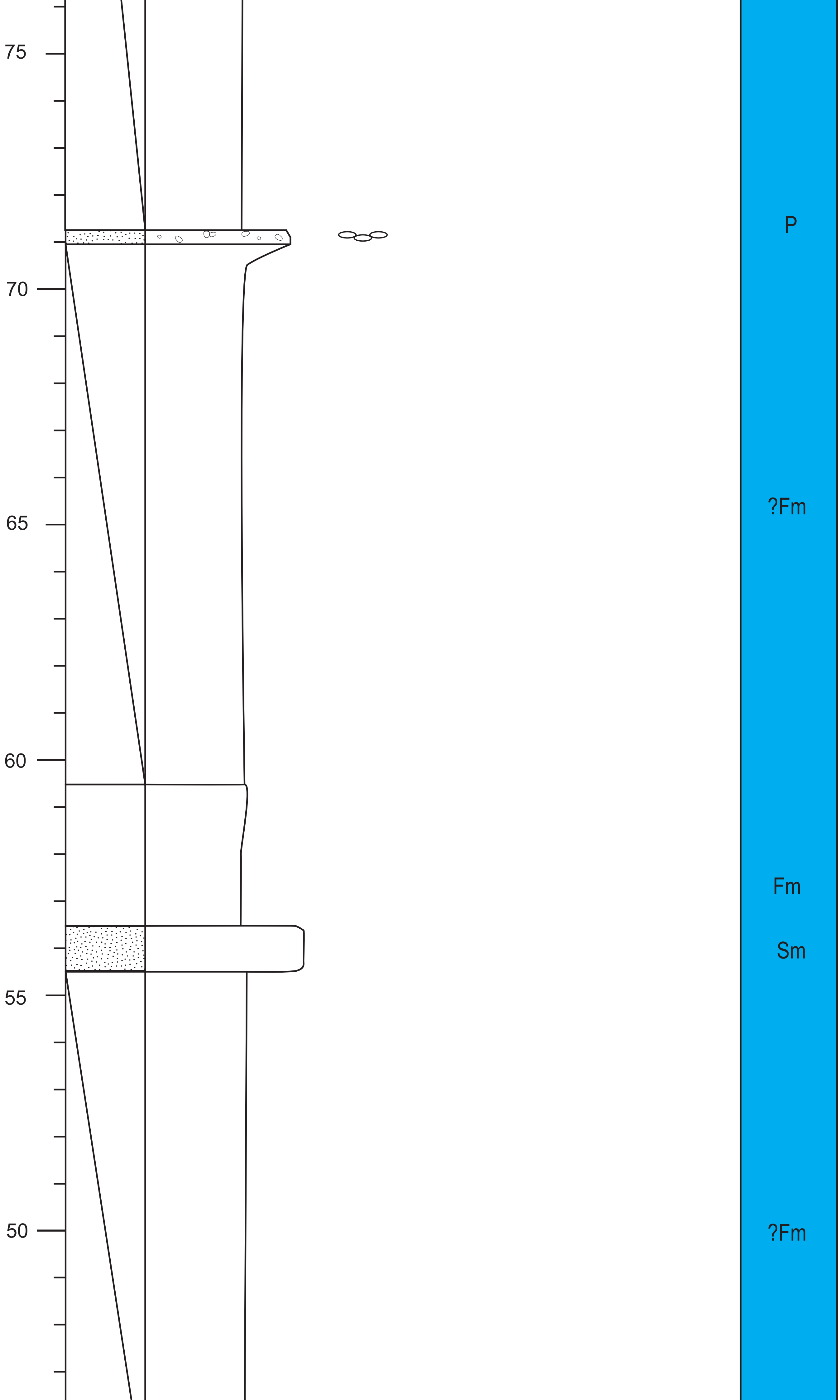
75
70
65
60
55
50
P
?Fm
Fm
Sm
?Fm

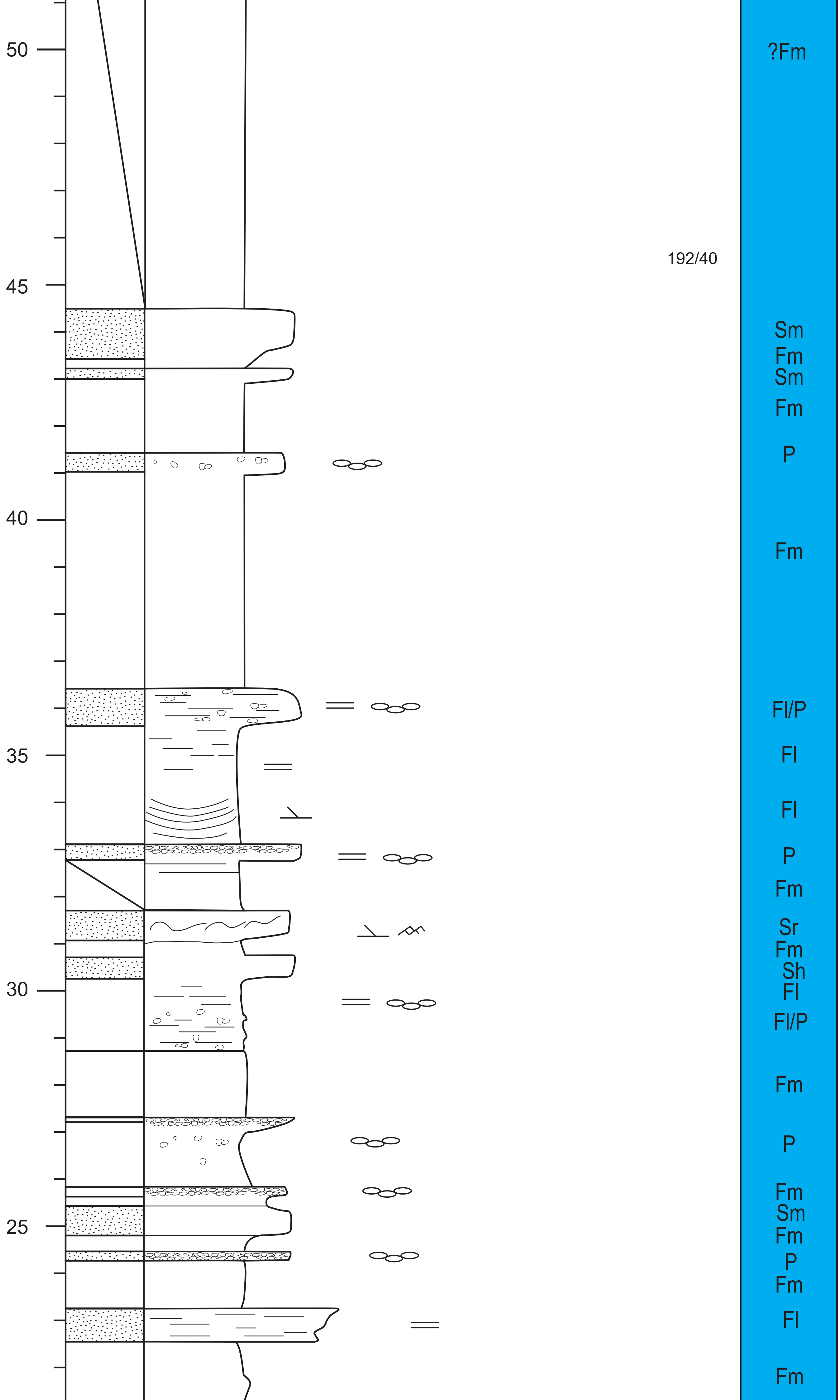
50
45
40
35
30
25
192/40
?Fm
Sm
Fm
Sm
Fm
P
Fm
Fl/P
Fl
Fl
P
Fm
Sr
Fm
Sh
Fl
Fl/P
Fm
P
Fm
Sm
Fm
P
Fm
Fl
Fm

Fi
(pg

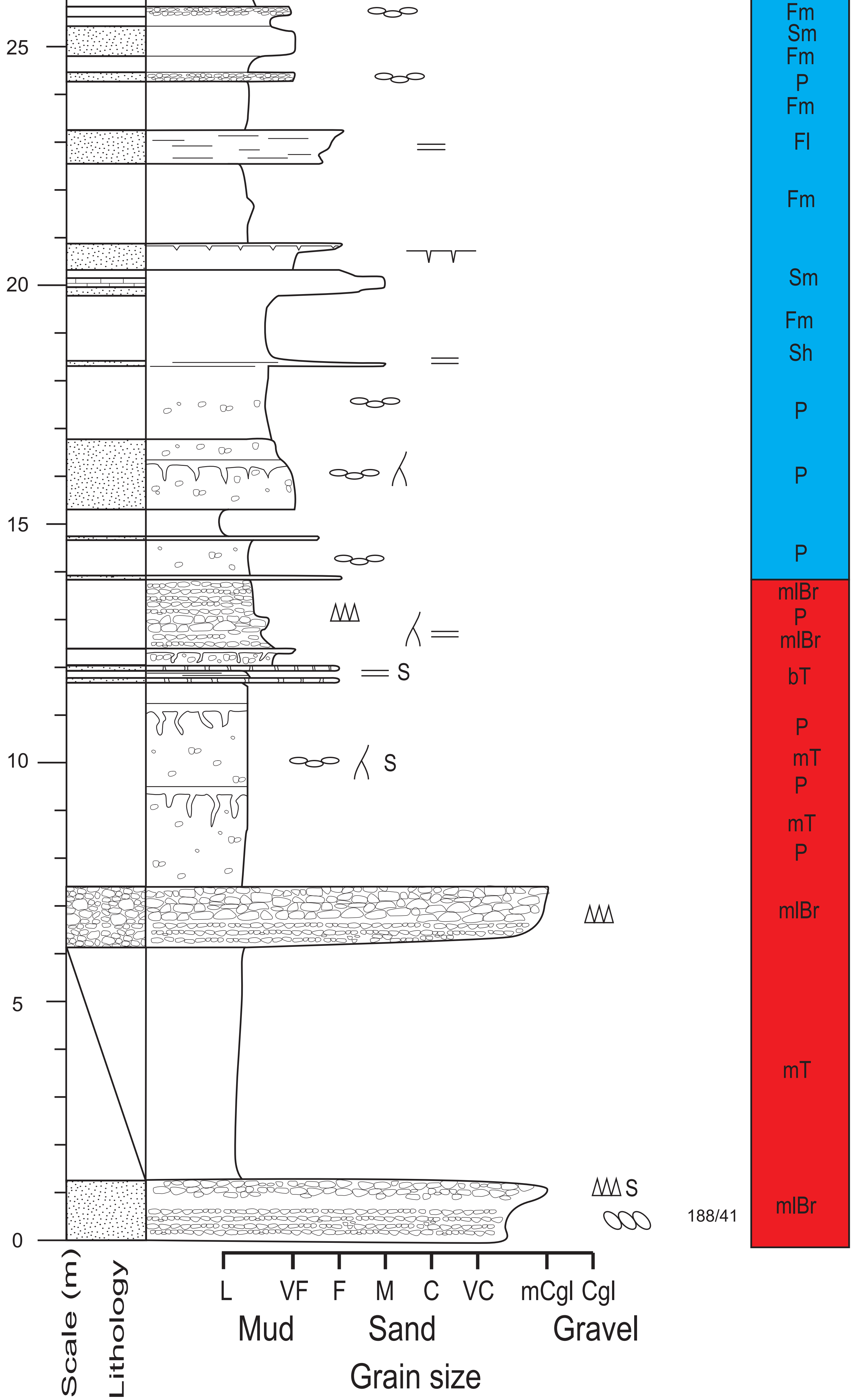

25
20
15
10
5
0
Scale (m)
Lithology
L VF F M C VC mCgl Cgl
Mud Sand Gravel
Grain size
S
S
S
188/41
Fm
Sm
Fm
P
Fm
Fl
Fm
Sm
Fm
Sh
P
P
P
mlBr
P
mlBr
bT
P
mT
P
mT
P
mlBr
mT
mlBr

Stratigraphical section of Coll Roig

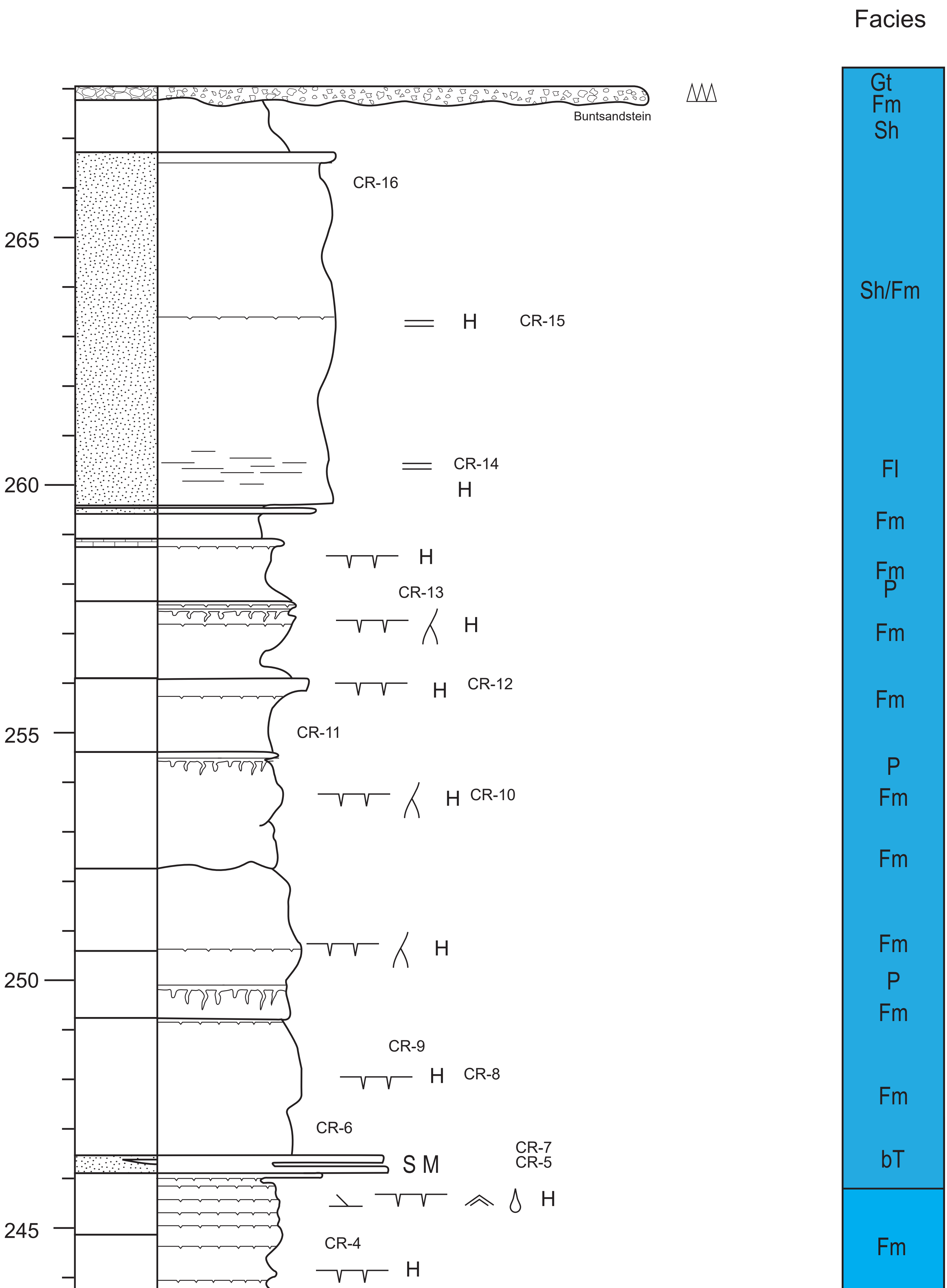

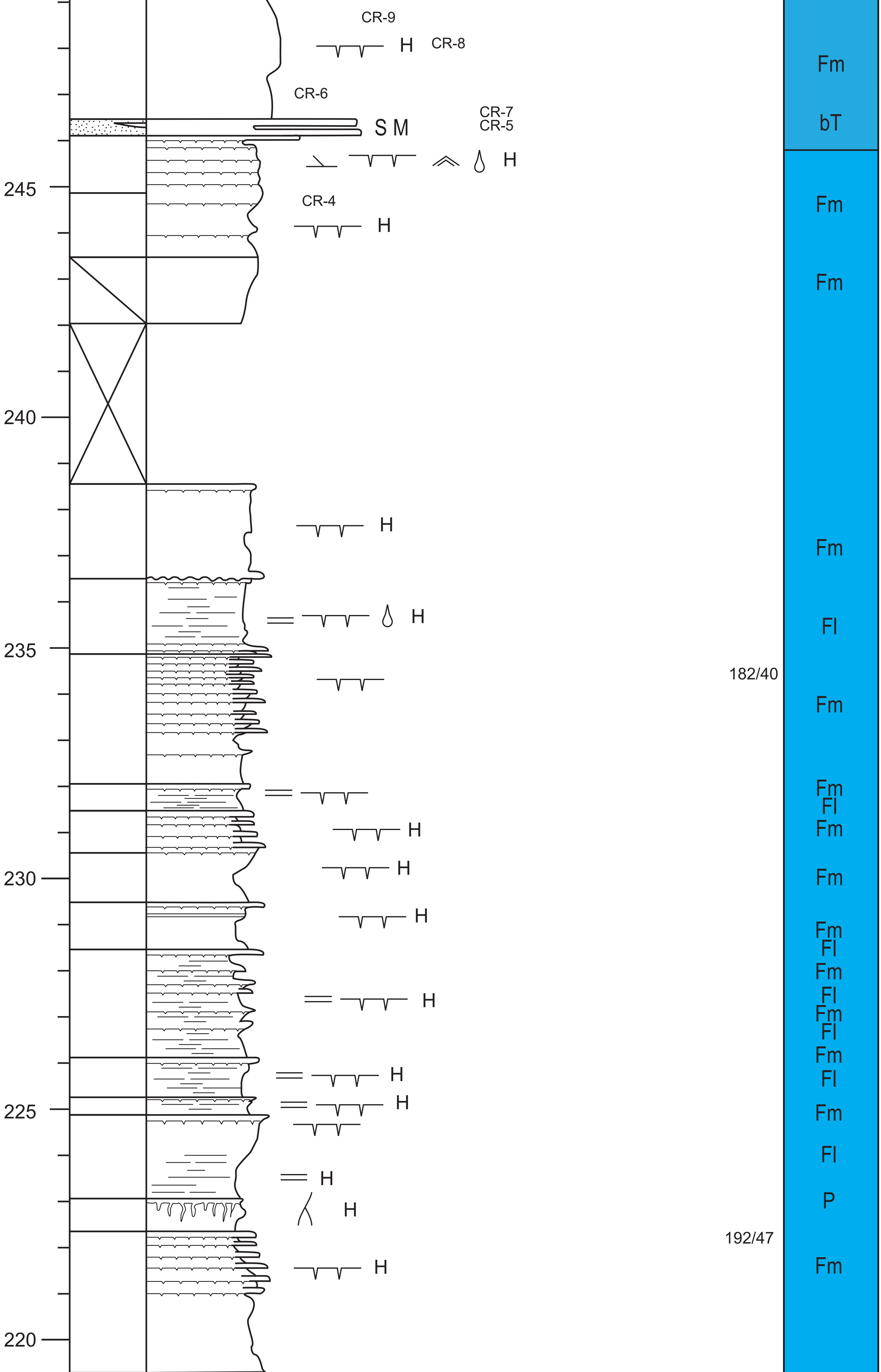

CR-9
H
CR-8
CR-6
S M
CR-7
CR-5
H
245
CR-4
H
240
H
H
235
182/40
H
H
230
H
H
H
H
225
H
H
192/47
H
220
Fm
bT
Fm
Fm
Fm
Fl
Fm
Fm
Fl
Fm
Fm
Fm
Fl
Fm
Fl
Fm
Fl
Fm
Fl
Fm
Fl
P
Fm

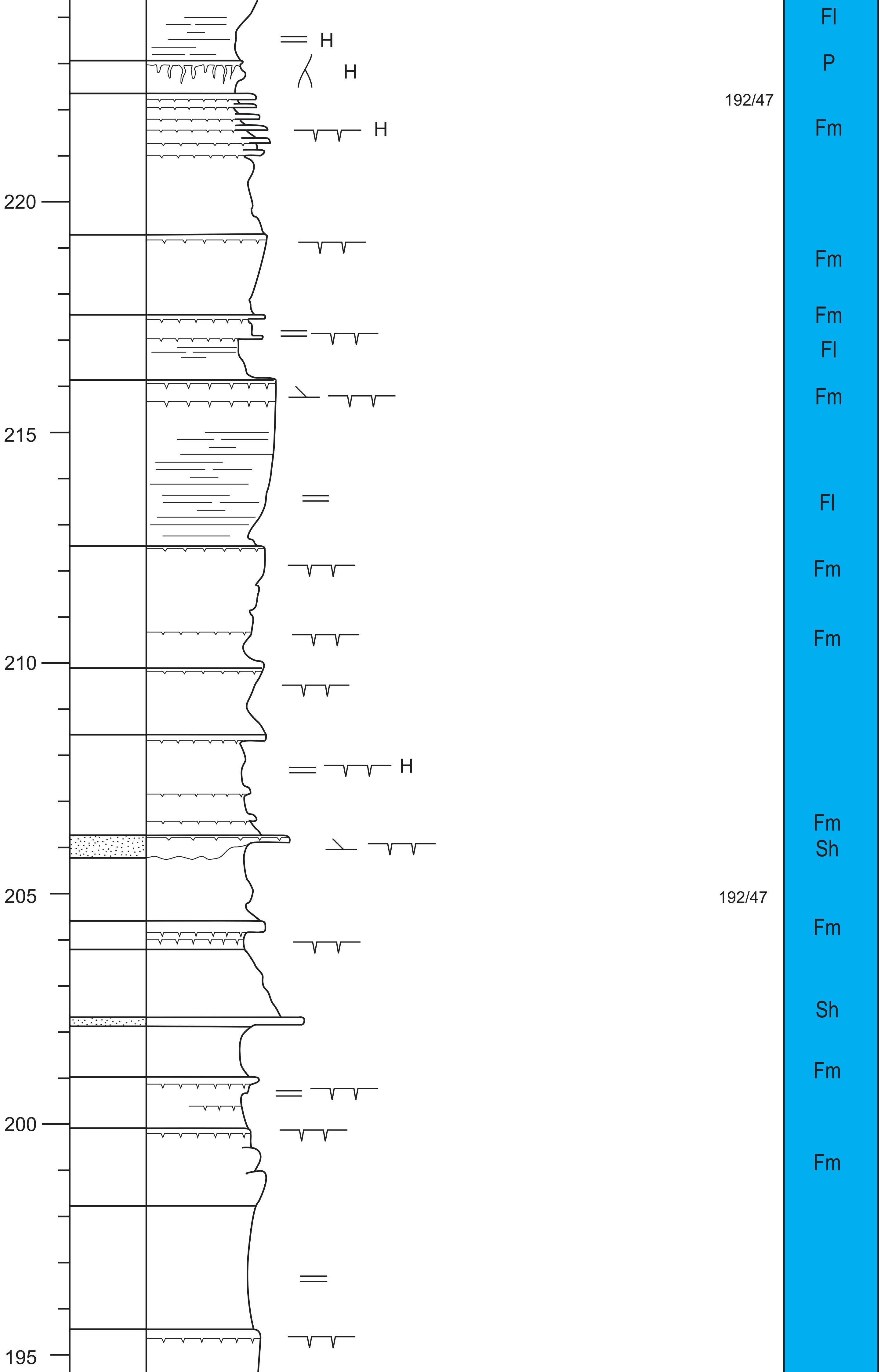

220
215
210
205
200
195
H
H
H
H
192/47
192/47
Fl
P
Fm
Fm
Fm
Fl
Fm
Fl
Fm
Fm
Fm
Sh
Fm
Sh
Fm
Fm

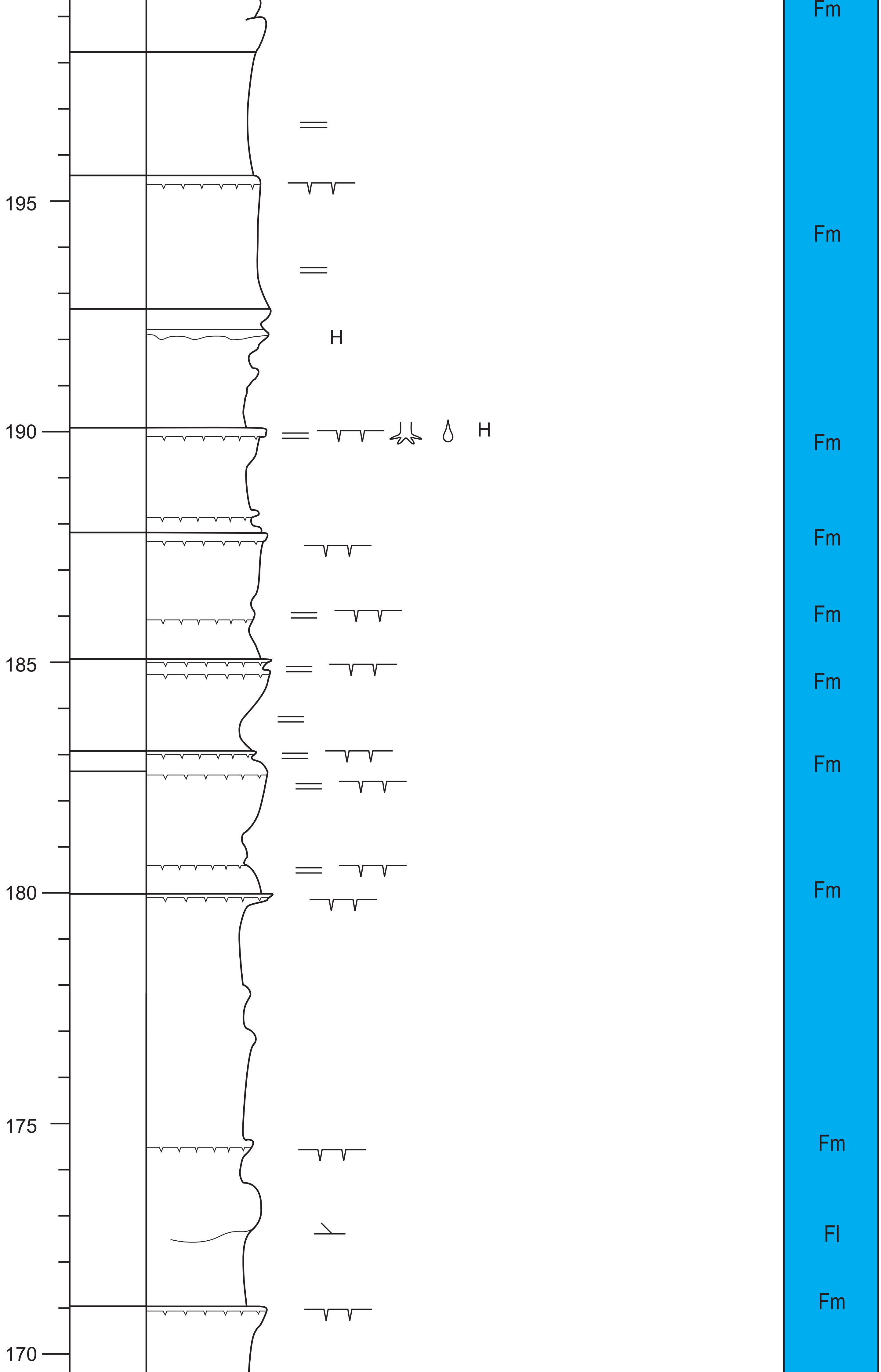

195
190
185
180
175
170
H
H
Fm
Fm
Fm
Fm
Fm
Fm
Fm
Fm
Fm
Fl
Fm

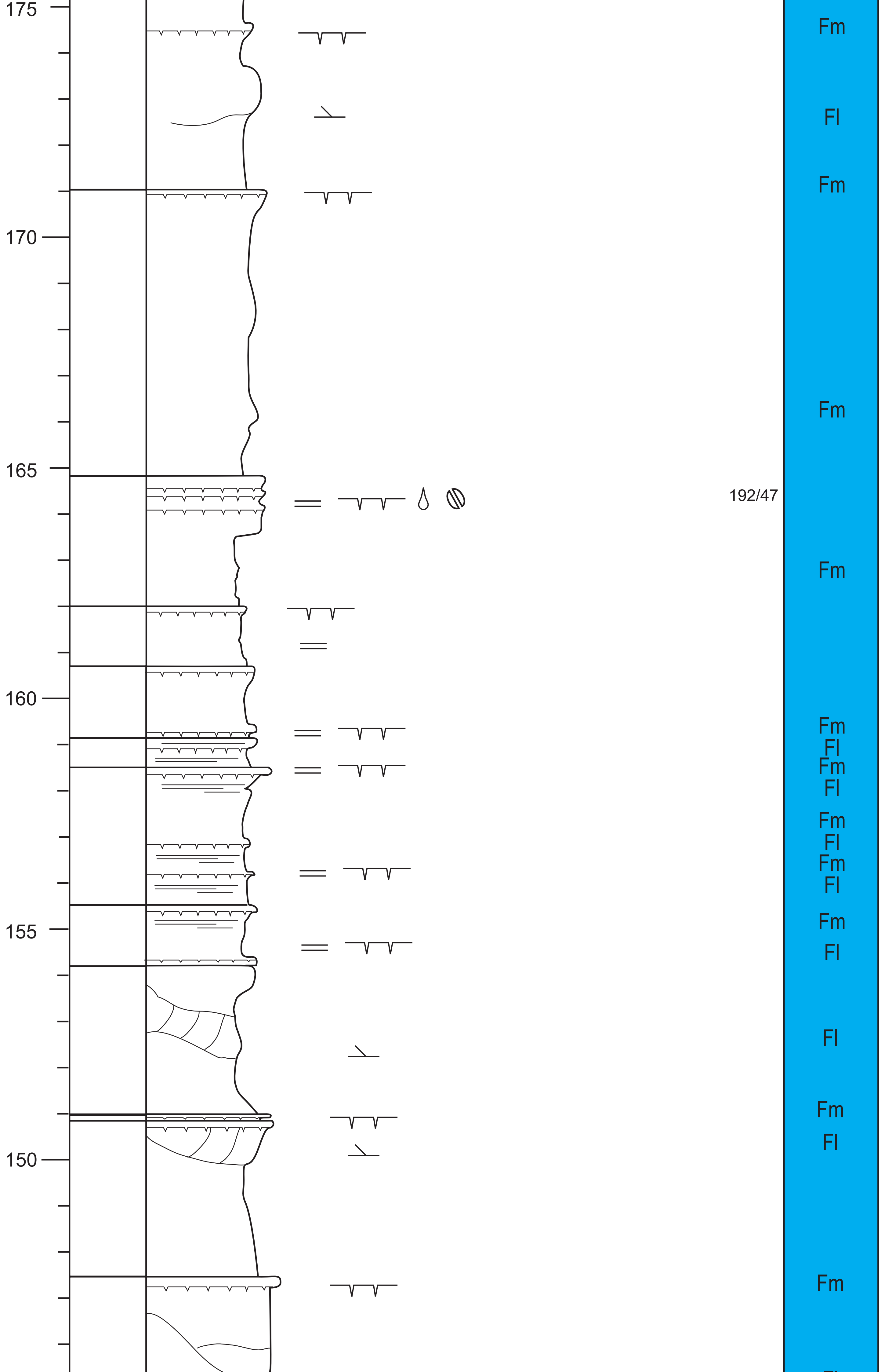
175
170
165
160
155
150
192/47
Fm
Fl
Fm
Fm
Fm
Fm
Fl
Fm
Fl
Fm
Fl
Fm
Fl
Fm
Fl
Fl
Fm
Fl
Fm

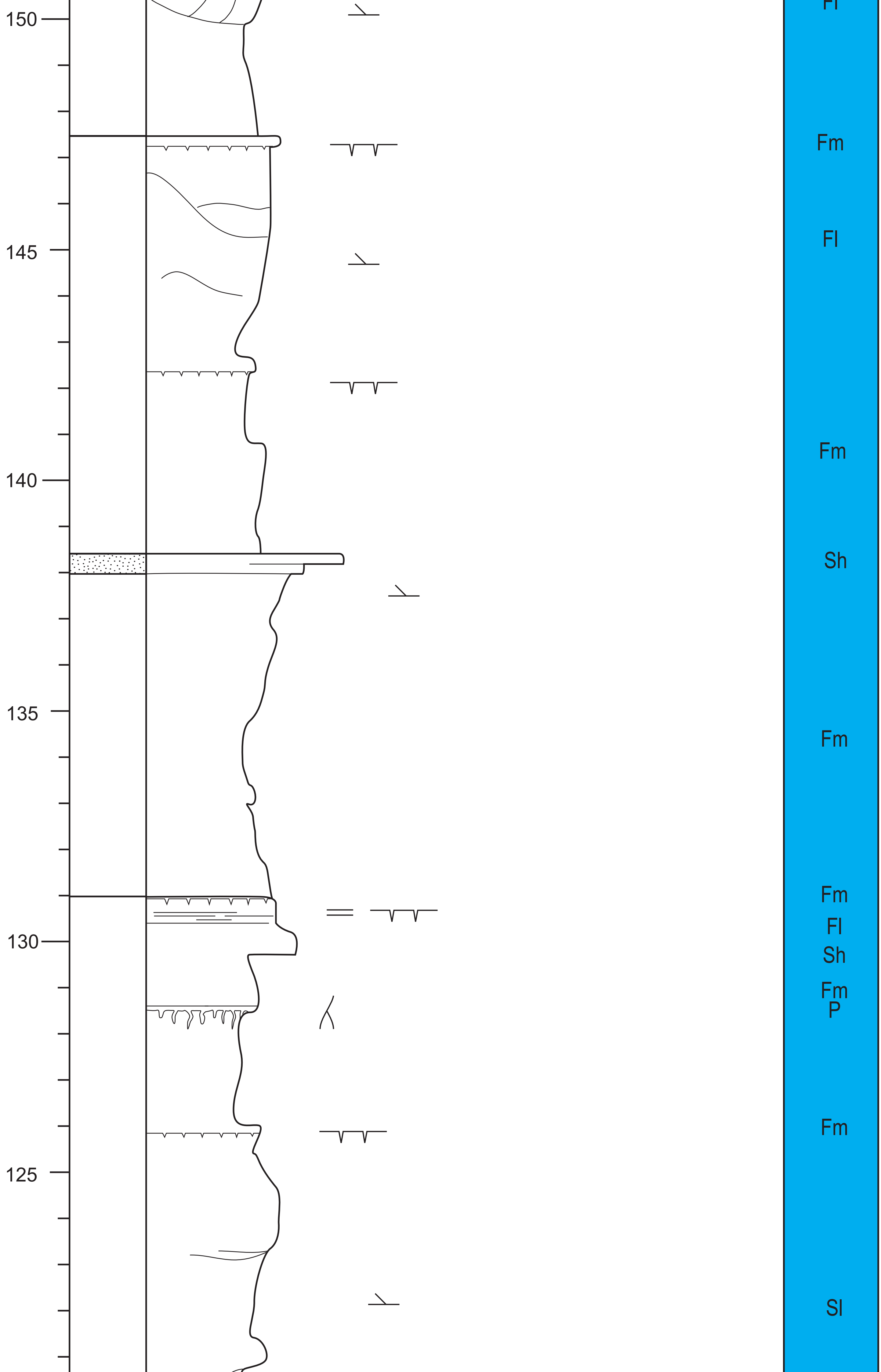

150
145
140
135
130
125
Fl
Fm
Fl
Fm
Sh
Fm
Fm
Fl
Sh
Fm
P
Fm
Sl

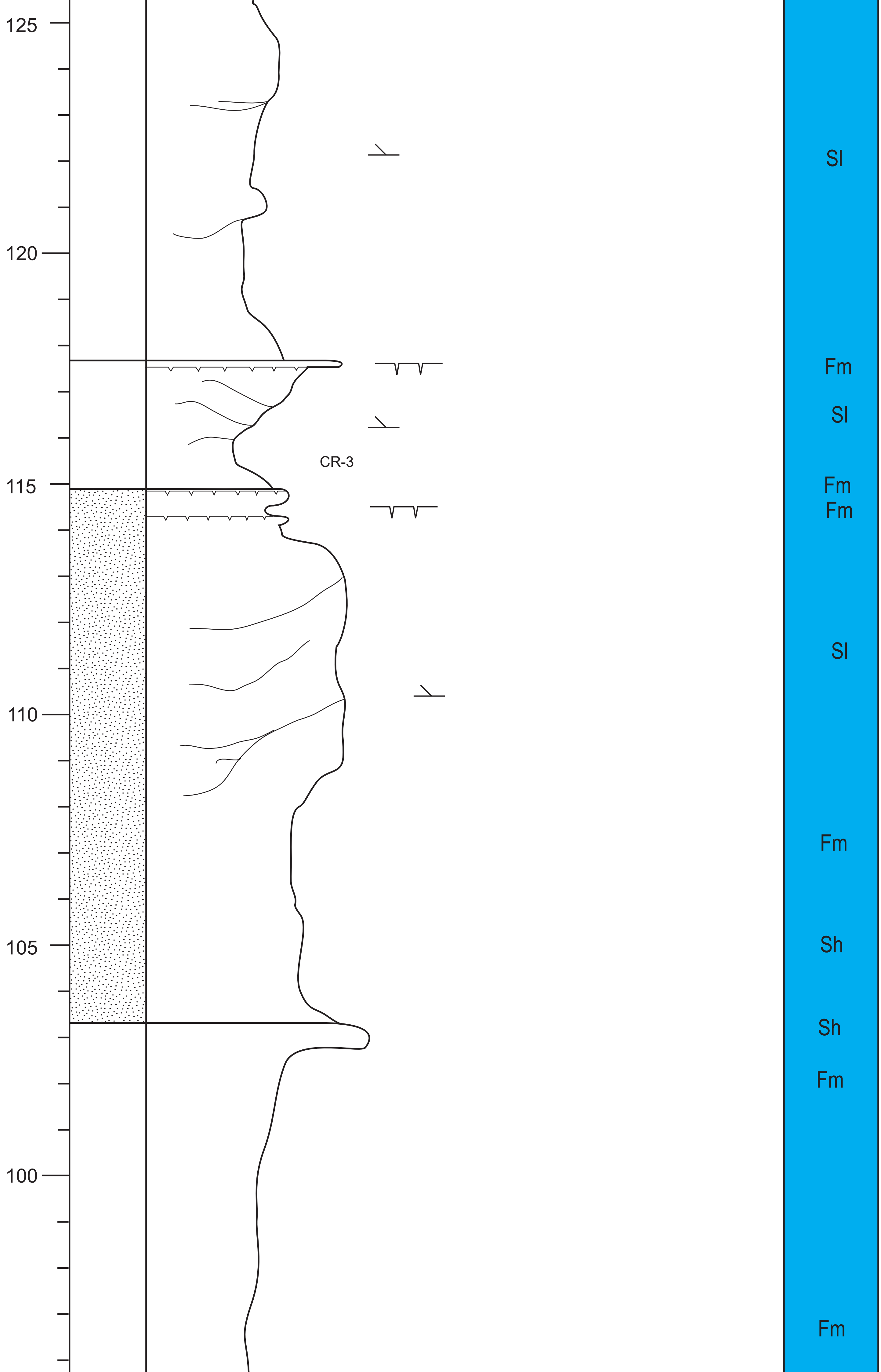

125
120
115
110
105
100
CR-3
Sl
Fm
Sl
Fm
Fm
Sl
Fm
Sh
Sh
Fm
Fm

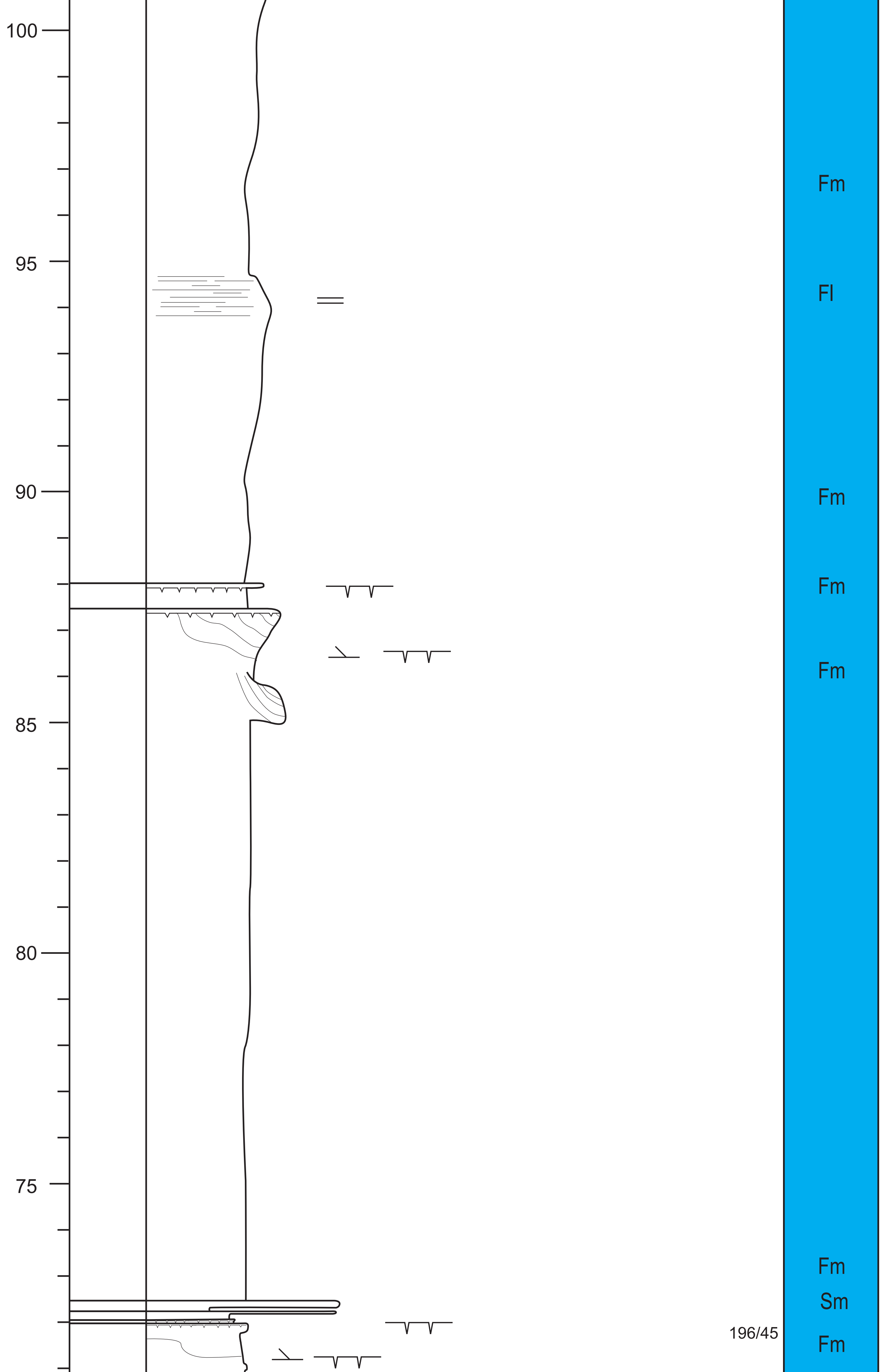
100
95
90
85
80
75
Fm
Fl
Fm
Fm
Fm
Fm
Sm
196/45
Fm

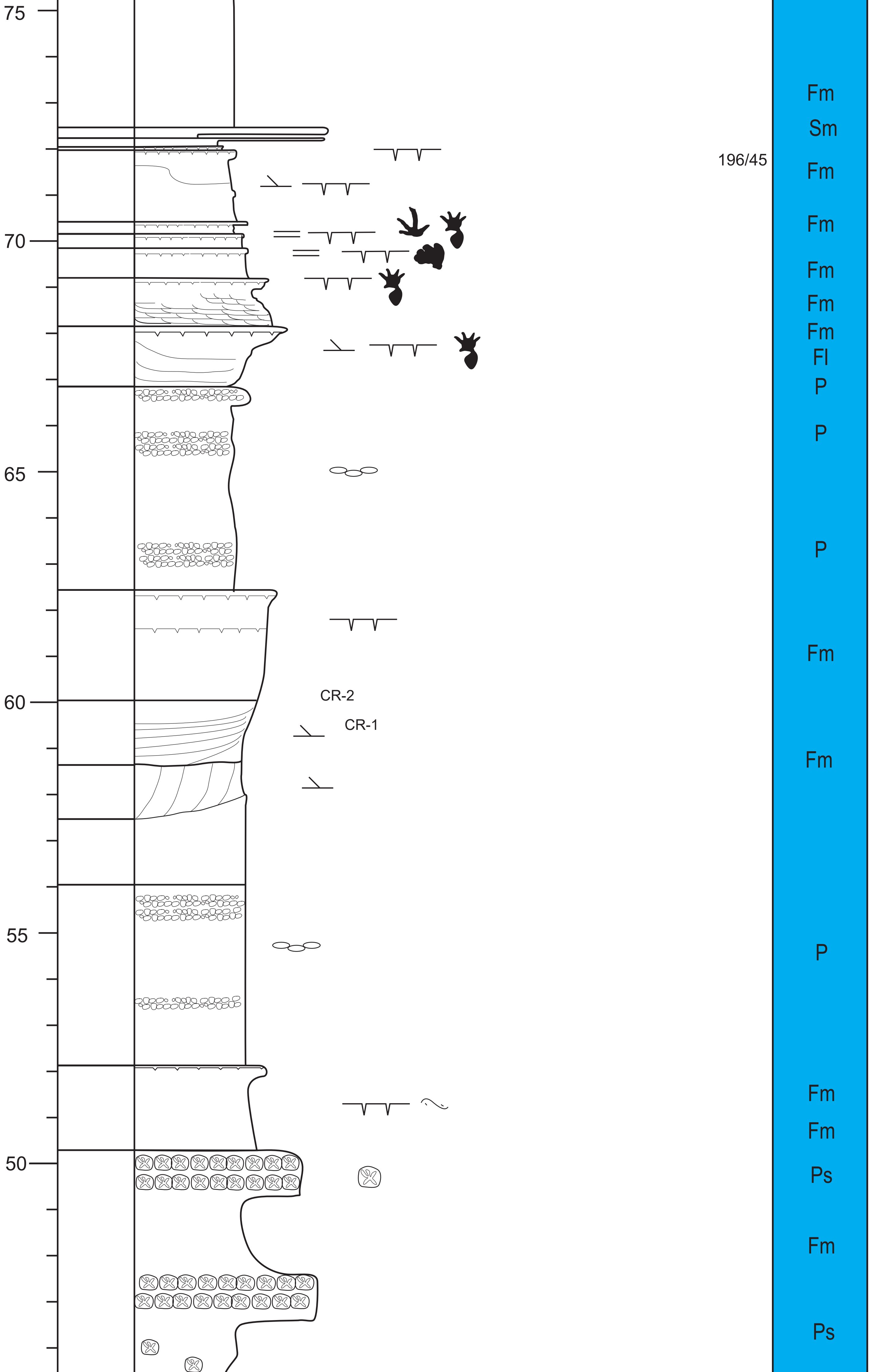

75
70
65
60
55
50
CR-2
CR-1
196/45
Fm
Sm
Fm
Fm
Fm
Fm
Fm
Fl
P
P
P
Fm
Fm
P
Fm
Fm
Ps
Fm
Ps

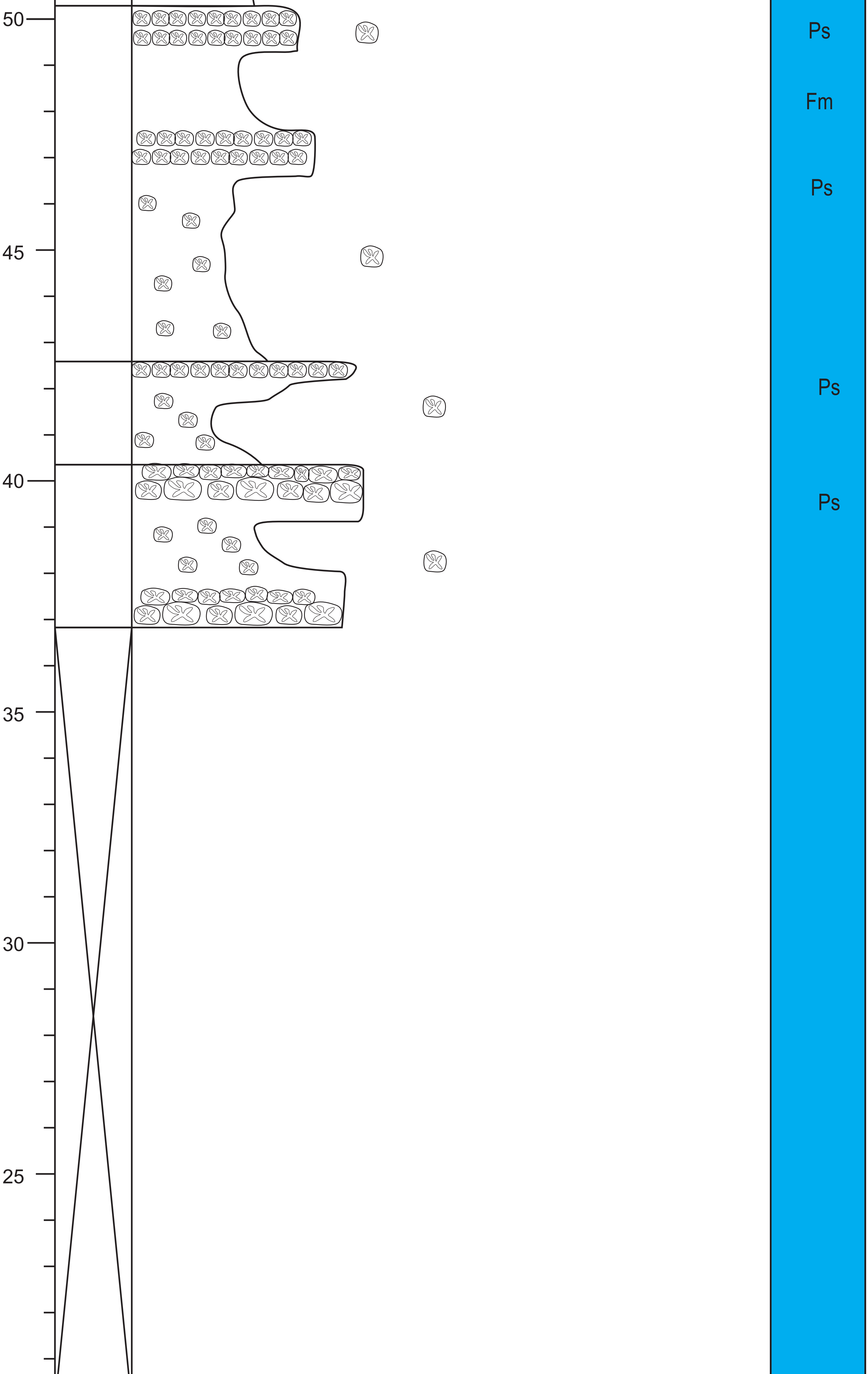

50
45
40
35
30
25
Ps
Fm
Ps
Ps
Ps

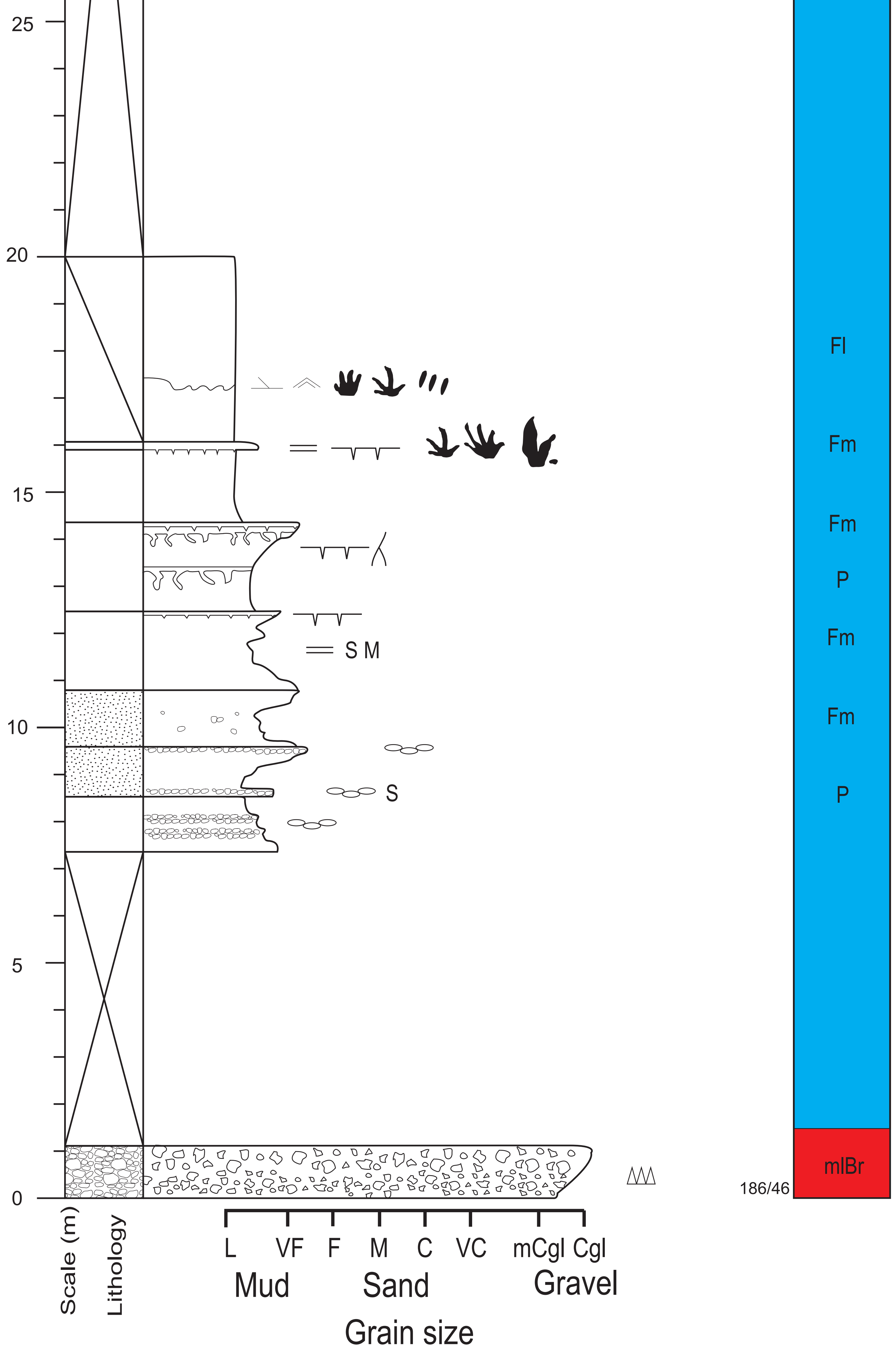
25
20
15
10
5
0
Fl
Fm
Fm
P
Fm
Fm
P
mlBr
S M
S
186/46
Scale (m)
Lithology
L
VF
F
M
C
VC
mCgl
Cgl
Mud
Sand
Gravel
Grain size

Legend of stratigraphic sections of CnH, RM and CR